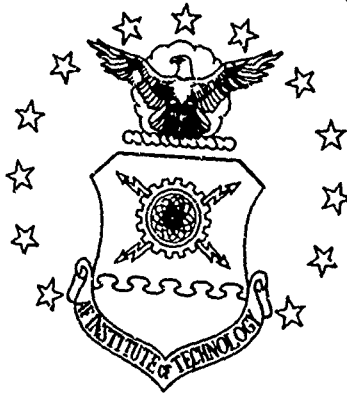
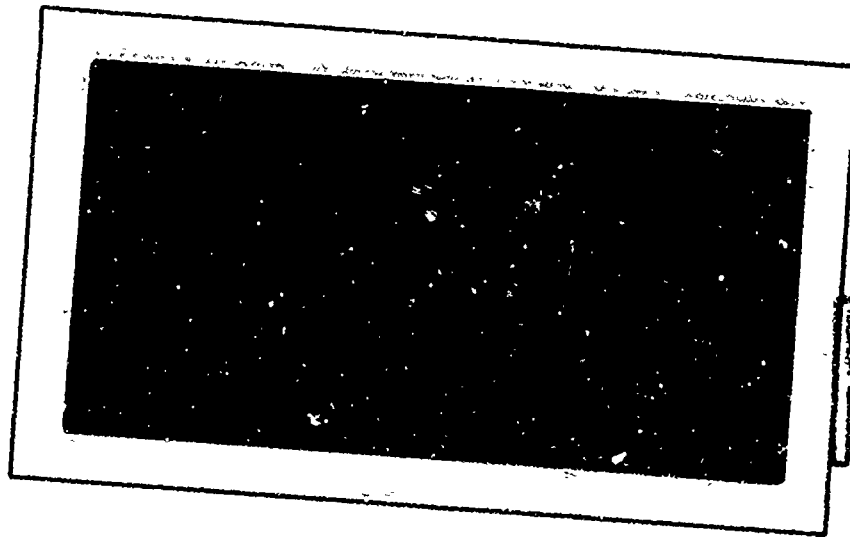


AD859717

AIR FORCE INSTITUTE OF TECHNOLOGY



AIR UNIVERSITY
UNITED STATES AIR FORCE



DDC
RECEIVED
OCT 6 1969
REGISTERED
D

SCHOOL OF ENGINEERING

WRIGHT-PATTERSON AIR FORCE BASE, OHIO

GRAVITY EFFECTS ON LOW VELOCITY
PENETRATION OF A PROJECTILE INTO
A COHESIONLESS MEDIUM

THESIS

GSF/MC/69-6

Anthony Paul Pyrz
Captain USAF

This document is subject to special export controls and each transmittal to foreign governments or foreign nationals may be made only with prior approval of the Dean of Engineering, Air Force Institute of Technology (AFIT-SE), Wright Patterson Air Force Base, Ohio 45433.

GRAVITY EFFECTS ON LOW VELOCITY PENETRATION
OF A PROJECTILE INTO A COHESIONLESS MEDIUM

THESIS

Presented to the Faculty of the School of Engineering
of the Air Force Institute of Technology
Air University
in Partial Fulfillment of the
Requirements for the
Master of Science Degree
in Astronautics

by

Anthony Paul Pyrzs, B.S.

Captain

USAF

June 1969

This document is subject to special export controls and each transmittal to foreign governments or foreign nationals may be made only with prior approval of the Dean of Engineering, Air Force Institute of Technology (AFIT-SE), Wright Patterson Air Force Base, Ohio 45433.

Acknowledgments

The assistance of Major Stewart M. Johnson of the Department of Mechanics, Air Force Institute of Technology, was guidance and counsel throughout the course of this study. Acknowledgments are due a great many other people who smoothed the path along the way.

Sincere thanks are expressed to:

Mr. Eldred Powell for his laboratory space, his tools, and his sage advice and assistance.

Mr. William Baker of the Mechanical Engineering Laboratory, AFIT, for the use of his equipment, his advise, and his constant encouragement.

Mr. Millard Wolfe, Supervisor of the AFIT shops, for the construction of experimental equipment.

Mr. Don Griggs, Capt. Jack Thompson, and Lt. James Lackey of the Zero-Gravity Section, Directorate of Flight Test, Aeronautical Systems Division, Wright-Patterson AFB, for their absolute cooperation and their assistance both on the ground and aboard the aircraft.

Mr. Merl Worland, Mr. Jack Warwick, and Mr. James Taylor of the Technical Photography Branch, Aeronautical Systems Division, for their cooperation and for the expertise with which they photographed a difficult subject.

TSgt George Alvarado, and SSgt Dominic Miglionico, photographers assigned to the Directorate of Flight Test, ASD, for their efficiency in operating the camera under somewhat less than ideal conditions.

Contents

	Page
Acknowledgments	ii
List of Figures	vi
List of Tables	ix
Abstract	x
I. Introduction	1
Purpose and Scope	1
Method of Attack	3
II. Factors Affecting Soil Penetration On Earth.	4
Historical Background	4
Semi-Analytic Approaches	4
Empirical Approaches	7
Soil Properties	8
Conclusions.	9
III. Gravity Effects On Soil Properties	10
Shear Strength	10
Shear Modulus	10
Compressional Wave Velocity	10
Previous Gravity Work	12
IV. Description of the Experiment	16
Materials	16
Equipment	16
Test Aircraft	17
Plywood Enclosure	18
Air Gun	18
Projectiles	18
Target Bed	19
Procedures and Conduct	20
Measurement of Impact Velocity	20
Measurement of Maximum Penetration	20
Preliminary Testing	21
Aircraft Environment	23
Quantity of Data	24

Contents (cont)

	Page
V. Presentation and Discussion of Results . . .	25
Laboratory Test Results	25
Gravity Testing	28
Deceleration Traces	42
VI. Conclusions and Recommendations	67
Terrestrial Penetration Into Cohesionless Media	67
Gravity Effects	67
Deceleration-Time Curves	68
General Conclusions	68
Recommendations	69
Bibliography	71
Appendix A. Tabulated Raw Data	74
Appendix B. Properties of the Target Media . . .	85
Appendix C. Description of Equipment	90
Appendix D. Measurements and Sources of Error. .	112
Appendix E. Derivation of a Semi-Analytical Equation	117
Appendix F. Computer Program for Plot P Production	126
Appendix G. Attempted Use of a Simulated Lunar Soil	132
Vita	135

List of Figures

Figure	Page
1. Shear Modulus vs Confining Pressure: Ottawa Sand	11
2. Sonic Velocity vs Confining Pressure. . . .	13
3. Crater Diameter vs Gravity: Moraski and Teal	15
4. Maximum Penetration vs Impact Velocity: Petry Equation	29
5. Maximum Penetration vs Impact Velocity: Moore Equation	30
6. Maximum Penetration vs Impact Velocity: Young Equation	31
7. Maximum Penetration vs Impact Velocity: Nara Equation	32
8. Maximum Penetration vs Gravity: Al-2-F, 1300 cm/sec	35
9. Maximum Penetration vs Gravity: Moore Equation	36
10. Maximum Penetration vs Gravity: Nara Equation	36
11. Time-To-Complete-Penetration vs Gravity . .	38
12. Maximum Penetration vs Time-To-Complete- Penetration	38
13. Time-To-Complete-Penetration vs Impact Velocity	41
14. \bar{G} (g) vs Gravity	43
15. Maximum Penetration vs Gravity: Modified Moore Equation	44
16. Typical Deceleration Traces: Ottawa Sand .	46
17. Normalized Penetration vs Time	48
18. Penetration vs Time: Al-2-F, 2.00 g, Number 5	49

List of Figures (cont)

Figure	Page
19. Deceleration vs Time: Al-2-F, 2.00 g, Number 5	50
20. Penetration vs Time: Al-2-F, 2.00 g, Number 6	51
21. Deceleration vs Time: Al-2-F, 2.00 g, Number 6	52
22. Penetration vs Time: Al-2-F, 1.00 g, Number 4	53
23. Deceleration vs Time: Al-2-F, 1.00 g, Number 4	54
24. Penetration vs Time: Al-2-F, 1.00 g, Number 5	55
25. Deceleration vs Time: Al-2-F, 1.00 g, Number 5	56
26. Penetration vs Time: Al-2-F, 0.38 g, Number 4	57
27. Deceleration vs Time: Al-2-F, 0.38 g, Number 4	58
28. Penetration vs Time: Al-2-F, 0.38 g, Number 3	59
29. Deceleration vs Time: Al-2-F, 0.38 g, Number 3	60
30. Penetration vs Time: Al-2-F, 0.17 g, Number 5	61
31. Deceleration vs Time: Al-2-F, 0.17 g, Number 5	62
32. Penetration vs Time: Al-2-F, 0.17 g, Number 2	63
33. Deceleration vs Time: Al-2-F, 0.17 g, Number 2	64
34. Mechanical Analysis Curve	86
35. Experimental Enclosure, Right-Front View . .	92

List of Figures (cont)

Figure	Page
36. Experimental Enclosure, Left-Front View . .	93
37. Experimental Enclosure, Back View	94
38. Experimental Enclosure, Interior View . . .	95
39. Compressed-Air Gun Schematic	99
40. Solenoid Trigger Schematic	101
41. Air Gun Performance Curves	104
42. Photograph of the A1-2-F Projectile	106
43. Schematic, Photo Diode Velocity Measurement	107
44. Sample Oscilloscope Trace	108
45. Wiring Diagram, High-Speed Photography Timing Circuit	111
46. Penetration in Crushed Basalt	133

List of Tables

Table		Page
I.	Maximum Penetration vs Gravity: A1-2-F, 1300 cm/sec	34
II.	Time-To-Complete-Penetration vs Gravity: A1-2-F, 1300 cm/sec	37
III.	Penetration Data: 2.00 g, Ottawa Sand. . .	75
IV.	Penetration Data: 1.00 g, Ottawa Sand. . .	76
V.	Penetration Data: 0.38 g, Ottawa Sand. . .	81
VI.	Penetration Data: 0.17 g, Ottawa Sand. . .	82
VII.	Deceleration-Curve Parameters, Type I Curves	83
VIII.	Deceleration-Curve Parameters, Type II Curves.	84

Abstract

The effects of gravity on the low velocity penetration of a projectile into Ottawa Sand are investigated in this study. A cylindrical aluminum projectile weighing 64.1 gm is fired at velocities in the range 800-1500 cm/sec into a bed of Ottawa Sand at gravity levels of 0.17, 0.38, 1.00, and 2.00 g. Maximum penetrations are compared at these levels. An inverse relationship is found between maximum penetration and gravity.

Terrestrial soil penetration equations are discussed and compared with the data from the experiment. A method to transform a terrestrial equation into an equation valid at gravity levels in the range of the experiment is suggested.

Deceleration traces are produced by computer from penetration-time data that is fit with a least-squares polynomial and mathematically differentiated. Double-peaked curves result at all gravity levels. Trends in properties of the curves are discussed.

Recommendations are made for further work in the area.

GRAVITY EFFECTS ON LOW VELOCITY PENETRATION
OF A PROJECTILE INTO A COHESIONLESS MEDIUM

I. Introduction

Low velocity penetration of projectiles into soil targets is interesting for several reasons. Early interest was aroused by the invention of artillery and the subsequent desire to protect men and structures with earth embankments. Modern interest has grown with the possibility that the soil penetration event might be used to determine the in situ properties of remote soils (Ref. 1,4,7,14,20,21,26). The remote penetrometer concept is considered applicable to interplanetary soil testing (Ref. 20:2) but the effects of a different gravity on the theories involved have not yet been experimentally demonstrated.

Purpose and Scope

The purpose of this investigation was to determine the effects of gravity on the maximum penetration resulting from a low velocity projectile impacting a cohesionless soil target. The choice of a cohesionless medium (Ottawa Sand) for the target was made because this is perhaps the easiest soil to control in an experimental environment. The basic experiment was designed to produce identical penetration events over a range of gravities which included the values 0.17 g, 0.38 g, 1.00 g, and 2.00 g, where g is the magnitude of gravitational acceleration on the Earth.*

* g on the Earth is 981 cm/sec^2 , at 45° latitude and at sea level

The ideal experiment would keep all other parameters of penetration perfectly constant while allowing gravity to vary in a controlled manner. Any changes observed in the maximum penetrations from one g level to another could then be attributed to the influence of gravity. A literature search was conducted to determine some parameters that were known functions of gravity, and extensive testing was done in the laboratory to determine the effects that other parameters had on maximum penetration.

Gravity simulation was accomplished aboard a KC-135A aircraft which flew controlled parabolic maneuvers (Ref.13). The desired gravity simulation was attained over the top of these maneuvers and the level attained depended on parabolic eccentricity. The use of the aircraft placed stringent limitations on the design of the experiment which are outlined in Section IV of this paper. The basic limit was on the size of the bed of sand. This, in turn, dictated the projectile mass and impact velocity that could be used.

In these experiments a cylindrical aluminum projectile weighing 64.1 grams was fired at a velocity of from 800 to 1500 cm/sec into the sand bed. The projectile which was flat-nosed, had a length of 33 cm. and a diameter of 1.27 cm.

Pre-impact projectile velocities for the air-borne experiments were determined by post-shot measurements made on successive frames of high-speed motion picture film. Because these films were available, it was possible to

determine penetration-time plots from them for each shot fired.

Deceleration-time traces from other experiments are available for impacts in soil in a 1 g environment (Ref. 4, 21,26) but possible effects of gravity on such traces have not been experimentally demonstrated. In theory, a least-squares polynomial fit could be made to the penetration-time data of this experiment and the result twice-differentiated to obtain deceleration-time curves.

The usual procedure in other experiments had been to place accelerometers in the noses of projectiles and to photograph an oscilloscope display of their response to impact. The deceleration-time plots thus obtained are integrated to obtain velocity-time and penetration-time plots. In this experiment a more difficult method was used. Curves were fitted to penetration-time data points and then twice differentiated to obtain deceleration time plots. The method was unproven, but was used anyway because of the lack of any such curves at gravity levels other than 1 g.

Method of Attack

The report begins with a section on attempted derivations of soil-penetration equations. This is followed by a discussion of soil properties that have been shown to be functions of gravity. The experiment and its results are presented in the next two sections. The final section contains conclusions drawn from the experimental results and makes recommendations for further work in the area.

II. Factors Affecting Soil-Penetration on Earth

A terrestrial soil-penetration is a function of many variables. The number of variables is the greatest reason why no purely analytical solution to the problem is currently available. Empirical solutions exist and the effects of easily isolated variables are quite well known. The most easily isolated variables are the characteristics of the penetrator and the energy that the penetrator delivers to the soil. The variables that are difficult to isolate and control are the properties of the target soil itself.

Historical Background

Semi-analytical Approaches. Early attempts at developing soil-penetration equations started with Newton's equation of motion in the form

$$Mg - F = Ma_p \quad (1)$$

where M = mass of a projectile and the soil traveling with it.

g = acceleration due to gravity

F = soil resistance force

a_p = projectile acceleration

(ref. 28:2)

From this point, most early investigators neglected the gravity force and the mass of soil traveling with the projectile and redefined Eq. (1) as

$$F = -M_p V \frac{dV}{dz} \quad (2)$$

where M_p was the mass of the projectile, V was velocity, and z was the depth the projectile traveled into the target.

The functional form of the soil resistance force was then assumed. Under the assumption that the soil target was homogeneous mass, considerations of fluid dynamic drag yielded a resistance force (Ref. 7) of the form

$$F = a + bV + cV^2 \quad (3)$$

where a , b , and c were constants. Various formulas for maximum penetration resulted from different assumptions about the constants.

One of the most widely used equations of this form was that of Jean Poncelet as discussed by Young (Ref. 28). He assumed a soil resistance force

$$F = f_1(z) f_2(V) \quad (4)$$

where

$$f_1(z) = kA$$

$$f_2(V) = a + bV^2 \quad (A = \text{cross-sectional area})$$

in which a , b , and k were constants. The resulting equation for maximum penetration was

$$P_m = \frac{W}{2Abk} \ln \left[\frac{1 + bV_o^2}{a} \right] \quad (5)$$

Where

P_m = maximum penetration

W = projectile weight

V_o = impact velocity

Investigators have since worked with the Poncelet equation in attempts to evaluate the constants for different soils and soil conditions. In 1910, Petry (Ref 28) experimentally evaluated the constants and developed an equation that has since been used extensively. The equation was of the form

$$P_m = \frac{W}{A} K \log_{10} \left[1 + \frac{V_o^2}{215,000} \right] \quad (6)$$

where K was a constant which described the penetrability of the soil target.

A recent innovation to the form of the soil resistance force was the assumption by H. J. Moore (Ref. 20) that the force was proportional to the confining pressure on the soil.*

Moore developed an equation to predict maximum penetration by integrating the resistance force, $F = Kpgz$, to a depth, P_m , and equating the resulting work to the kinetic energy of the projectile at impact. (See Appendix E.) The equation was

* Confining pressure varies with depth, soil density, and gravitational acceleration. It is defined by the expression $P = pgz$, where P is confining pressure, p is soil density, and z is depth into the soil. (See Ref. 24:184-200.)

$$P_m = K' \left(\frac{\rho_p}{\rho} \right)^{\frac{1}{2}} \left(\frac{L}{g} \right)^{\frac{1}{2}} V_o \quad (7)$$

where ρ_p = projectile mass density
 K' = a constant
 L = projectile length

Moore's equation has been shown (Ref. 20:44) to give good fit to a set of low velocity penetration data obtained by Sandia Laboratories (Ref 29).

The dependence on gravity and soil density, evident in Moore's equation, was a change from the semi-analytical equations previously discussed. The dependence on gravity in these other equations was usually found in the weight of the projectile, while dependence on soil density was hidden in the various constants.

Discussion. The thing that has prevented a completely analytical solution to the problem has been lack of knowledge of the exact form of the soil resistance force. If this form were known and if it were integrable over the depth of penetration, Eq. (1) would yield an exact solution. (See Appendix E.)

Empirical Approaches. C. W. Young (Ref. 28) of Sandia Laboratories has developed a completely empirical equation. His basic assumption was that the correct form of the equation was

$$P_m = f_1(N) f_2(A) f_3(W) f_4(V) f_5(S) \quad (8)$$

where

N = projectile nose-performance

coefficient

A = frontal area

W = projectile weight

V = velocity

S = soil constant or function

The results of more than 200 full-scale earth penetration tests were used by Young to evaluate the five functions of Eq. (8). The resulting equation was (for velocities less than 200 feet per second)

$$P_m = 0.53 SN \frac{W}{A}^{\frac{1}{2}} \ln(2V_o^2 \cdot 10^{-5} + 1) \quad (9)$$

Soil Properties. Little work has been done to isolate the effects of specific soil properties on the penetration process. Nearly all existing equations lump soil properties into a constant or function. The Moore equation (Eq. (7)) is an example that shows explicit dependence on soil density. An equation attributed to Nara and Chem (Ref. 11) shows dependence on both density and angle of internal friction. This equation is

$$P_m = \frac{M}{2Ab} \ln \left[\frac{\frac{M}{2Ab} \rho g N_q + 0.6 \rho g N_f R_f + b V_o^2}{\frac{M}{2A_b} \rho g N_q + 0.6 \rho g N_f R_f + \rho g N_q P_m} \right] \quad (10)$$

where

R_f = frontal radius of projectile

b = a constant

N_q, N_γ = bearing capacity factors (functions of angle of internal friction)

Though it is not experimentally or analytically proven, one must expect the shear modulus of a soil to have an effect on maximum penetration since the primary mode of failure in soils is most often shear. This is especially true of granular soils (Ref. 22:14).

The dynamic nature of the problem should make it dependent on compressional and shear wave velocities as well.

Conclusions. The following general conclusions can be stated:

1. Maximum penetration is proportional to projectile mass and inversely proportional to cross-sectional area.
2. Maximum penetration is proportional to the impact velocity of the projectile.
3. Maximum penetration is inversely proportional to soil density.
4. Maximum penetration is affected by the shape of the nose of the projectile.
5. Maximum penetration can be related to different soils through a constant or function which is dependent on the properties of the soils. The soil properties which make up this constant or function are not completely known.

III. Gravity Effects on Soil Properties

Soil properties are the only parameters that will be altered when a penetration takes place at a different gravity level. The characteristics of the projectile are fixed, and the energy that the projectile brings to the target is fixed (neglecting potential energy). Changes in maximum penetration can, therefore, be attributed to changes in the properties of the soil. Some soil properties are known to be functions of gravity. They are discussed in this section.

Shear Strength

The yield strength of a cohesionless medium is the shear strength of the material because shearing is the primary mode of failure. The shear strength on any plane in a cohesionless medium is directly proportional to gravity (Ref. 13:9).

Shear Modulus

The shear modulus of a material is defined as the ratio of shear stress to shear strain (Ref. 6:129). The shear modulus of Ottawa Sand has been shown (Ref 8) to be a function of gravity. Figure 1, on the following page, is a graph of the variation of shear modulus with gravity for Ottawa Sand from B. O. Hardin (Ref. 8).

Compressional Wave Velocity

Compressional waves are developed in cohesionless media by penetration events. They seem to be important to the

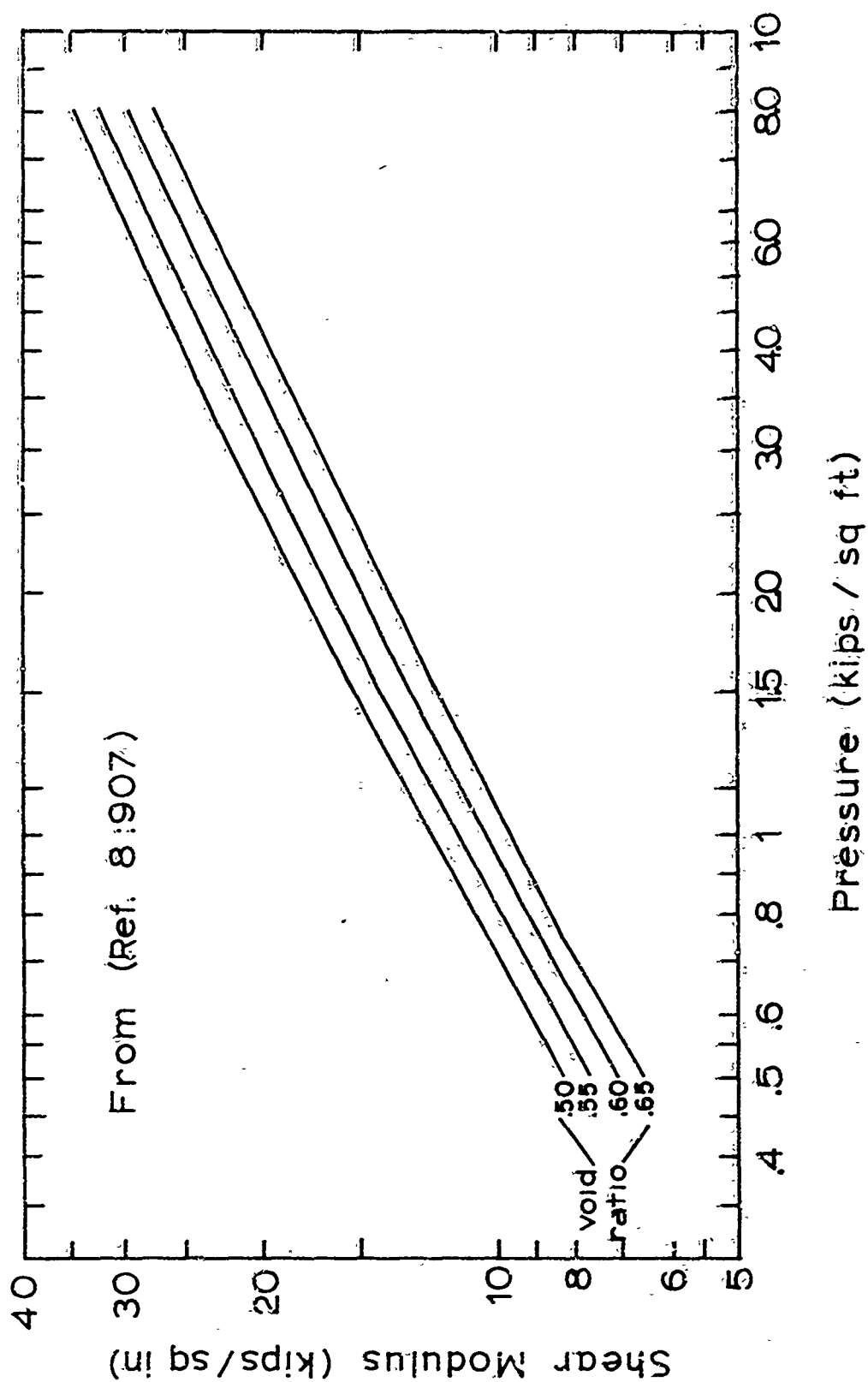


Figure 1. Shear modulus vs Confining pressure.

process (Ref. 3). Allen, Mayfield, and Morrison, in experiments with Ottawa Sand, noted that the drag coefficient changed abruptly as the velocity of the projectile in the sand reached the compressional wave velocity of the surrounding matter. This indicated two different regions of penetration that were described by different equations. The variation of compressional wave velocity with gravity (confining pressure) is shown in Figure 2 on the following page.

Velocities in this work remain below the compressional wave velocity of the Ottawa Sand at all times.

Other properties of the sand are not expected to vary with gravity. Mass density, water content, and void ratio certainly will not. (See Appendix B).

Previous Gravity Work

The effects of gravity on results in other experiments involving dynamic-loading of cohesionless media have been reviewed. The effects on simulated meteorite impact craters were studied by Smith and Franklin (Ref. 22). Moraski and Teal (Ref. 19) used deflagrating explosives to study cratering in Ottawa Sand at different depths of burst over a range of gravities. Victorov and Stepenov (Ref. 25) used accelerated frames to vary gravity while studying cratering in moist sand at 1, 25, 45, and 66 g. The results of the first two experiments gave a range of dependence which increased as the scaled depth of burst of the explosive increased. The dependence noted by Victorov and Stepenov was slightly less.

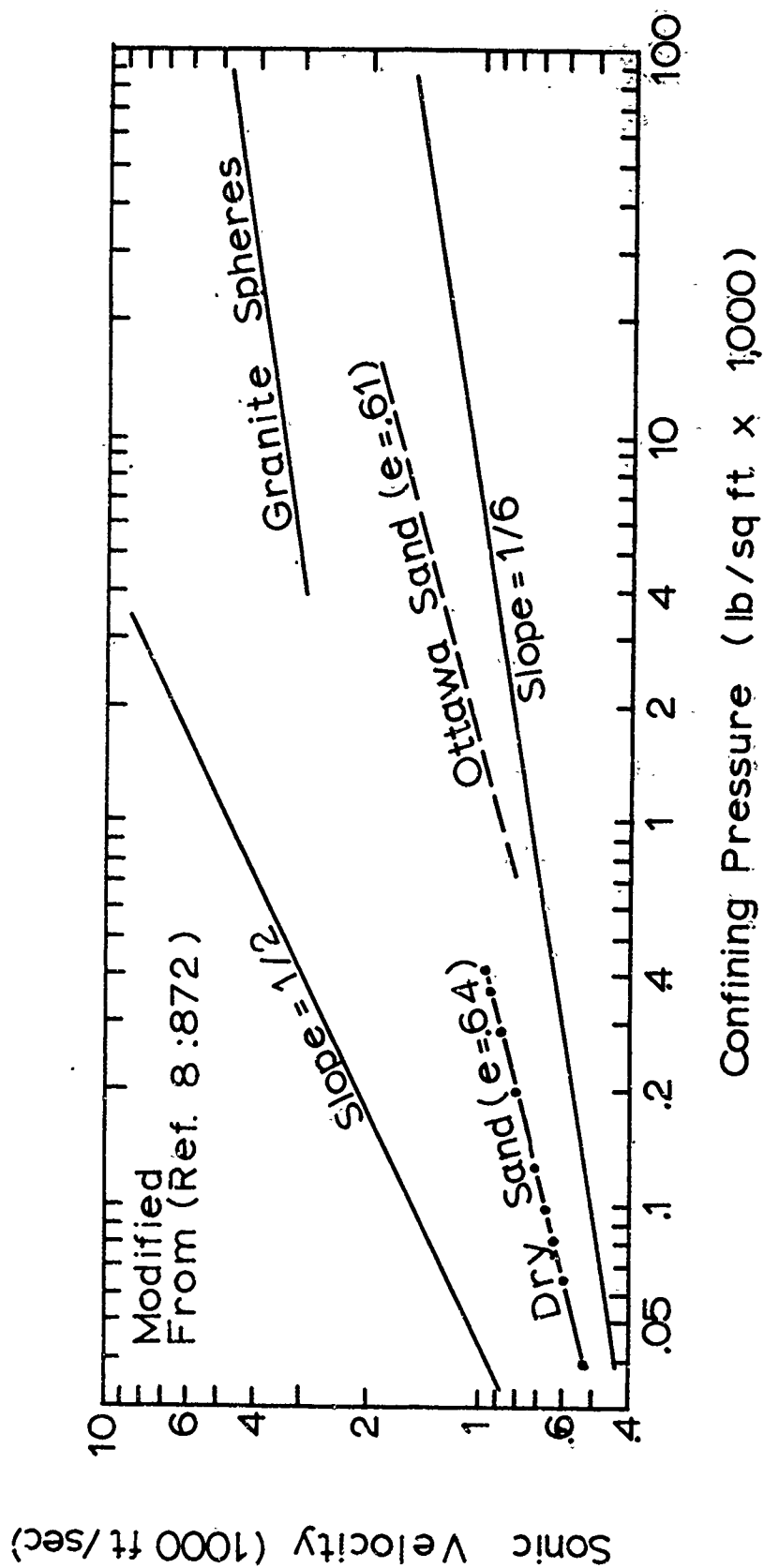


Figure 2. Sonic velocity vs. Confining Pressure.

Figure 3, page 15, is a log-log plot of crater diameter versus gravity at a one inch scaled depth of burst as determined by Moraski and Teal. The range of slopes from their experiment was from -0.11 to -0.16, varying with scaled depth of burst.

Lynch and Higgins (Ref. 13) performed bearing capacity tests on Ottawa Sand at varying gravity levels and found that bearing capacity increased with gravity. Their experiment used very small loading rates and may have been a static-loading problem.

The Russians I. I. Cherkasov, et al (Ref. 5) discussed the results of a soil penetrometer experiment aboard the automatic lunar station Luna 13. They determined that penetration would increase with decreased gravity such that a penetrometer would penetrate 1.7 times deeper on the lunar surface than on the earth.

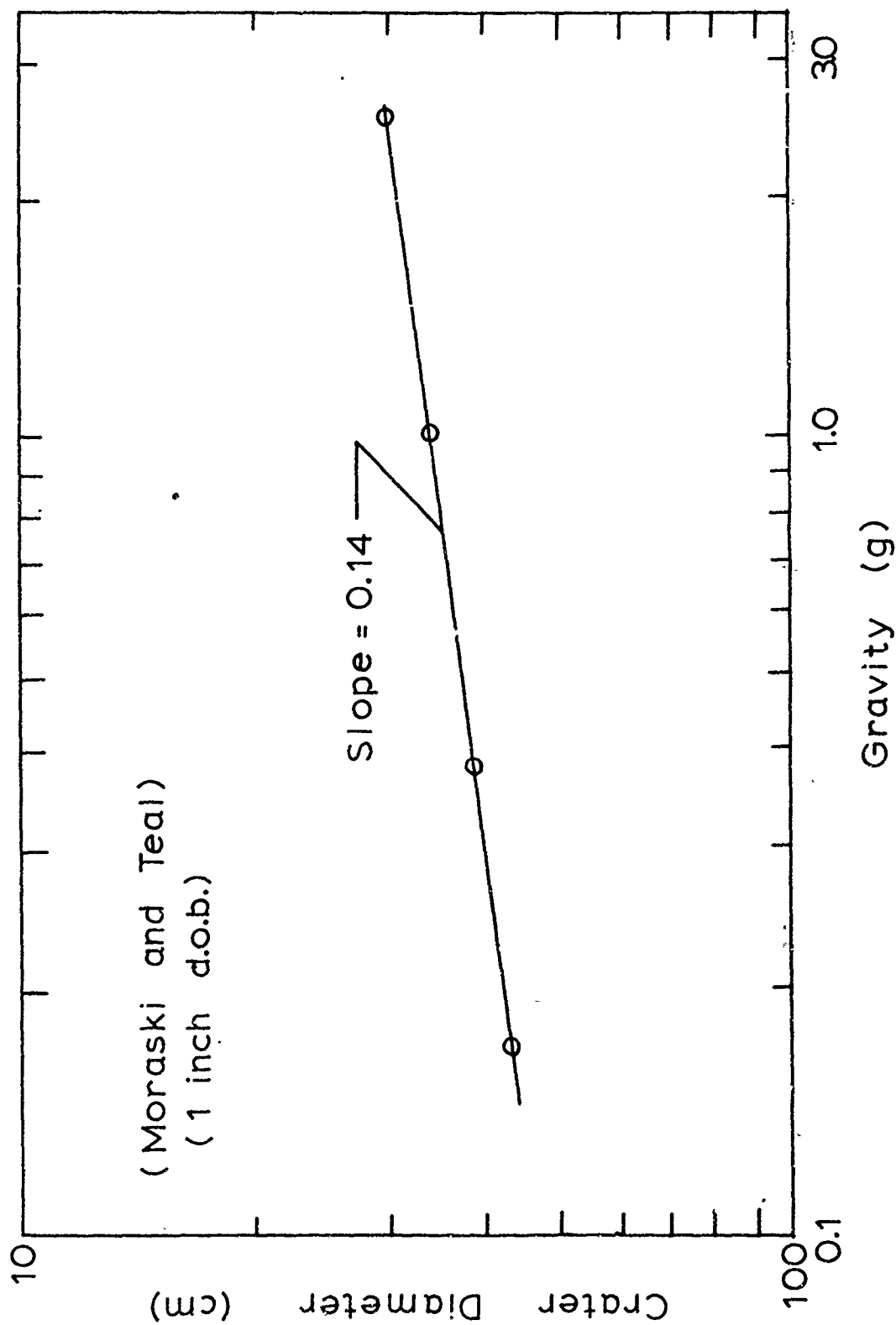


Figure 3. Crater diameter vs Gravity.

IV. Description of the Experiment

Based primarily on the previous two sections of this paper, an experiment was designed and performed to determine the effects of gravity on maximum penetration in Ottawa Sand. A general description of the experiment is given in this section.

Materials

The primary material in the experiment was Density Sand, CN-501, obtained from Soiltest Corporation, Evanston, Illinois. It was used as a representative cohesionless medium because of its lack of moisture, its stable void ratio, and its cleanliness. These properties are detailed and discussed in Appendix B.

Compressed air was used as the propellant to produce impact velocities. It was stored in a standard 2000 psi pressure bottle.

Equipment

A detailed description of all equipment is found in Appendix C. It basically consisted of an air gun which fired projectiles at measured velocities into a bed of sand. Additional equipment consisted of firing circuitry and velocity measurement systems.

The basic projectile configuration was an aluminum cylinder with a flat nose. The basic impact velocity was about 1300 cm/sec.

Gravity simulation was obtained aboard an aircraft

which flew controlled parabolic maneuvers.

Test Aircraft. The aircraft used to provide gravity simulation was a United States Air Force KC-135A, operated by the Directorate of Flight Test, Aeronautical Systems Division, Wright-Patterson AFB, Ohio. It flew parabolic maneuvers during which the values of 0.17, 0.38, and 2.00 g were attained with an accuracy of plus or minus 0.01 g. The average duration of the altered gravity condition was about 30 sec, except for the 2.00 g maneuvers which lasted about 10 seconds.

The requirements and limitations presented by this aircraft were largely responsible for the design of equipment and procedures.

The experimental package was limited in size by the dimensions of the fuselage of the aircraft and the size of the cargo hatch through which it had to be loaded.

Sand particles could not be allowed in any of the electrical or mechanical equipment within the fuselage, so the target bed had to be completely contained. All equipment and instrumentation had to be braced so that nothing would tear loose under a load of 16.00 g along the roll axis of the aircraft. Vibrations were present which required that the equipment be designed as simple and durable as possible. Simplicity and durability were also important because the experimental package was transported to and from the aircraft by a forklift.

It was important in these tests that the manipulative

effort required of the experimenter be minimized. This was because the parabolic maneuvers of the aircraft are difficult to adjust to and often produce nausea. Although one becomes accustomed to the experience with time, true comfort is impossible. The detrimental effects on the experimenter of performing in an environment with rapidly changing g values were anticipated and the experimental procedure was simplified as much as possible.

Plywood Enclosure. Safety requirements dictated that sand particles could not be allowed in the fuselage of the aircraft. A plywood container for use in aircraft-borne experiments had been constructed previously (Smith and Franklin, 1967; Moraski and Teal, 1965). The same container was adapted for this work. It contained all of the equipment with the exception of the compressed air supply line, gauges and valves; the solenoid triggering circuit; and the camera equipment. (See Appendix C.)

Air Gun. The air gun used to fire the projectiles was designed and constructed at the Air Force Institute of Technology. (See Appendix C.) It was basically a pressure chamber that was sealed only when a projectile was held in the barrel.

Triggering was done electrically with the pull of a solenoid. This method was used because a nearly constant trigger pull was needed for consistency in the velocities produced at a given chamber pressure (Ref. 23).

Projectiles. The projectiles were cylindrical in

general shape and were constructed from either aluminum bar stock or tubing. Replaceable noses were made for each of the projectiles, one flat and the other hemispherical. Four basic configurations were thus possible and were designated Al-1-F, Al-1-R, Al-2-F, and Al-2-R. Al-1 referred to the heavier body (made from bar stock) and Al-2 referred to the lighter body (made from tubing). The final F or R denoted the flat or the round nose. Al-1-F and Al-1-R weighed 90.9 gm. Al-2-F and Al-2-R weighed 64.1 gm.

Al-2-F proved to be the projectile which penetrated the least at a given impact velocity in the laboratory. For the remainder of this paper, references to the basic projectile will be references to the Al-2-F configuration.

Target Bed. The size of the box which held the sand target was chosen to negate boundary effects. The upper limit on its size was the space available within the enclosing box, with reductions made for the space to be occupied by the air gun and other equipment. The dimensions were determined during preliminary testing by trying sand beds of graduated size. A small bed was penetrated initially and progressively larger beds were tried until no apparent change was observed in the maximum penetration of the basic projectile at 1300 cm/sec. This occurred with a cubical container that was 36 cm on each side. More penetration was expected at lower gravities, so an arbitrary factor was incorporated, bringing the dimensions of the box up to 61 cm on each side.

The container for the sand was made of plywood. It was laid on the floor of the enclosing box and securely braced.

Procedures and Conduct

Measurement of Impact Velocity. There were two methods used to measure impact velocities. The simplest method recorded the time that the falling projectile shaded a photo diode from a point light source. This time was used to calculate an average velocity over a drop equal to the length of the projectile.

The more complicated method used high-speed photography. The film speed was monitored to give a time base, and a grid was pre-exposed onto each frame of film for a distance scale.

The results of the two methods were compared and found to give approximately equal velocities. The methods were incompatible because of the intense lighting required for the high-speed camera and could not be used together. However, given pressure settings produced equal velocities as measured by the two methods.

The photo diode method was used for nearly all of the preliminary laboratory testing. The high-speed camera was used for all tests aboard the aircraft.

Measurement of Maximum Penetration. Maximum penetration was measured in two ways. One method was used on all tests. It used a scale graduated in millimeters to determine how much of the projectile remained above the surface

of the sand after penetration was complete.

When high-speed photography was used to measure impact velocity, the penetration could be read directly from the exposed film by noting the positions in the grid of the back of the projectile at impact and when penetration was complete. Maximum penetration was the difference between the two positions, since the projectile was assumed not to deform during the event.

When measurements were made for the same shot with both methods, values were never found to vary more than 0.25 cm.

Preliminary Testing. Extensive ground testing was done to determine the optimum container size for the target bed, the maximum velocity that could be stopped by this container size, chamber pressure-velocity curves for the air gun, the best method of target preparation, and the effects on maximum penetration caused by varying certain parameters at 1.00 g in the laboratory.

Calculations showed that the two feet of free fall of the projectile at different gravity levels would not cause the impact velocity to vary appreciably. Since this was the case it was possible to get an almost constant impact velocity over a series of impacts by only once adjusting the pressure in the gun chamber to a predetermined value.

Tests by other persons (Ref. 17) had indicated that target preparation was extremely important for consistent data. Each penetration caused a crater to form and greatly

disturbed the sand around the impact point. To prepare the target bed for the next shot, it was found that the following procedure gave the best results:

1. The projectile was taken out of the sand.
2. The crater which remained was filled with fresh sand, piled to a height of about 10 cm above the normal surface of the sand bed.
3. The mound of sand was slapped and remounded 25 times with a flat aluminum striking plate.
4. The surface was scraped level.

Since a great deal of vibration was known to exist aboard the aircraft (Ref 22), and since vibrations would tend to settle the sand bed to its densest state, this densest state was the goal of the procedure described above. The density of the sand was not expected to change more than five percent (see Appendix B), but the effect of such a change on the dynamic properties which were known functions of density (Section III) was not certain.

Time had to be conserved aboard the aircraft because of the expense involved in flying and the difficulties encountered in trying to schedule flying time. A definite sequence of tasks was developed and practiced on the ground for this reason. All camera related tasks were assigned to a photographic assistant. Preparation of the air gun, projectiles, and sand bed was divided into the following tasks which were performed by the author:

1. The target bed was prepared and leveled.

2. The projectile was chambered in the air gun.
3. The sequence card was placed in the card clip to identify the next shot. Information of the card included the projectile, the chamber pressure, the gravity level, and the sequence number.
4. The pressure chamber was charged to the correct pressure and the shut-off valve was closed.
5. The box was shut and the access door latched.
6. The firing cycle was initiated.
7. When the firing cycle was complete, the door was opened and the penetration was measured with the scale.
8. The routine was repeated from step 1.

In the laboratory, the procedure required about three minutes to complete. This was less than the time it took the photographic assistant to clean and reload the camera. Total time for one shot in the laboratory was therefore about five minutes.

The same basic procedure was followed aboard the aircraft. The only important addition resulted from the fact that the aircraft commander monitored the accelerometers in the cockpit and had to inform the researchers in the back when the gravity level had been reached. He did this by giving the command, "Release", over the internal communications system. Step 6, triggering of the firing cycle, was held until this command was heard.

Aircraft Environment. The cabin pressure in the aircraft was kept at about 634 mm Hg. This was the same for

all flights. Some lag existed during the parabolic maneuvers but is probably insignificant and is neglected in this report. The temperature in the cabin was kept at approximately 60 degrees Fahrenheit.

Because of the difference in ambient pressure between the aircraft and the laboratory, a number of shots were fired in level flight for comparison with the laboratory tests. The inaccuracies resulting from the lack of precise control of gravity in level flight are ignored.

Quantity of Data. A total of 105 penetrations were recorded at 1.00 g, 7 in level flight, and 98 in the laboratory. 27 usable shots were fired aboard the aircraft at different gravity levels.

All of the data at 0.38 g was taken on the first flight. Data at 0.17 and 2.00 g were taken on the three following flights. Shots in level flight were fired on each flight. The data from all recorded penetrations are tabulated in Appendix A.

V. Presentation and Discussion of Results

In this section, the results of the experiment are presented and discussed. The three phases, in order of appearance, are laboratory test results, gravity test results, and deceleration-time curve results.

Laboratory Test Results

Testing was done in the laboratory to learn as much as possible about the soil penetration event. Many shots were fired only to help in organizing the work to be done aboard the aircraft. Most of these shots were spent in the development of a procedure for repairing craters in the sand bed (Section IV). Others were used to obtain chamber pressure-velocity curves for the air gun. (See Appendix C.)

Data on both maximum penetration and impact velocity were taken for 105 shots at the 1.00 g gravity level, 98 in the laboratory, and 7 in level flight aboard the aircraft. 14 shots at 1.00 g were recorded on high-speed film.

There seemed to be a significant difference between the sample means of the maximum penetrations in the laboratory and the maximum penetrations in level flight. The sample mean of the laboratory penetrations with the basic projectile configuration at an impact velocity of 1300 cm/sec was 11.9 cm with a standard deviation of 1.50. For this reason, the 7 shots at 1.00 g in level flight were used exclusively for comparison with shots fired at the different gravity levels obtained in flight.

The difference noted between laboratory and level-flight penetrations can possibly be explained by listing the variations in experimental environment. The most obvious difference was in ambient pressures. The cabin pressure maintained aboard the aircraft was less than laboratory ambient pressure by about 120 mm Hg. The confining pressure on a soil element at a given depth in a bed of cohesionless sand will be a function of the pressure at the surface of the bed. The effects of confining pressure on dynamic soil properties have been indicated in a previous section. Reduced ambient pressure would imply reduced confining pressure and penetrations would be expected to increase. It is doubtful, however, that such a small decrease in ambient pressure would be enough to cause the differences in penetration observed in this work.

Changes in the void ratio of the target bed could definitely have occurred between the laboratory and the aircraft, but the changes should have densified the sand and caused less penetration.

Level flight in the aircraft cannot be a controlled gravity maneuver, and it is conceivable that slight pockets of less dense air were encountered by the aircraft during the shots. Such pockets would cause the aircraft to drop and produce a condition of lowered gravity.

All measurements of impact velocity were made from high-speed film for the shots aboard the aircraft, but the majority of laboratory velocities were measured with the

photo diode circuit. There may have been a consistent difference in impact velocities that was not noticeable in the two measurement systems.

In the laboratory, the characteristics of the projectile and the impact velocity were varied in attempting to correlate observed maximum penetrations with the predictions of existing equations.

Nose-Performance Coefficients. The change in maximum penetration between a flat-headed and a round-headed projectile, with all other parameters held constant, was found to be different than was predicted by Young (Ref. 28:16). Young determined a factor of 0.56 for a flat-headed projectile and 0.72 for a round headed projectile, based on a bullet-shaped, 9.0 CRH tangent ogive nose with a value of 1.00.

Shots 54 through 73, in Table IV, Appendix A, were used specifically to check this variation. The mean penetration of Al-2-R in shots 54 through 63 was 12.3 cm, that of Al-2-F in shots 64 through 73 was 11.5 cm. Assuming that all other parameters in the Young equation were constant, the soil constant required that the nose-performance coefficients for the flat-headed and round-headed projectiles be 0.60 and 0.65 respectively.

The data from which Young extracted his values was from penetrations with projectiles three inches in diameter, much larger than the diameter of Al-2-R and Al-2-F. The importance of differences in nose shape seems to decrease

as the body diameter of the projectile decreases.

Soil Constants. The soil constants for the Petry, Moore, and Young equations (Eqs. (6), (7), and (9)) were determined from the observed penetrations of the basic projectile at an impact velocity of 1250 cm/sec. Each equation was forced to predict the sample mean of 11.9 cm with all parameters except the soil constant either known or assumed. The constants were the following:

$$\text{Petry } -K = 0.281 \text{ (cm}^3/\text{gm)}$$

$$\text{Moore } -K' = 0.0017(\text{sec}/\text{cm}^{\frac{1}{2}})$$

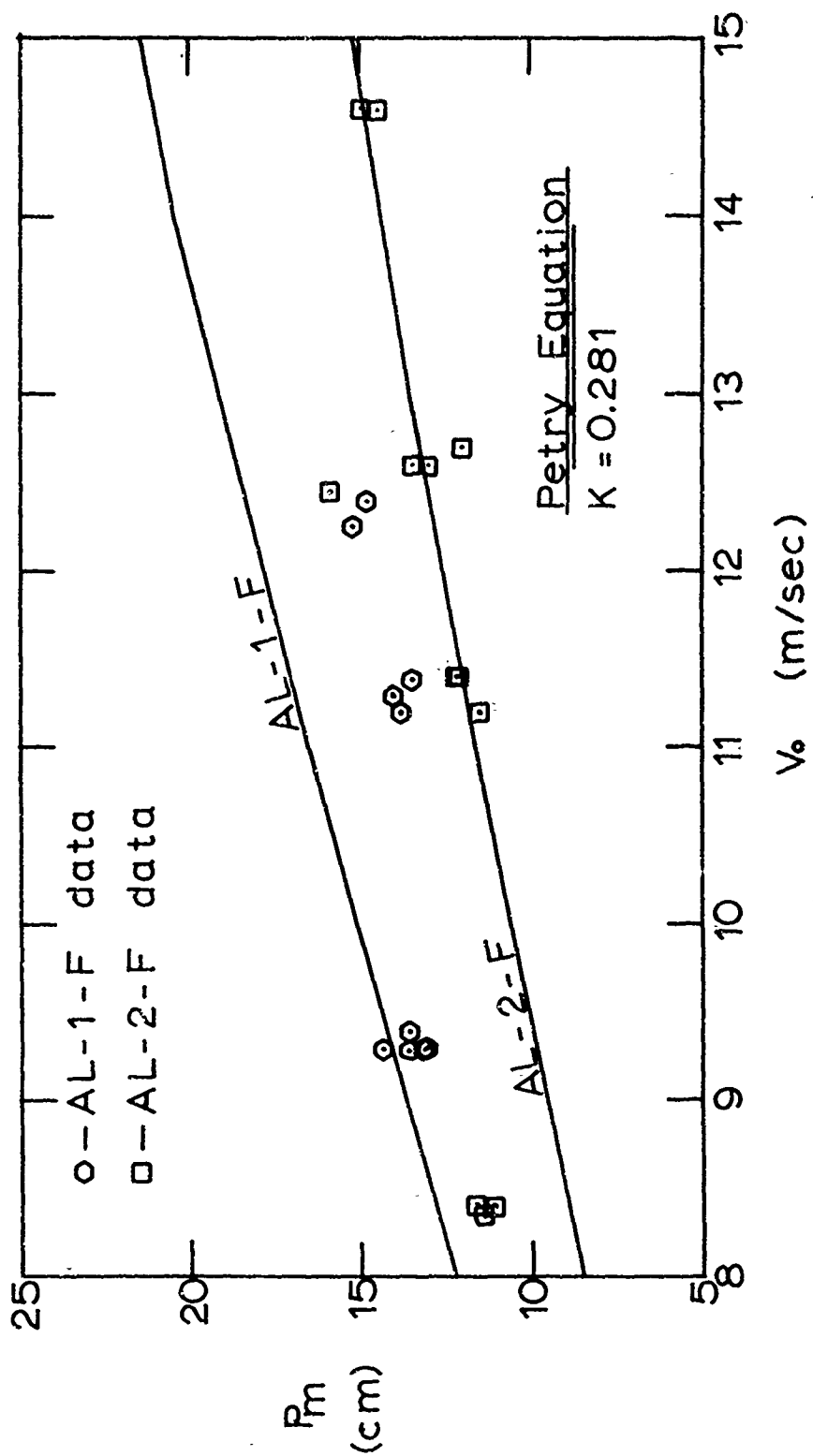
$$\text{Young } -S = 1.70 \text{ (dimensionless)}$$

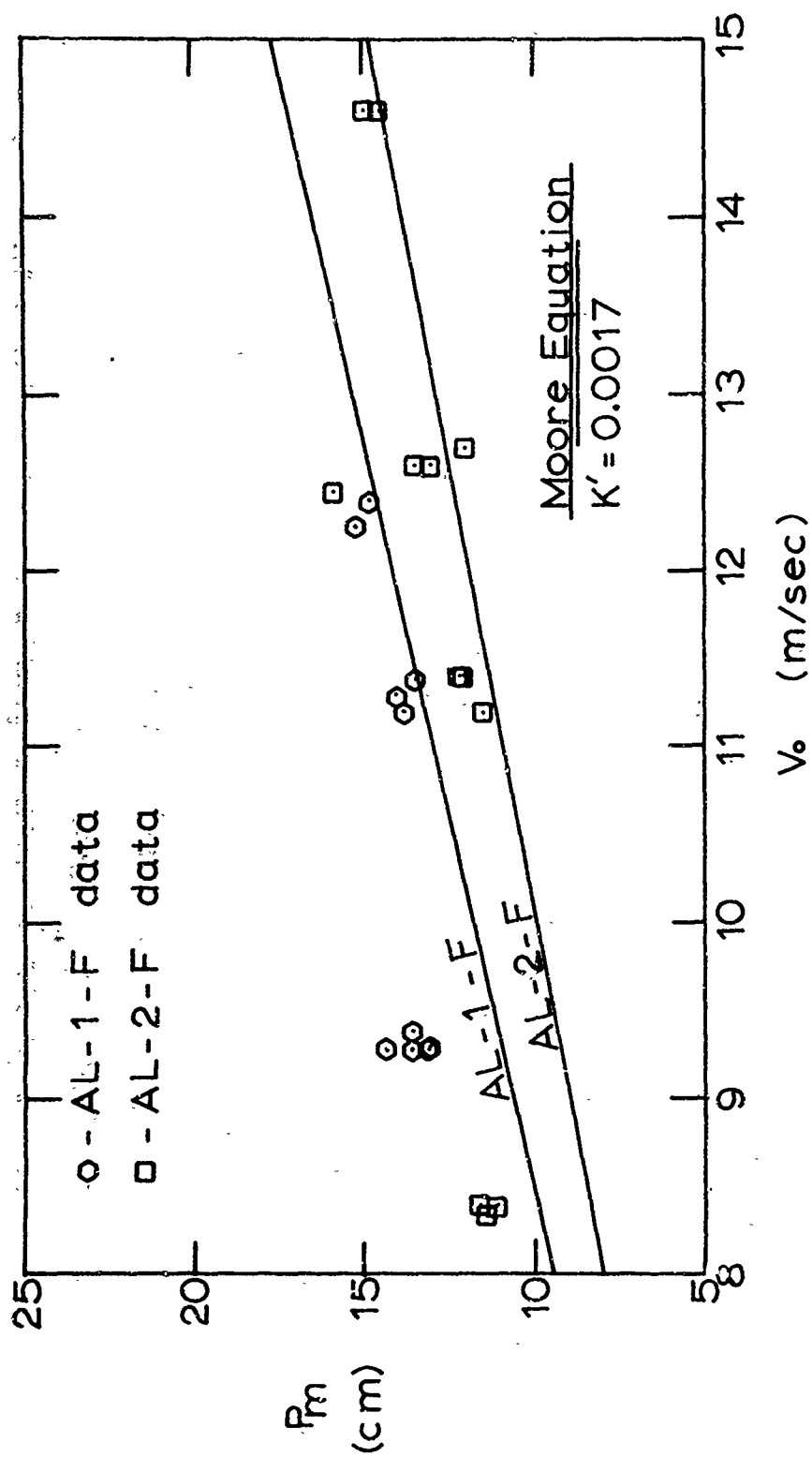
The Nara equation (Eq. (10)) was also solved for the value of its constant using the same data. Solution by computer was required, and the value of b was found to be 0.001 gm/cm³.

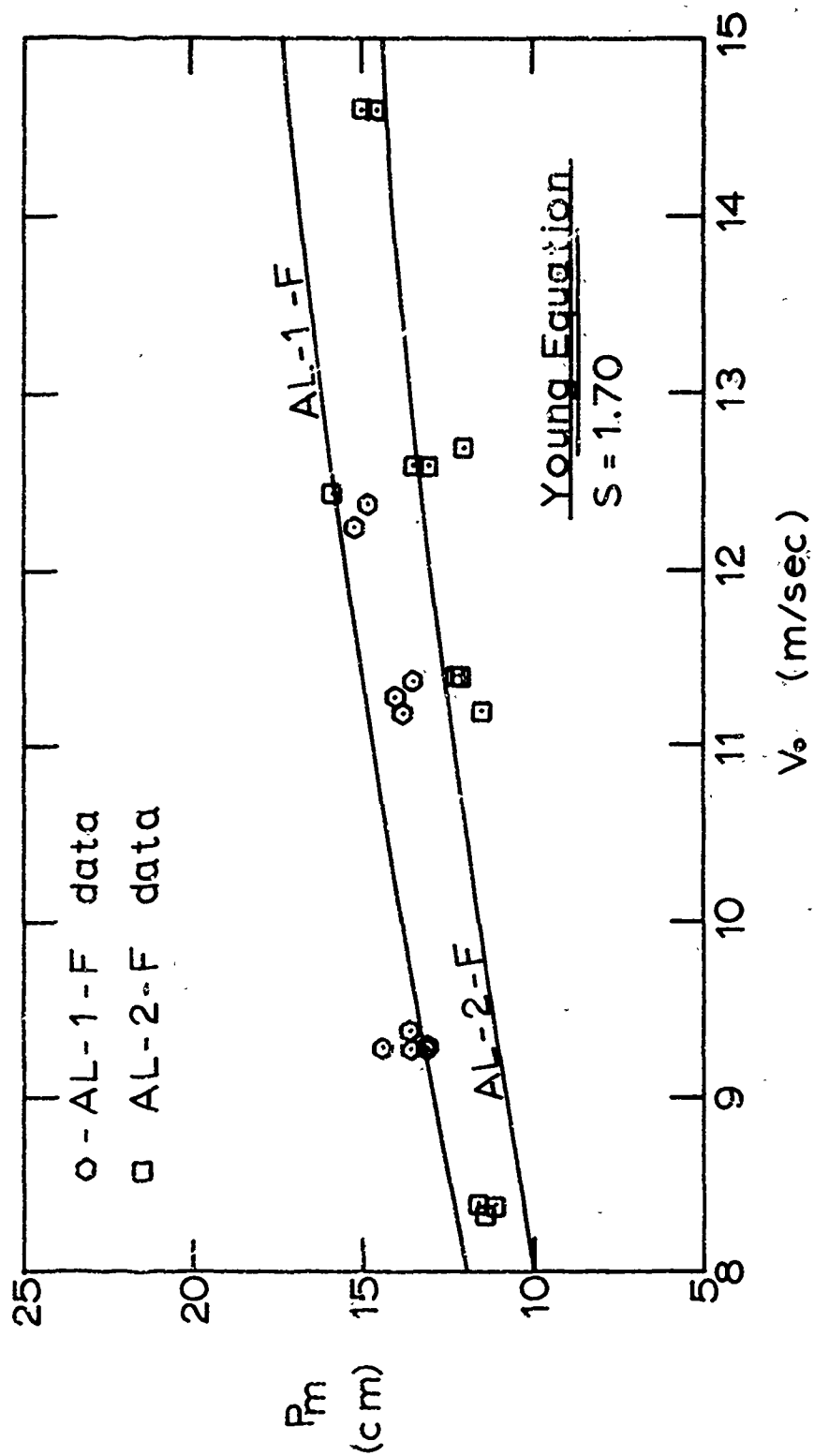
With these values of the soil constants, the equations were plotted over a range of impact velocities and the data from shots 31 through 53 were plotted against the resulting curves. The graphs are found in Figures 4, 5, 6, and 7 on the following four pages. Shots 31 through 53 include data from both A1-1-F and A1-2-F penetrations. They differ only in projectile mass, so curves for each mass are drawn for each of the four equations.

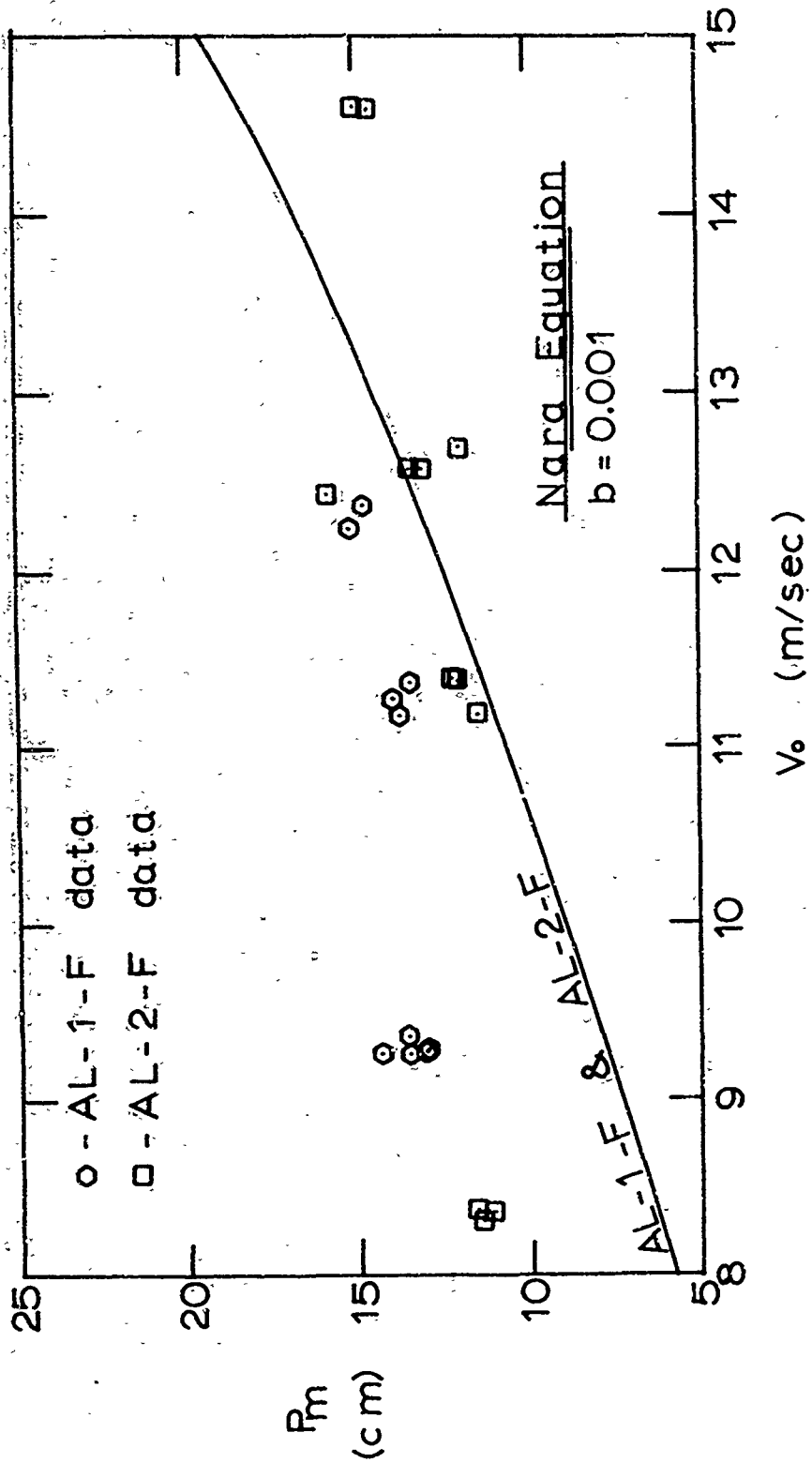
Gravity Testing

In the section on laboratory testing, it was pointed out that a difference was noted between the maximum

Figure 4. P_m vs V_0 , 1.00g Data vs Petry.

Figure 5. P_m vs V_0 , 1.00g Data vs Moore.

Figure 6. P_m vs V_o , 100g Data vs Young.

Figure 7. P_m vs V_0 , 1.00g Data vs Nara.

penetrations of 1.00 g shots with the basic projectile in the laboratory and 1.00 g shots with the same projectile during level flight. 1.00 g shots, 1 through 7 only, are included in this section. In this way, the factors that caused the difference in penetration should act on each shot aboard the aircraft and not mask variations due to gravity.

Cratering. A crater was formed in the sand with each penetration. Although measurements were not made, crater dimensions seemed to increase with decreasing gravity. The high-speed films showed that the crater in each shot did not begin to form immediately at impact, but that formation was delayed a significant time. It appeared that the projectile had nearly come to rest before a noticeable amount of ejecta was thrown from the forming crater.

Maximum Penetration Versus Gravity Level. Time and scheduling difficulties restricted the amount of data that could be taken at different levels of gravity aboard the aircraft. For this reason, the basic projectile, A1-2-F, at an impact velocity of 1300 cm/sec was the only arrangement that was tested at each gravity level enough times to draw statistical conclusions about the resulting penetrations. The following table is a collection of the penetrations used to obtain results indicated in this section:

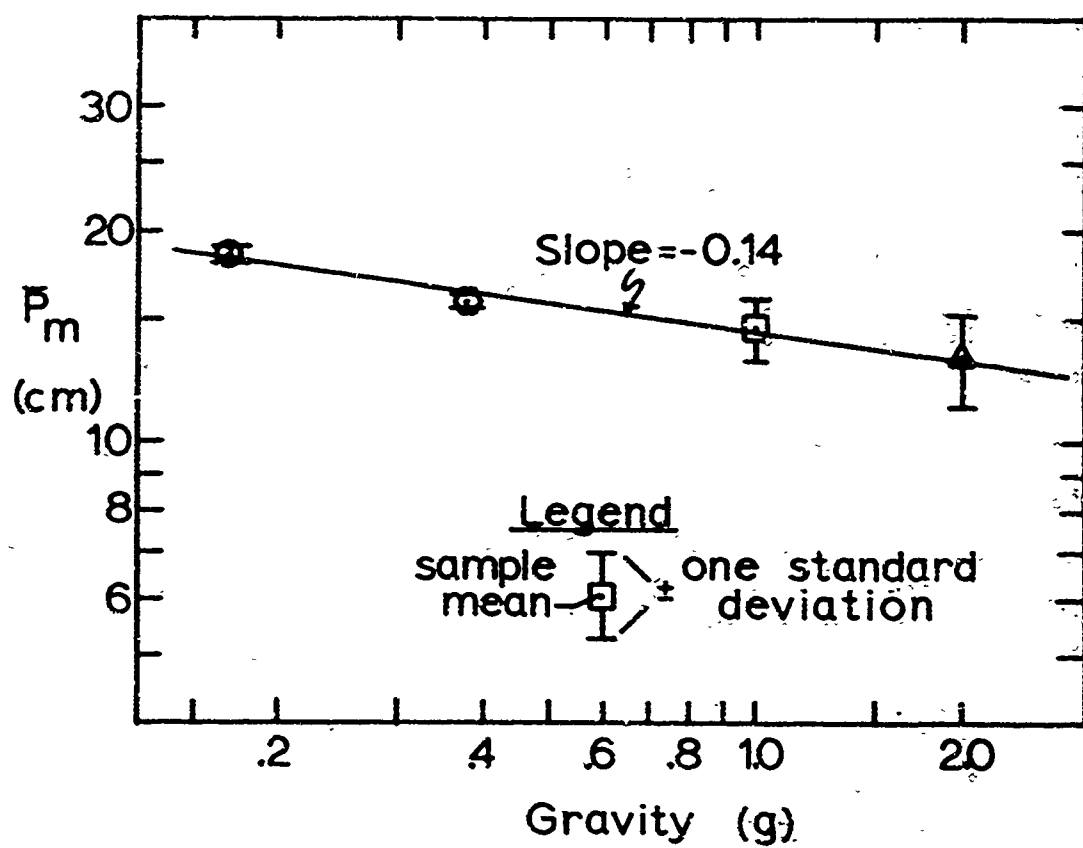
TABLE I

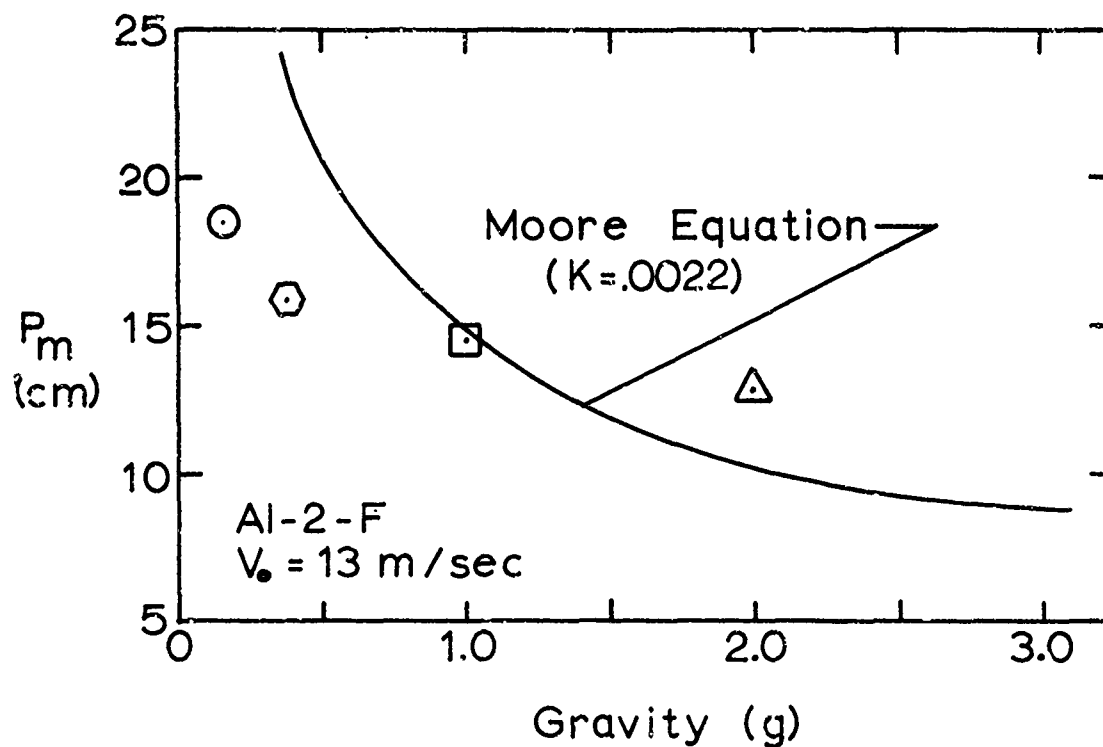
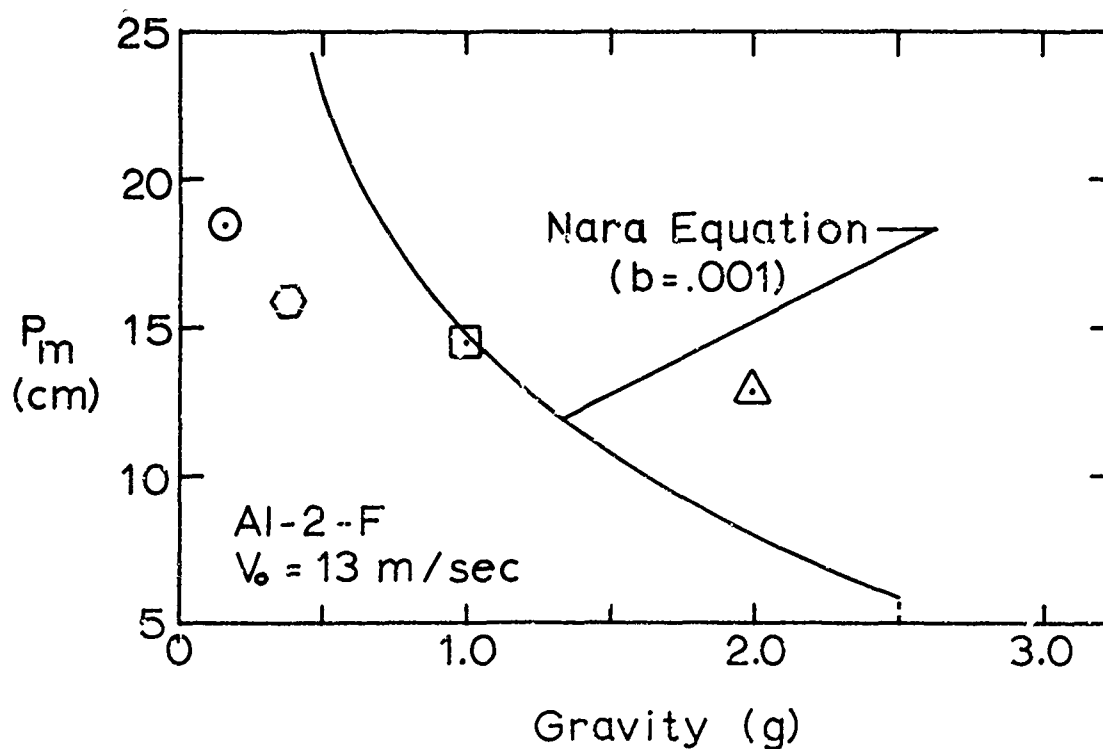
Maximum Penetration vs Gravity Level(A1-2-F, 1300 cm/sec)

GRAVITY LEVEL	NUMBER OF SHOTS	RANGE (cm)	MEAN (P_m) (cm)	STANDARD DEVIATION
2.00 g	8	10.9-16.5	13.2	2.1
1.00 g	6	12.4-16.0	14.6	1.5
0.38 g	10	15.5-16.7	15.9	0.3
0.17 g	8	17.7-19.3	18.6	0.5

A least squares fit was made to the data from Table I after the data was plotted on log-log graph paper. The graph is shown in Figure 8 on the following page. The slope of the straight line fit was 0.14, identical to the results obtained by Smith and Franklin and by Moraski and Teal for a one inch depth-of-burst (Ref 10).

The equations of Petry, Moore, Young and Nara were compared to the observed penetrations. The equations of Petry and Young had gravity dependence only in the weight of the projectile. This simple prediction was obviously in error and the two equations were not plotted against the data. The equations of Moore and Nara showed an inverse dependence on gravity. They were plotted against the data of Table I. The graphs are found in Figures 9 and 10 on page 36. In these plots, the soil constants determined in the previous section are assumed independent of gravity and

Figure 8. \bar{P}_m vs g.

Figure 9. P_m vs g , Moore.Figure 10. P_m vs g , Nara.

used to calculate the predicted values over the range of gravities.

Time-to-Complete Penetration vs Gravity. The high-speed photography method of measuring impact velocity allowed measurement of the time spent by the projectile traveling in the bed of sand. This time was defined as t_m . A variation of t_m with gravity was noted when the following table of mean time-to-complete-penetration versus gravity was construct

TABLE II

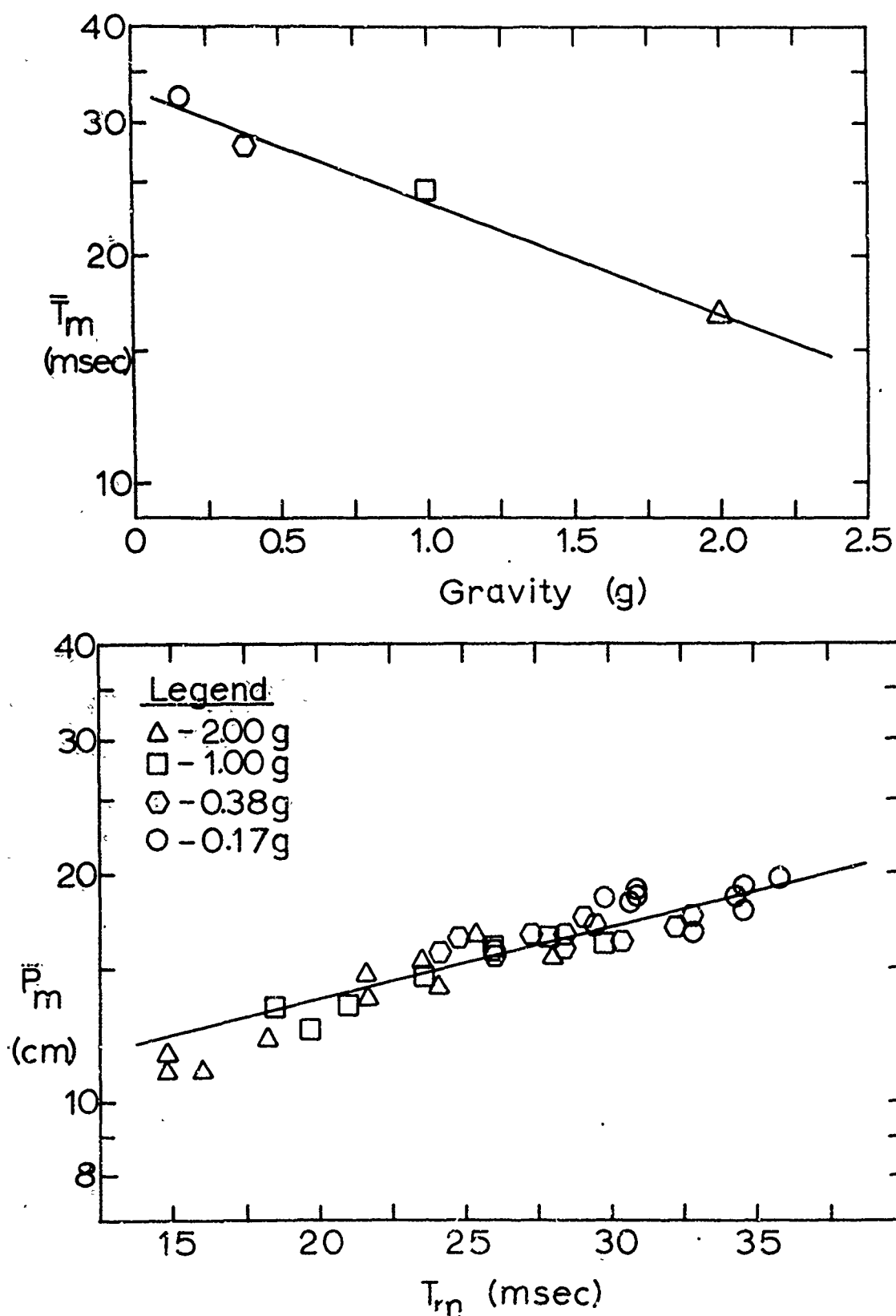
Time-to-Complete-Penetration vs Gravity

(A1-2-F, 1300 cm/sec)

GRAVITY	\bar{t}_m
(g)	(msec)
2.00	16.86
1.00	24.70
0.38	27.99
0.17	32.78

The data of Table II was plotted on semi-logarithmic graph paper (Figure 11, page 38) and found to fit a straight line determined by the least squares method. The intercept and slope of this line were used to develop an expression for t_m as a function of gravity. The expression was

$$t_m = 33.7e^{-.341g} \quad (11)$$

Figures 11 and 12. \bar{T}_m vs g , P_m vs T_m .

which indicates a definite relationship between gravity and the time required to stop a projectile penetrating a cohesionless medium.

Maximum Penetration vs Time-to-Complete-Penetration.

P_m was plotted against t_m for each shot for which both were determined. The graph is shown in Figure 12, page 38. The first-order least squares fit to the plotted data gave a slope and intercept which dictated a relationship of the form

$$P_m = 9.02e^{.021t_m} \quad (12)$$

which indicated a relationship between maximum penetration and the time it takes a projectile to reach maximum penetration in a cohesionless medium.

Maximum Penetration Scaling Law. Equations (11) and (12) were combined by equating t_m and \bar{t}_m . The result was a relationship between P_m and g of the form

$$P_m = 9.02e^{.71e^{-.341g}} \quad (13)$$

Eq. (13) predicts the values of maximum penetration determined by this experiment for the conditions under which it was conducted. It is a gravity scaling law but may have greater usefulness.. Replacement of the numerical factors, which apply to this experiment, with undetermined constants might lead to a more general equation for maximum

penetration.

One use of the relationship was investigated. Based on the assumption that t_m and, hence, Eq. (11) were independent of at least impact velocity, a method was devised by which an existing penetration equation could be caused to agree with the gravity dependence observed in this experiment.

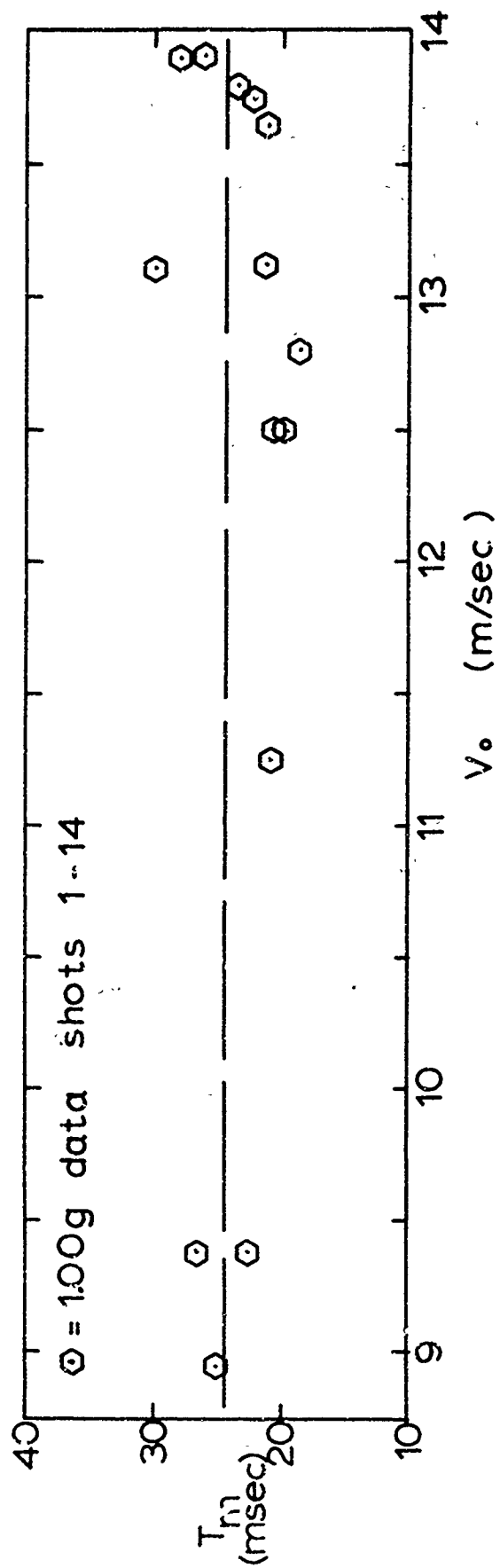
The assumption that t_m was independent of impact velocity was upheld by a plot of these variables which was made for each shot for which they both were determined. This plot is shown in Figure 13; on the following page. Further support was obtained in a conversation with Dr. H. J. Moore (Ref. 18) who had knowledge of an uncompleted work that had shown the same intermediate result.

The soil constant or function was the thing that was expected to change in a different gravity field, so a logical method of approach was to make the constant that appeared in an existing equation a function of gravity.

An example is perhaps the best way to show the procedure involved. Moore's equation can be modified in the following way:

1. The existing dependence on gravity is treated as a terrestrial constant (unity). Projectile weight thus becomes mass.
2. Eq. (13) is rewritten as

$$P_m = P_0 S \bar{G}(g) \quad (14)$$

Figure 13. T_m vs V_0 at 100g

where P_0 is Moore's equation (Eq. (7)) divided by the soil constant, K' . $\bar{G}(g)$ is the expression

$$e^{-.71e^{-.341g}} \quad (15)$$

which is shown plotted in Figure 14 on page 43.

$S'\bar{G}(g)$ is the modified soil function.

2. The value of S' is determined by equating K' and $S'\bar{G}(g)$ at Earth gravity. The value of S' for Moore's equation is 0.00105.

3. $S'\bar{G}(g)$ is substituted for K' in the original equation. The modified Moore equation becomes

$$P_m = S'\bar{G}(g) \left(\frac{\rho_p}{\rho} \right)^{\frac{1}{2}} (L)^{\frac{1}{2}} v_0 \quad (16)$$

A plot of the modified Moore equation is shown in Figure 15 on page 44.

The method can be applied to any existing soil-penetration equation unless the soil constant cannot be isolated. An equation modified in this way is good, however, only under the conditions which applied to the experiment. Further applications may or may not be possible.

Deceleration Traces

Distance-time data were obtained from the high-speed films by recording the position of the back end of the projectile in every other frame from impact until penetration was complete. (See Appendix D.) Every other frame

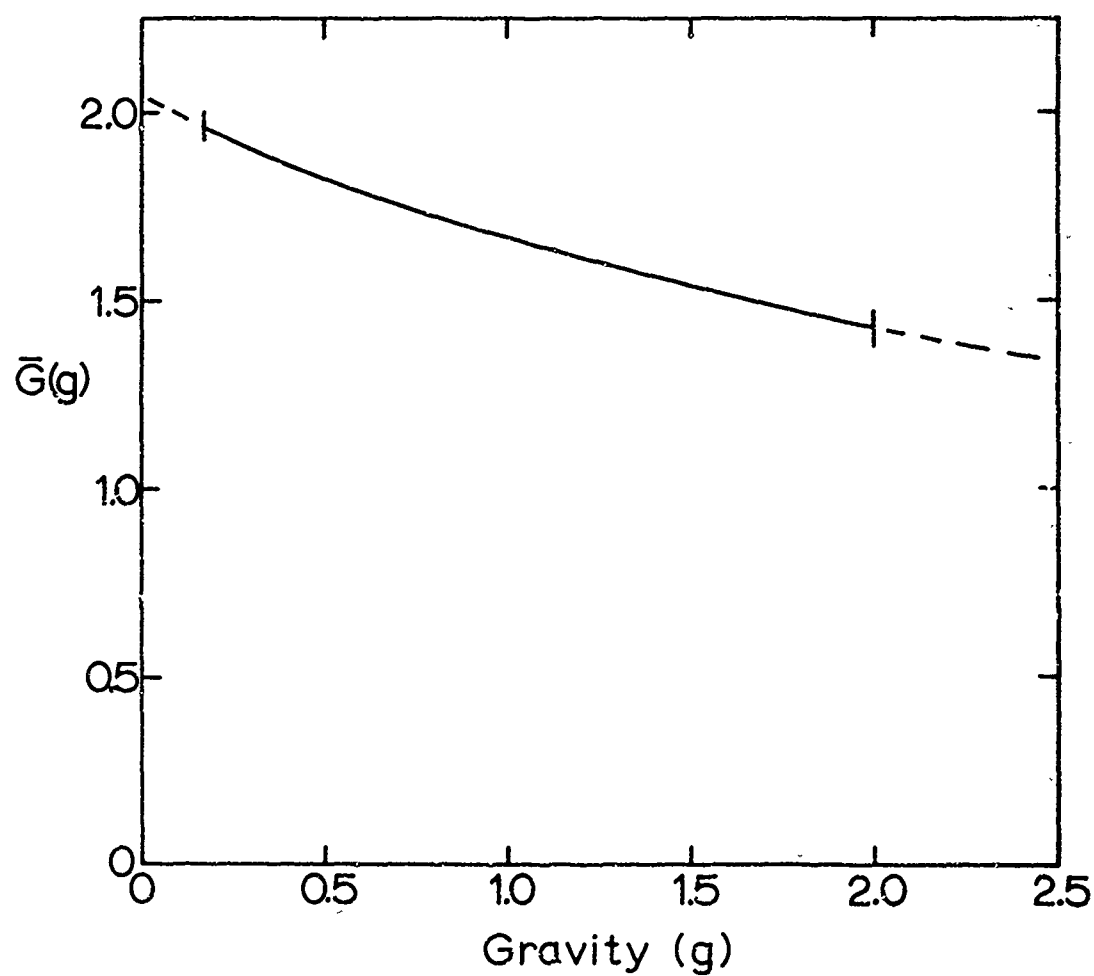
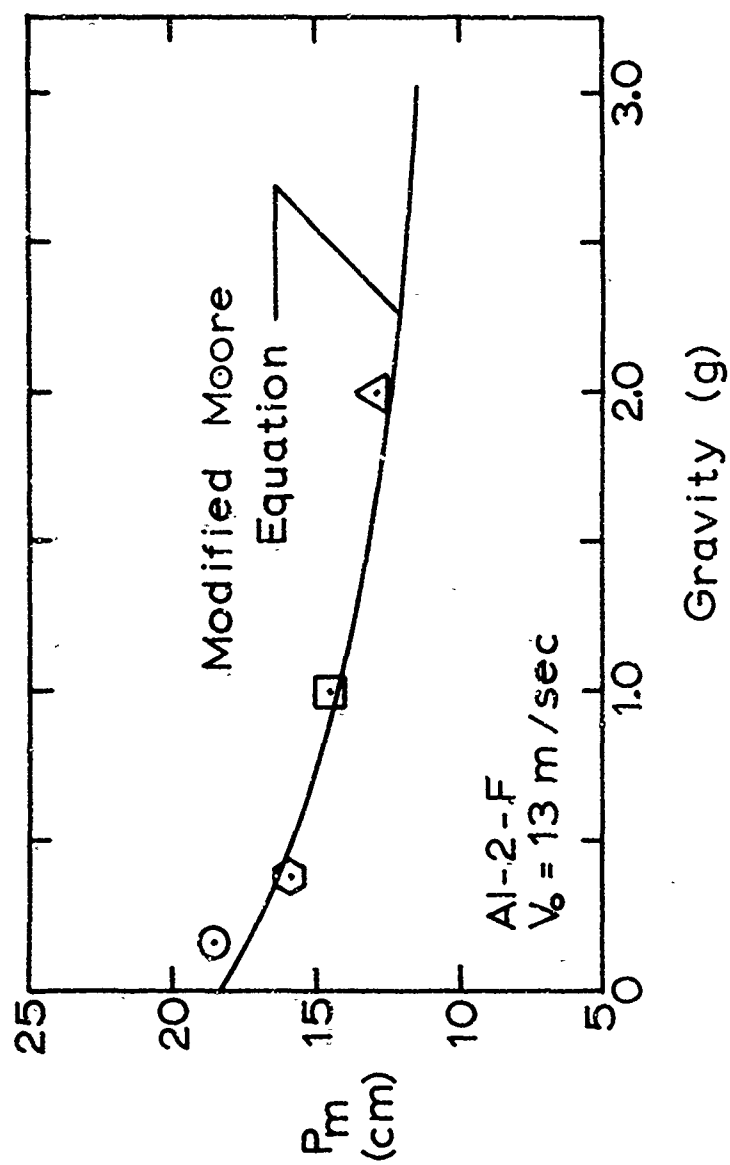


Figure 14. $\bar{G}(g)$ vs g .

Figure 15. P_m vs g , Modified Moore.

gave an elapsed time of 0.62 msec between readings. The number of data points per event varied from 35 to 60 depending on the magnitude of t_m .

To obtain deceleration-time curves, a least squares polynomial fit was made to the distance-time data, and the resulting expression double-differentiated. Polynomials from order 1 to order 10 were fitted to each set of data by a computer, and the best fit in terms of root-mean-square residue was noted.

The fits became increasingly better with increasing polynomial order, but computer plots of the polynomials showed that from order 7 to order 10 the functions were not monotonically increasing at high values of time. Such curves were felt to be unrealistic because no bouncing of the projectile during penetration had ever been observed. In all cases, the sixth-order polynomial fit had the least residue and was chosen as the best depiction of the actual function.

Further support for a sixth-order polynomial fit came from the computer-produced plots of the double-differentiated functions. Double-peaked curves were produced in all cases. This general shape agreed with the curves produced from low velocity penetrations into Ottawa Sand by previous investigators (Ref. 21, 26). Samples of such curves are found in Figure 16, on the following page.

Four shots, one at each gravity level, were chosen for their nearness to the sample mean values of P_m and t_m .

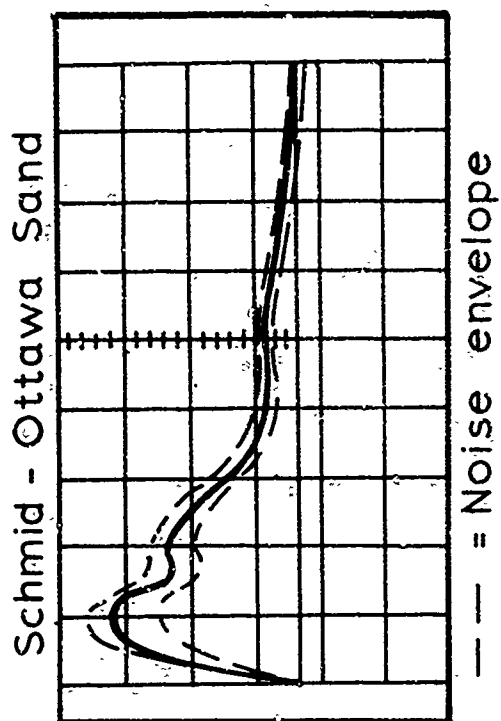
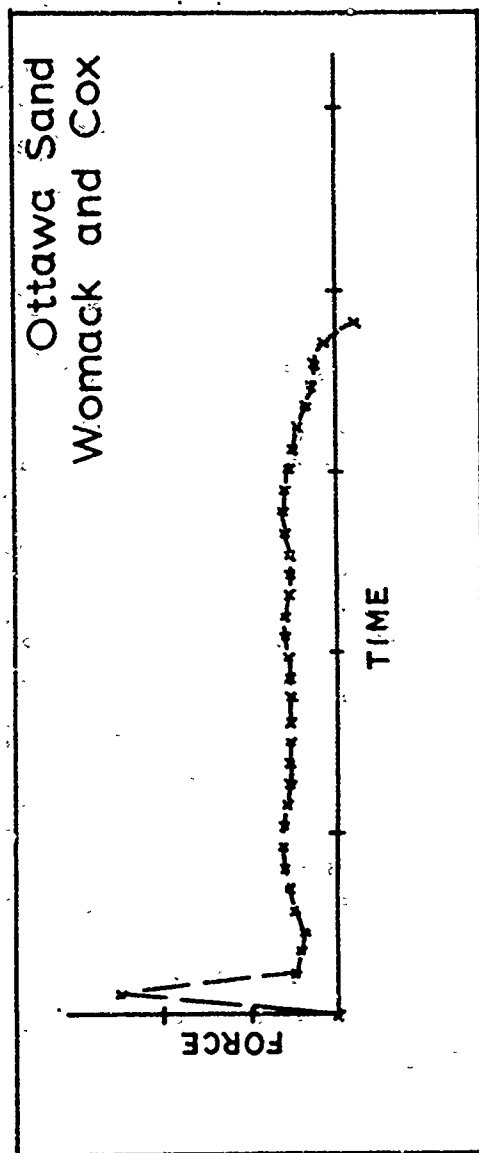


Figure 16. Typical deceleration traces, Ottawa Sand.

The distance-time data from all four shots was normalized to the forms P/P_m and t/t_m and plotted on one graph. The graph is shown in Figure 17 on page 48. There was no apparent trend in this plot. This gave support to the choice of one functional form (the sixth-order polynomial) for the distance-time expression at all gravity levels.

A computer program was written to produce sixth-order polynomials of best fit from the distance-time data of every shot fired for which high-speed films were available. The program would also double-differentiate the polynomial when desired, and produce a continuous plot of the function. It plotted all data points on the plot of the distance-time polynomial. The program can be found in Appendix F.

Analysis of the Deceleration Curves. Two basic curves were generated. They were designated Type I and Type II. Type I curves had the first peak deceleration at impact, and the Type II curves took some time to reach it. The following parameters were defined and read from each curve:

- t_1 = time to reach first peak (msec)
- a_1 = magnitude of first peak (g)
- t_v = time to reach minimum between peaks (msec)
- a_v = minimum between peaks (g)
- t_2 = time to reach second peak (msec)
- a_2 = magnitude of second peak (g)

Thirteen Type I and twelve Type II curves were produced. At least one curve of each type was generated from the data of each gravity level. Figures 18 through 33 on

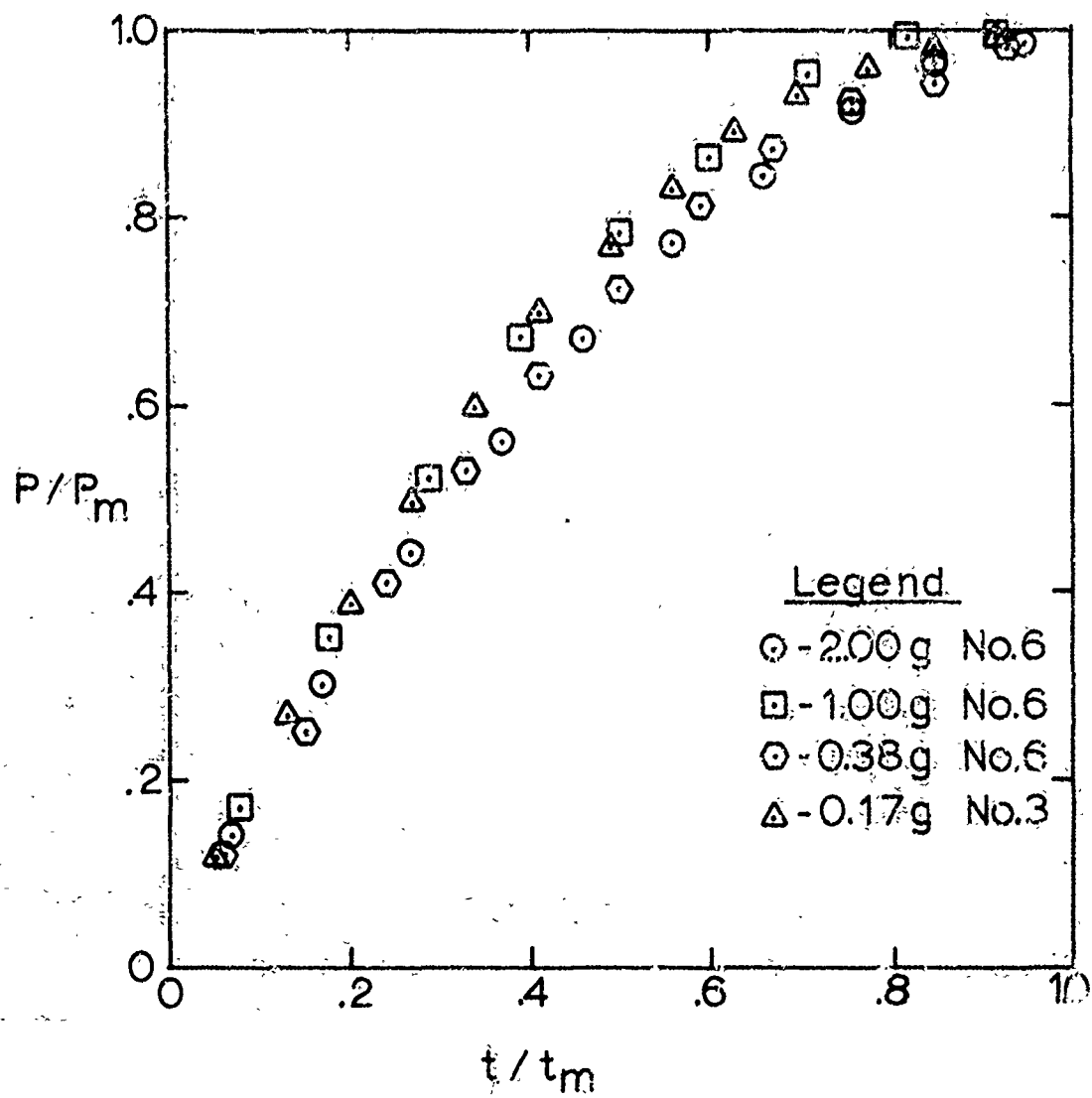


Figure 17. P/P_m vs T/T_m .

PENETRATION VS TIME
LEAST SQUARES FIT
AL-2-F 2.00G NO 5A

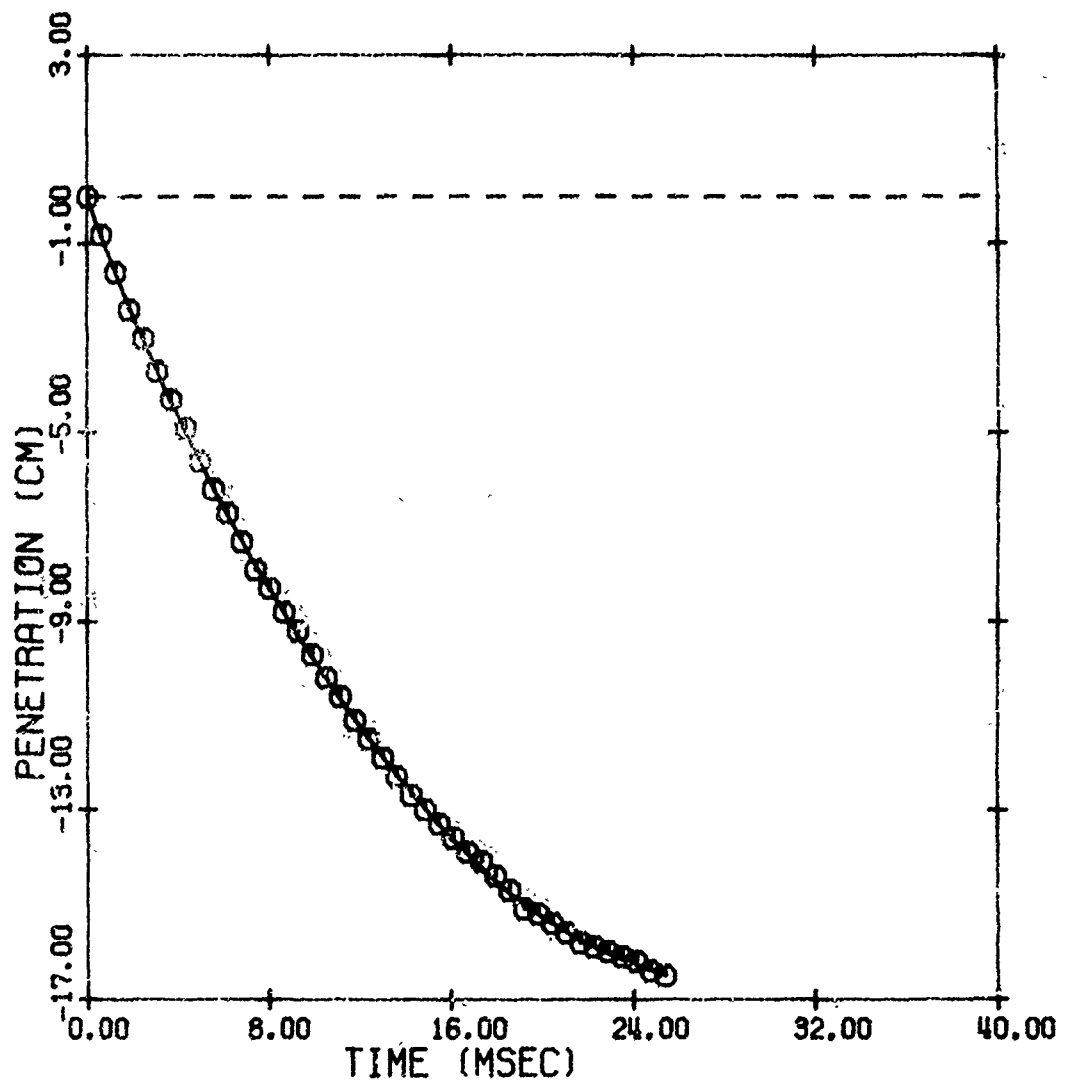


Figure 18.

DECELERATION VS TIME
2ND DERIVATIVE OF LEAST SQUARES FIT
AL-2-F 2.00G NO 5A

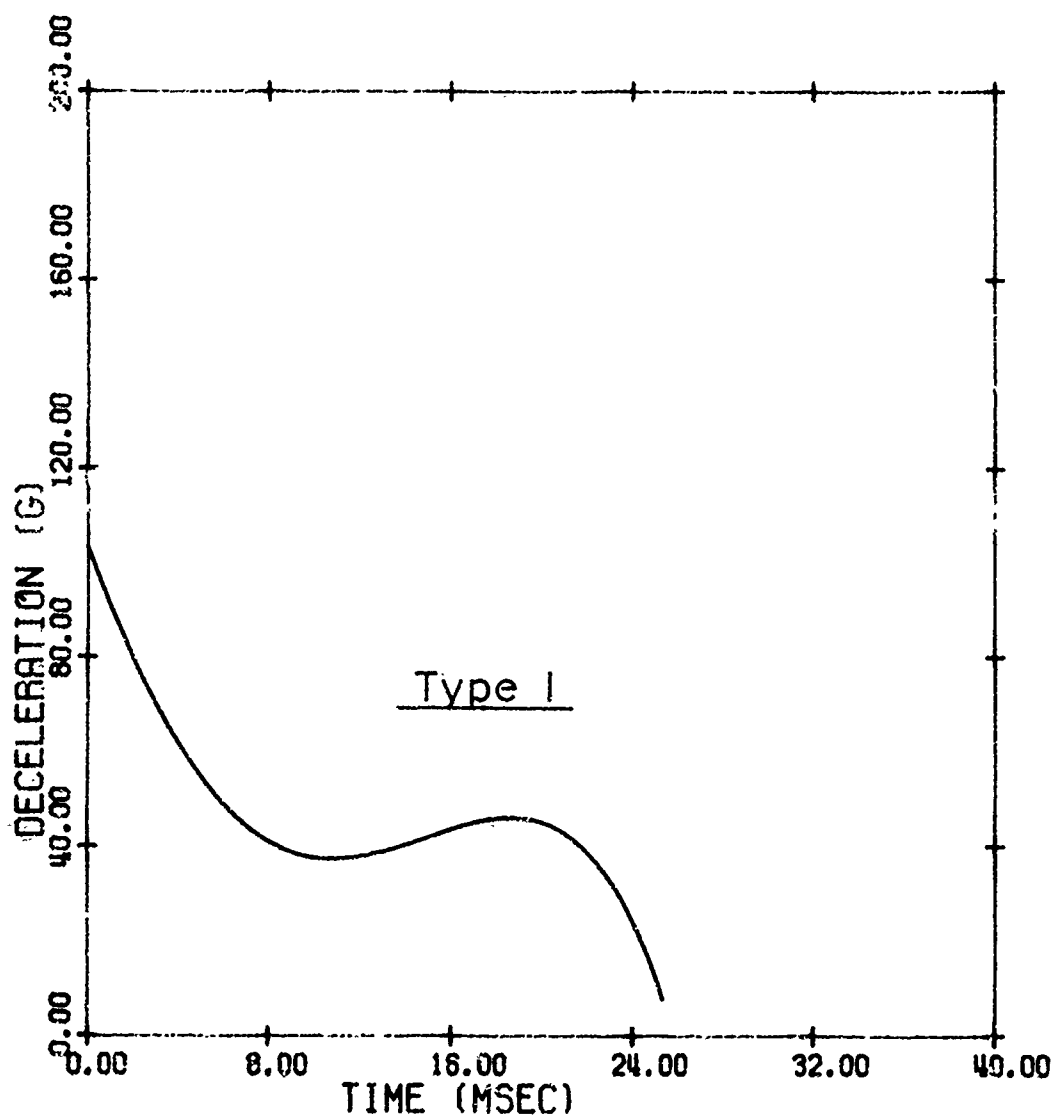


Figure 19.

PENETRATION VS TIME
LEAST SQUARES FIT
AL-2-F 2.00G NO 6

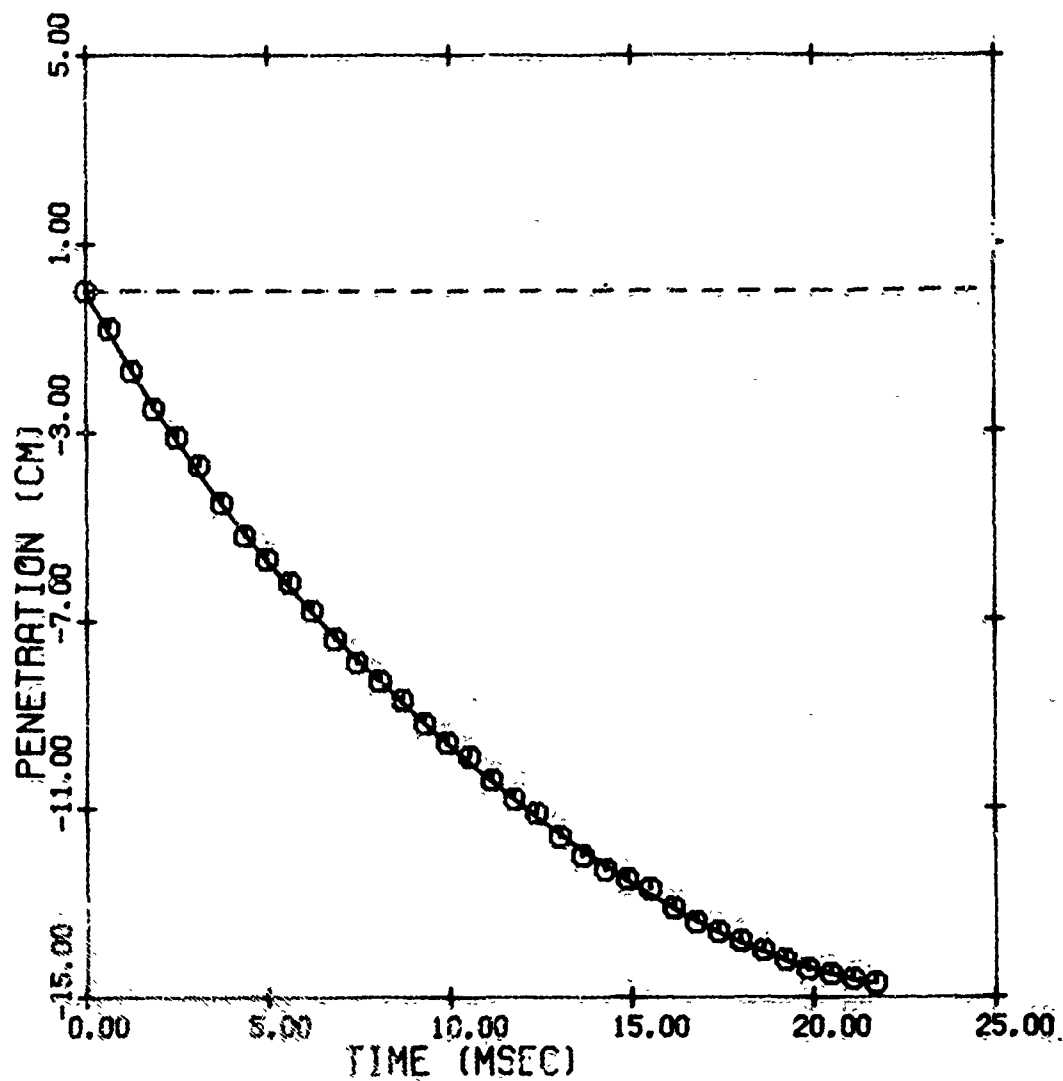


Figure 20.

DECELERATION VS TIME
2ND DERIVATIVE OF LEAST SQUARES FIT
AL-2-F 2.00G NO 5

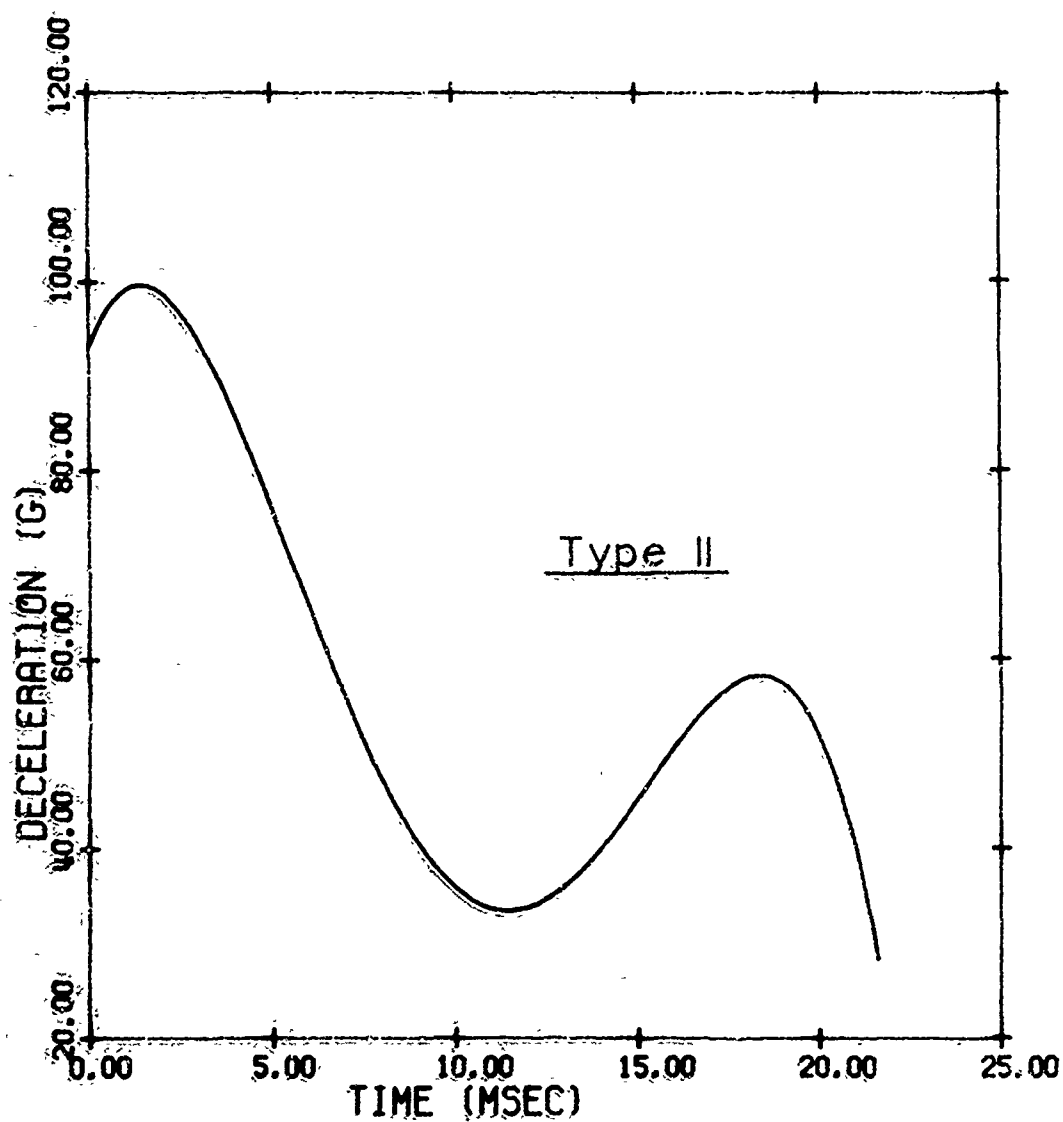


Figure 21.

PENETRATION/TIME
LEAST SQUARES FIT
AL-2-F 1.00G NO 4

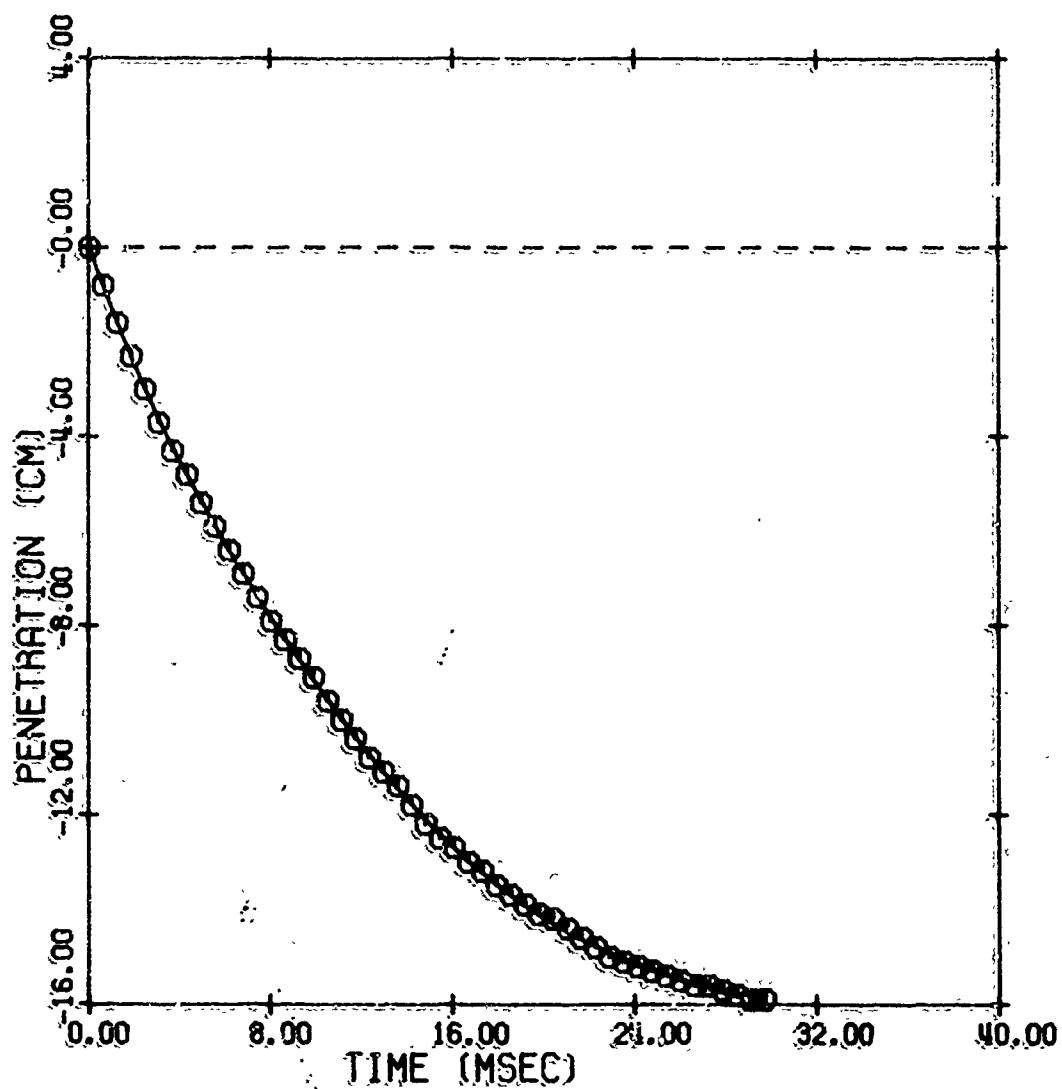


Figure 22.

DECELERATION VS TIME
2ND DERIVATIVE OF LEAST SQUARES FIT
AL-2-F 1.00G NO 4

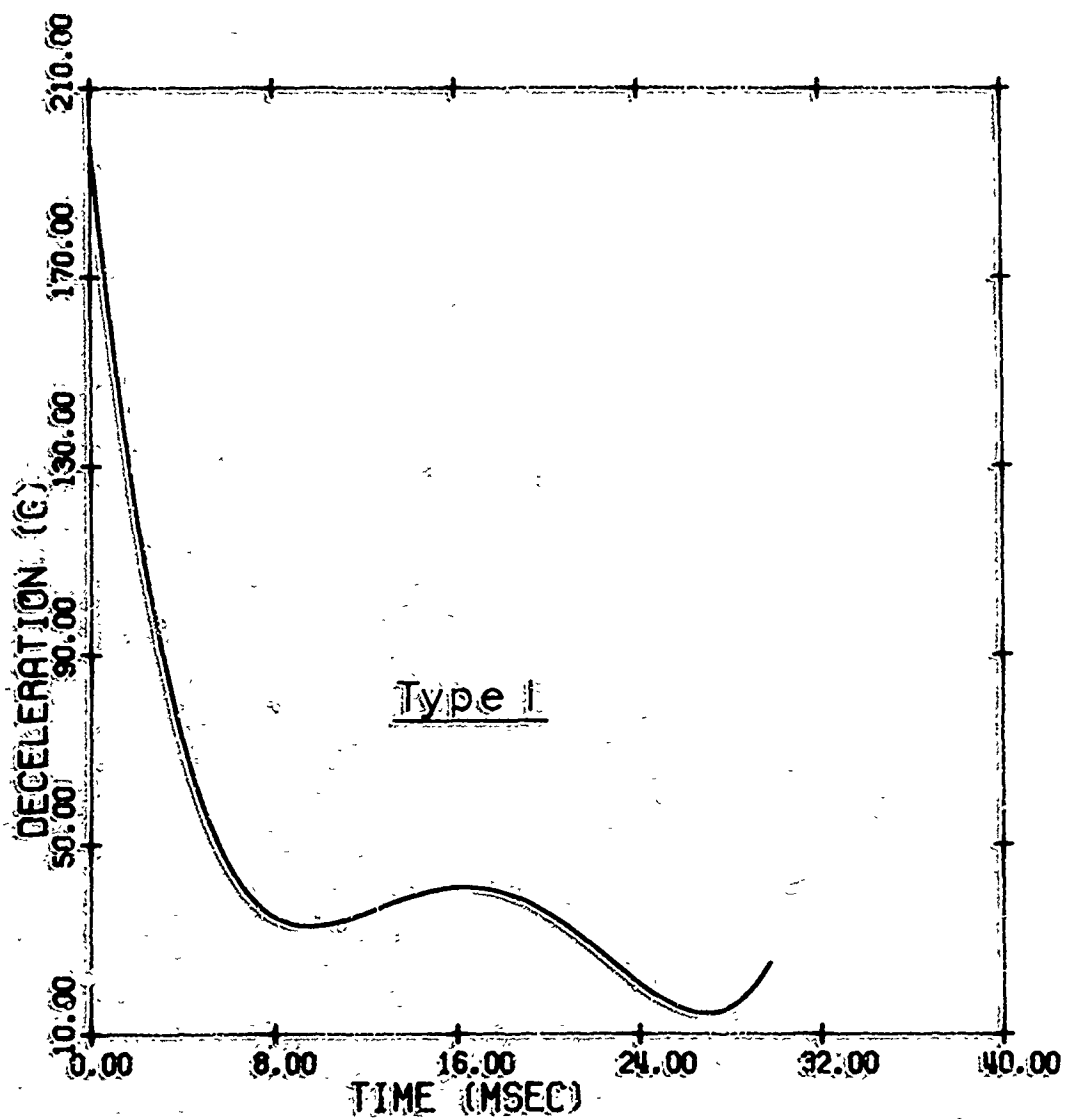


Figure 23.

GSF/MC,'59-6

PENETRATION/TIME
LEAST SQUARES FIT
AL-2-F 1.00G NO 5

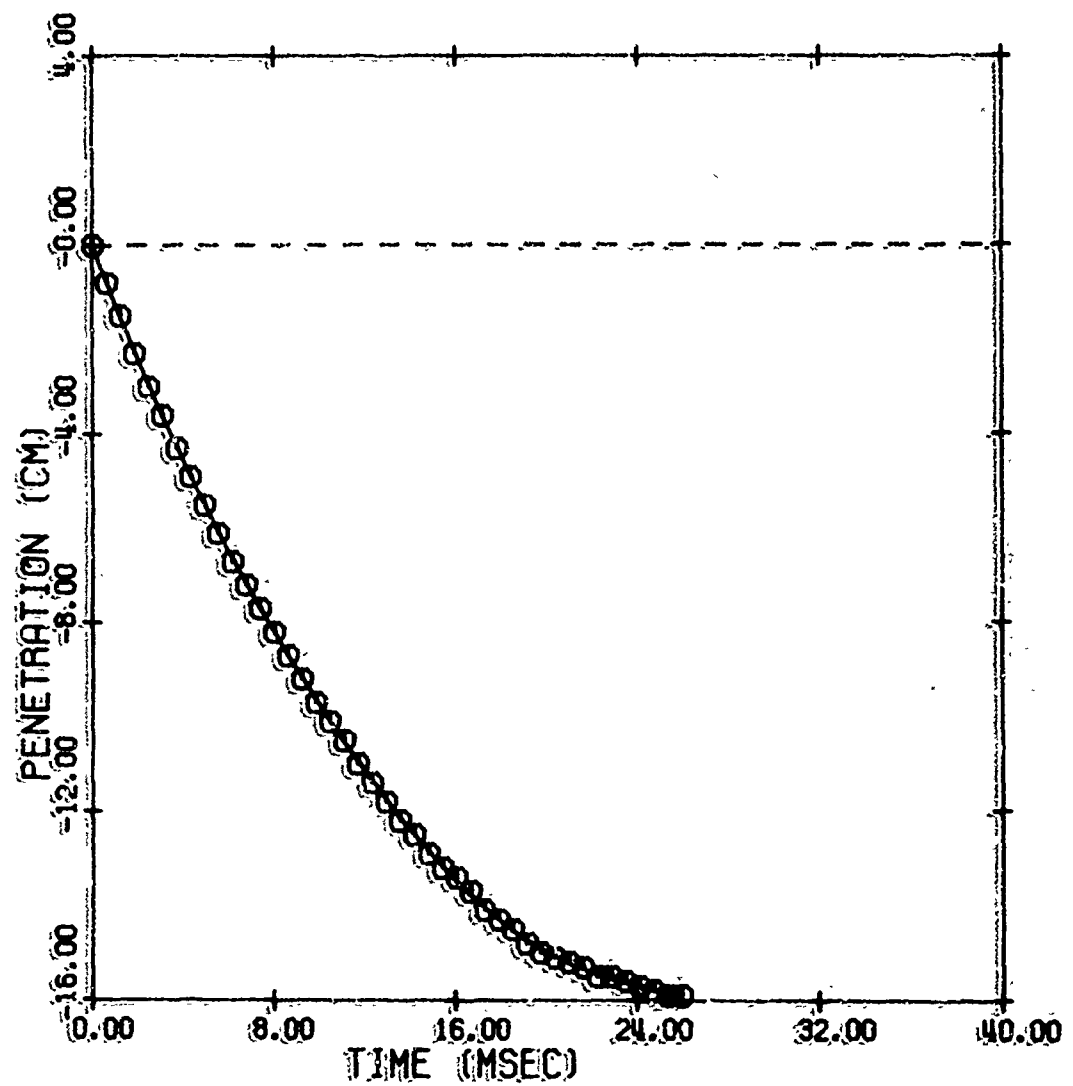


Figure 24.

DECELERATION VS TIME
 2ND DERIVATIVE OF LEAST SQUARES FIT
 PL-2-F 1.00G INO 5

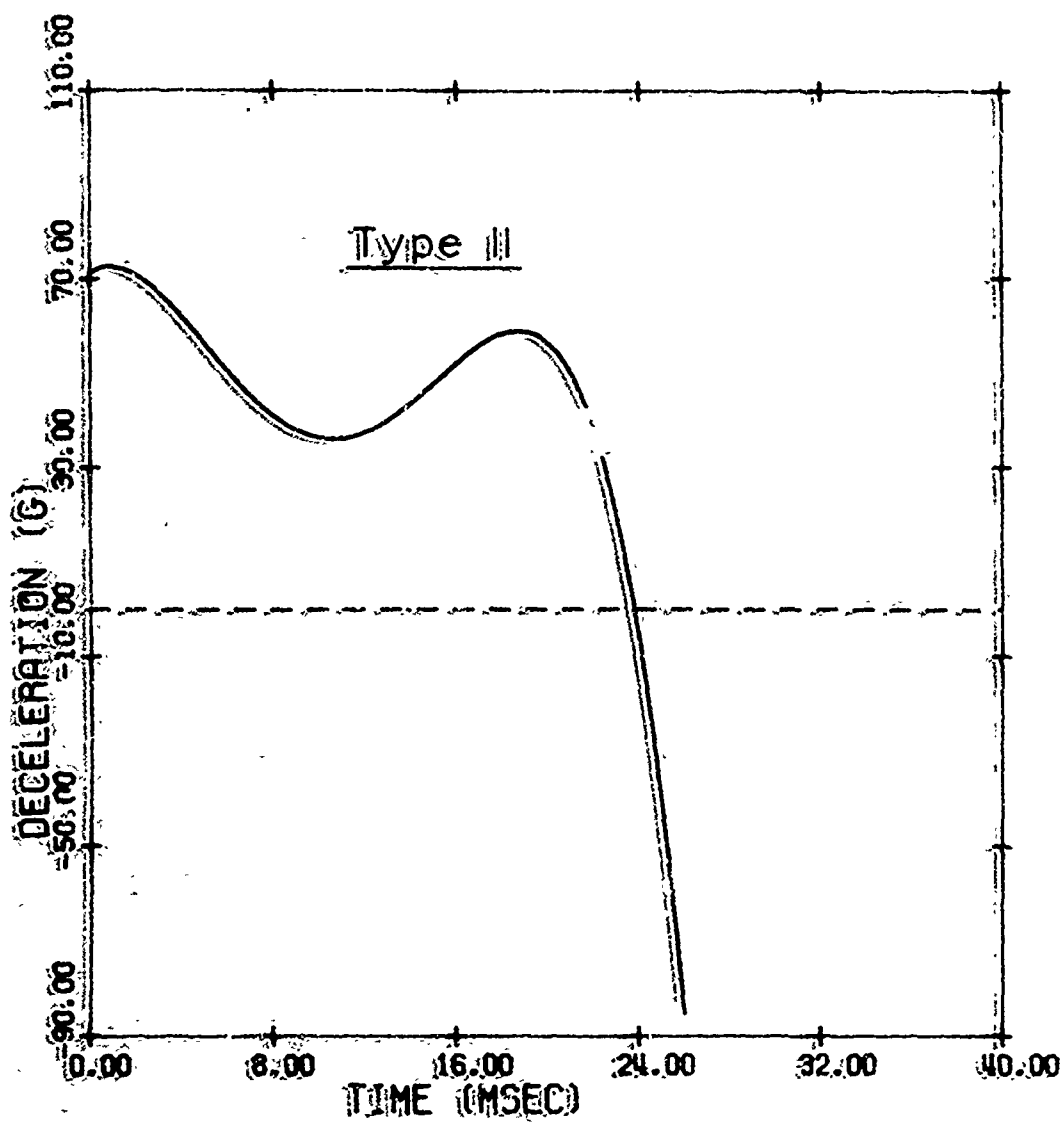


Figure 25.

PENETRATION VS TIME
LEAST SQUARES FIT
IAL-2-F 0.38G NO 4

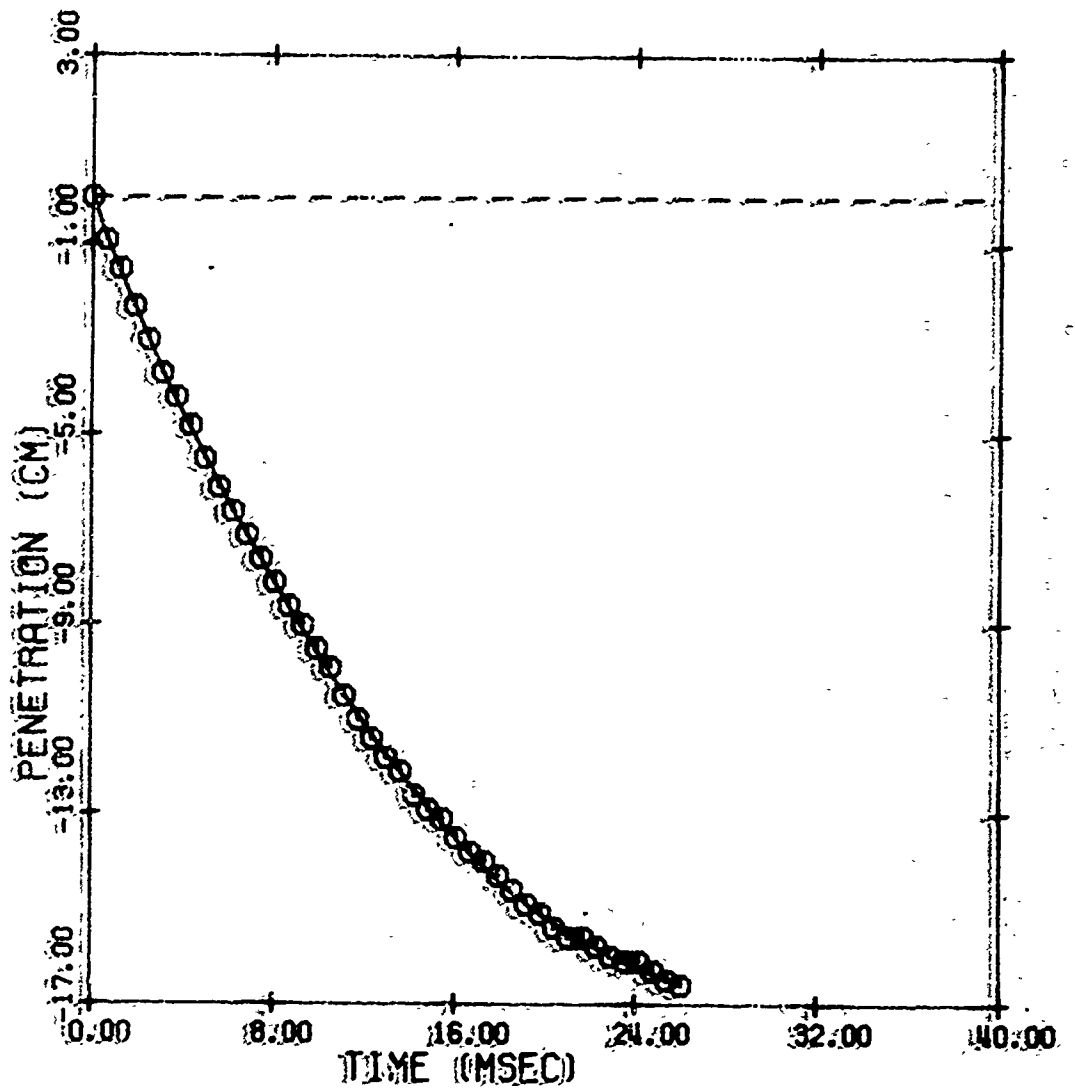


Figure 26.

DECELERATION VS TIME
2ND DERIVATIVE OF LEAST SQUARES FIT
AL-2-F 0.38G NO 4

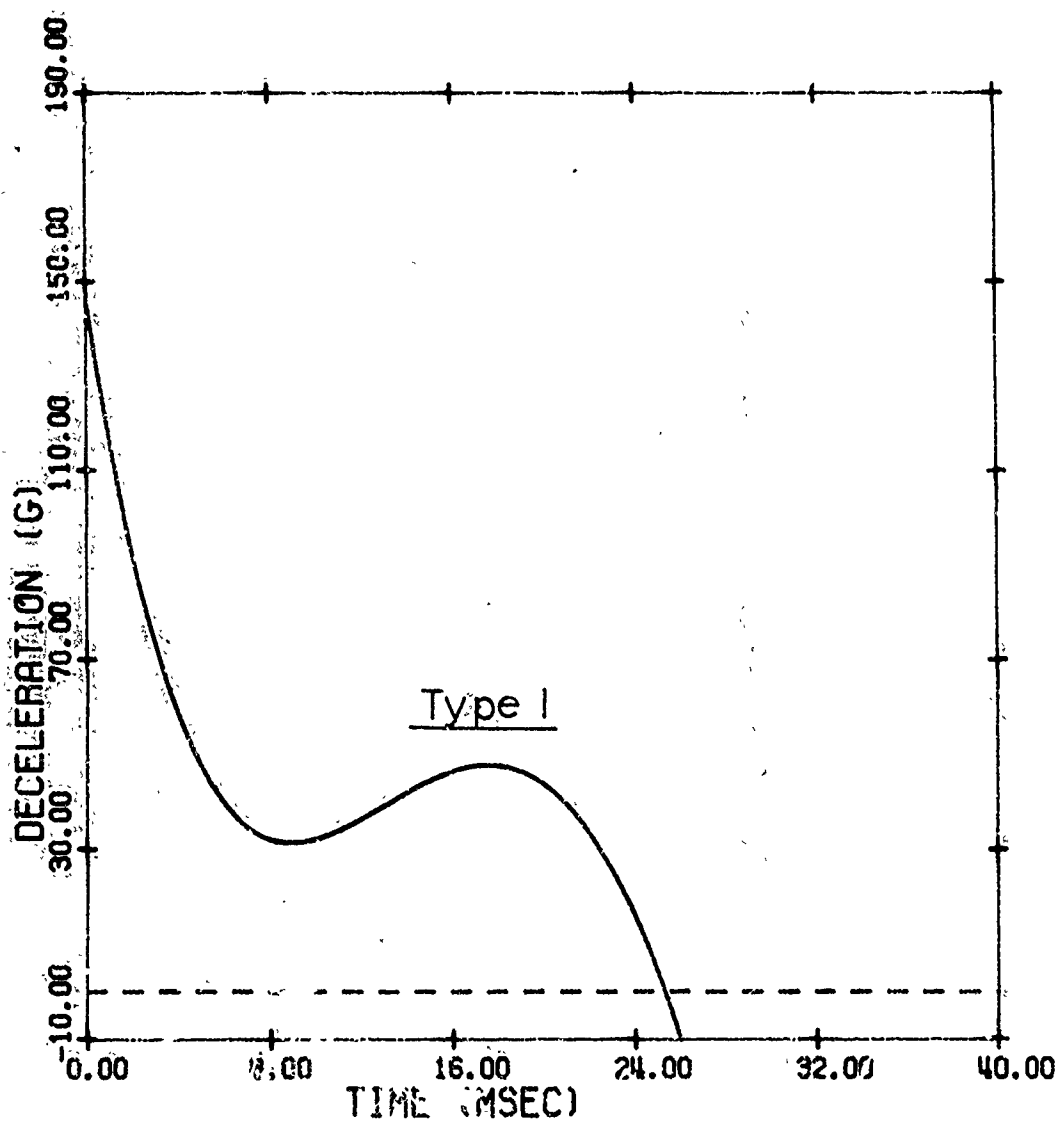


Figure 27.

PENETRATION VS. TIME
LEAST SQUARES FIT
AL-2-F 0.38G NO 3

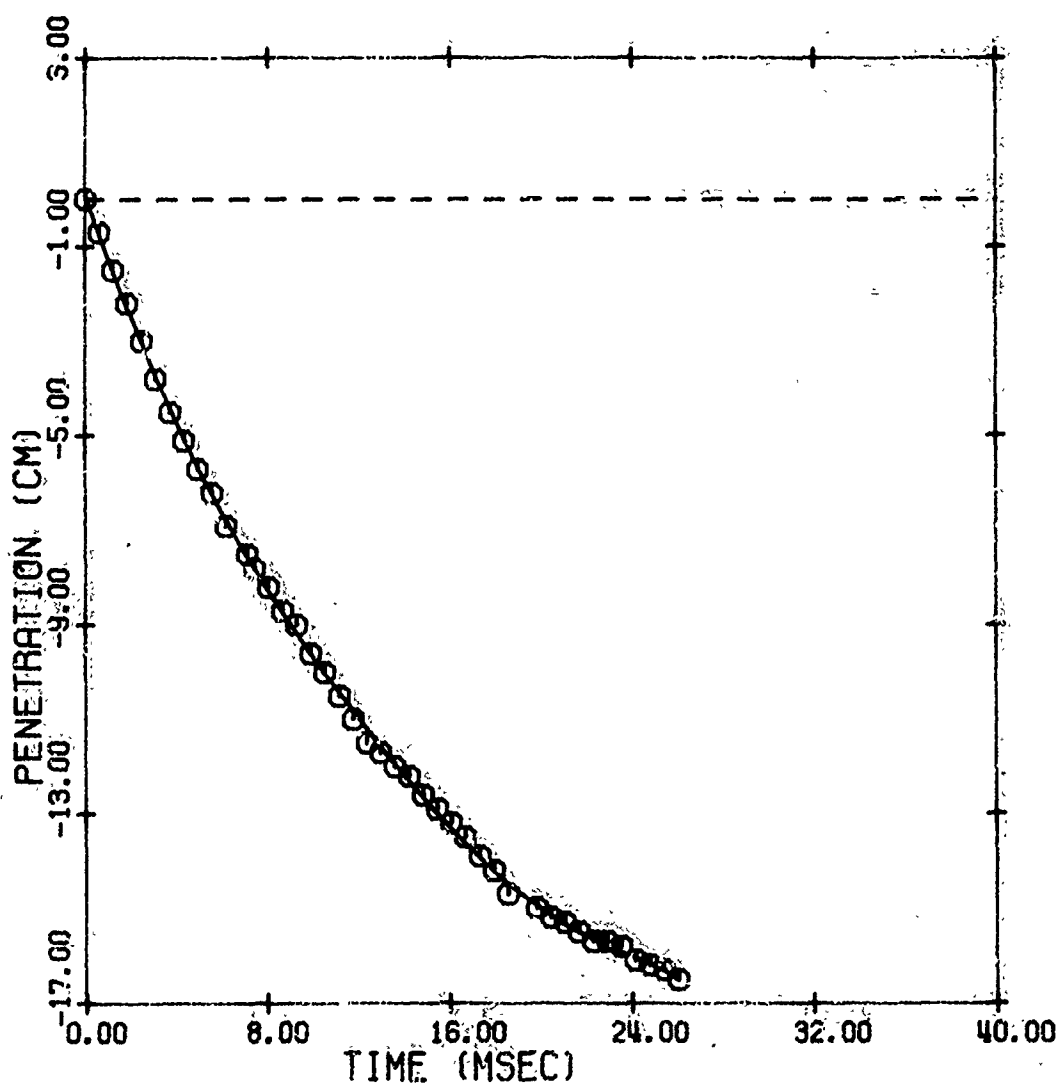


Figure 28.

DECELERATION VS TIME
2ND DERIVATIVE OF LEAST SQUARES FIT
AL-2-F 0.38G NO 3

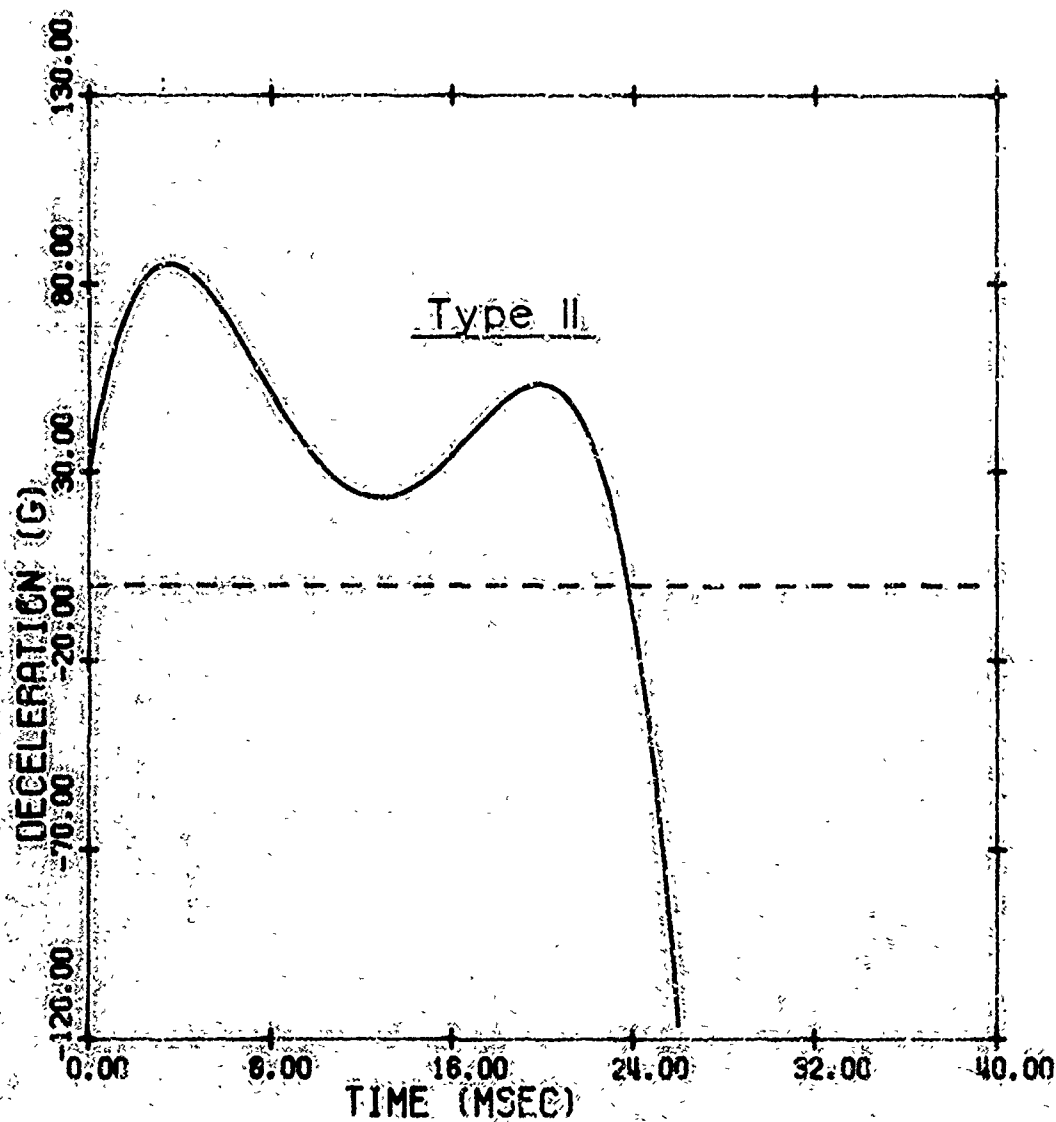


Figure 29.

PENETRATION VS TIME
LEAST SQUARES FIT
AL-2-F 0.17G NO 5

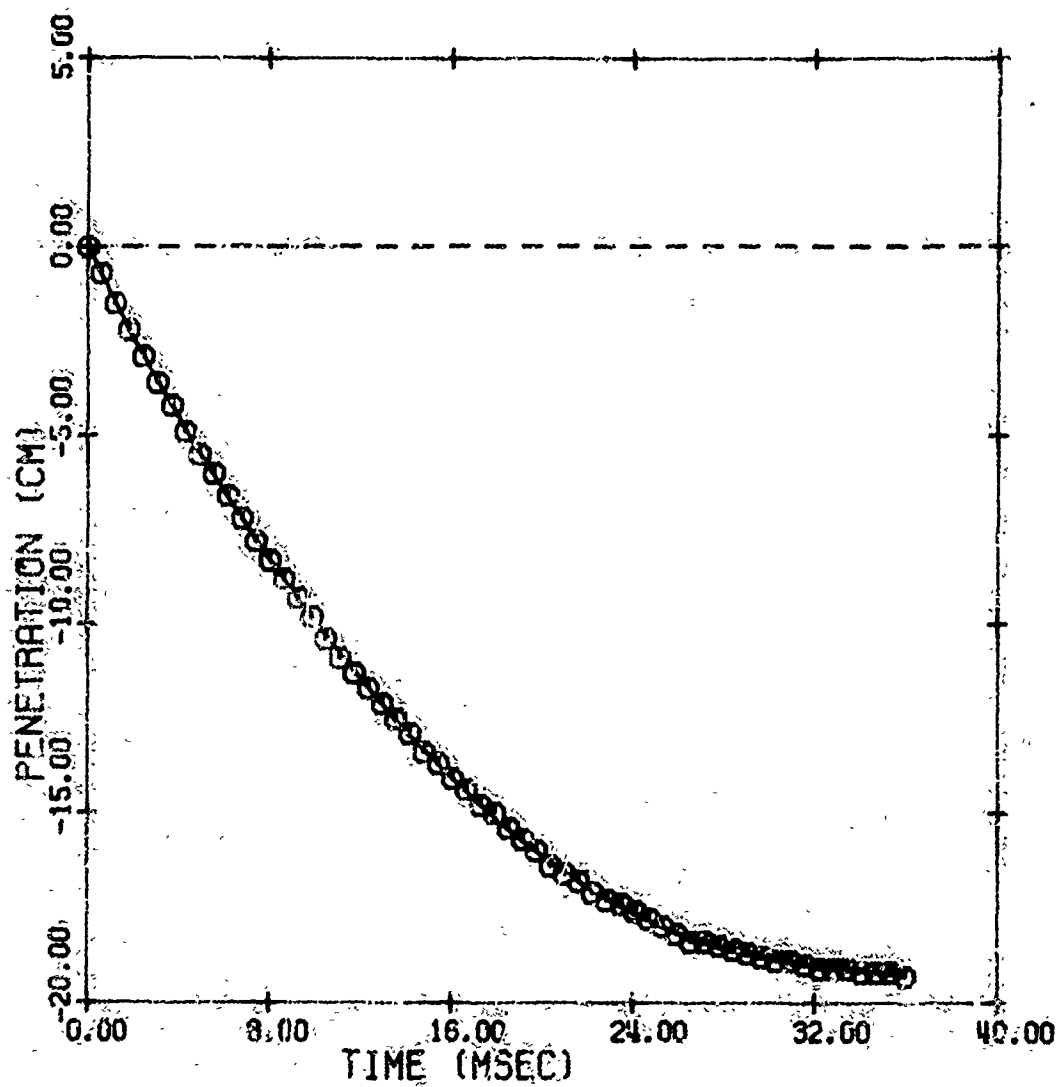


Figure 30.

DECELERATION VS TIME
2ND DERIVATIVE OF LEAST SQUARES FIT
AL-2-F 0.17G NO 5

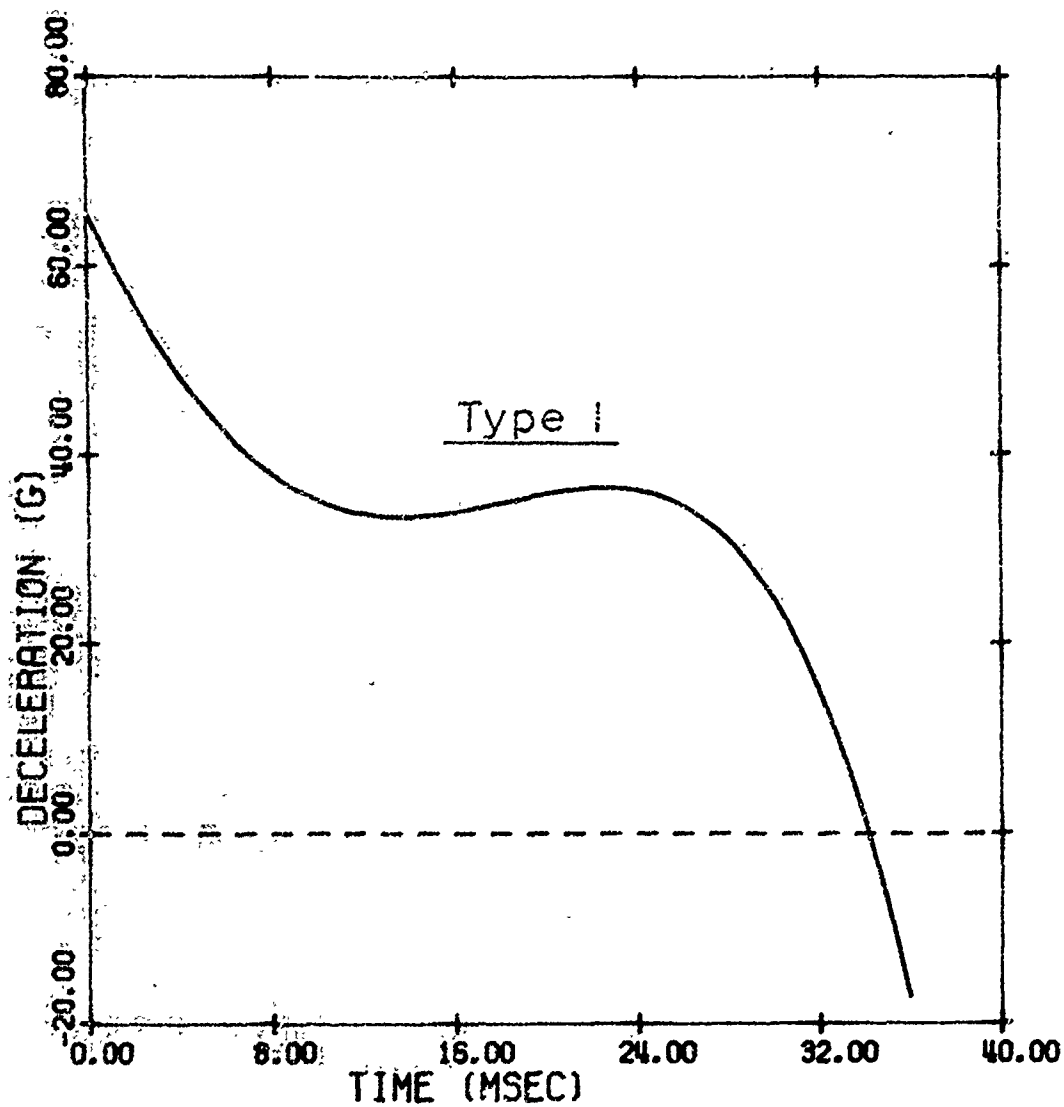


Figure 31.

PENETRATION VS TIME
LEAST SQUARES FIT
AL-2-F 0.17G NO 2

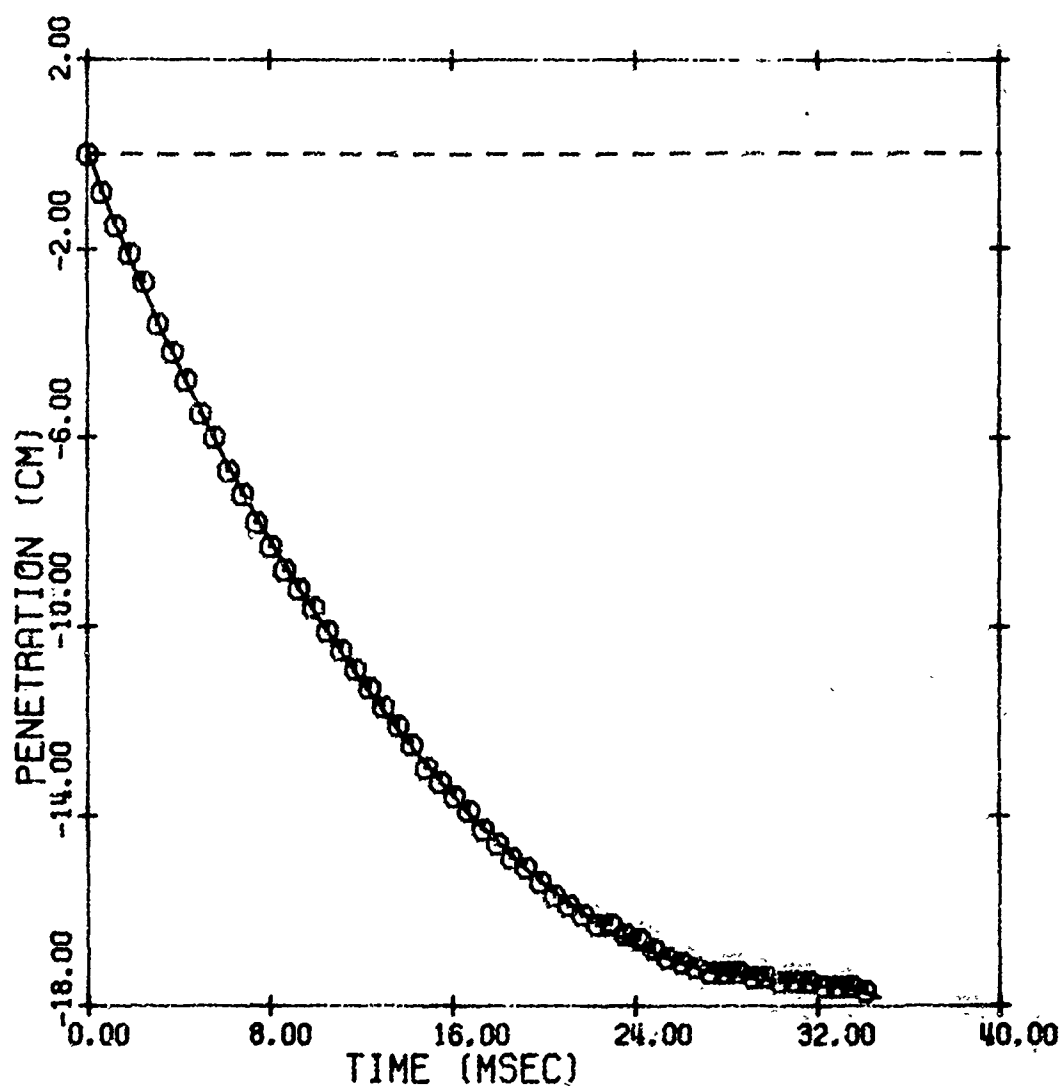


Figure 32.

DECELERATION VS TIME
2ND DERIVATIVE OF LEAST SQUARES FIT
AL-2-F 0.17G NO 2

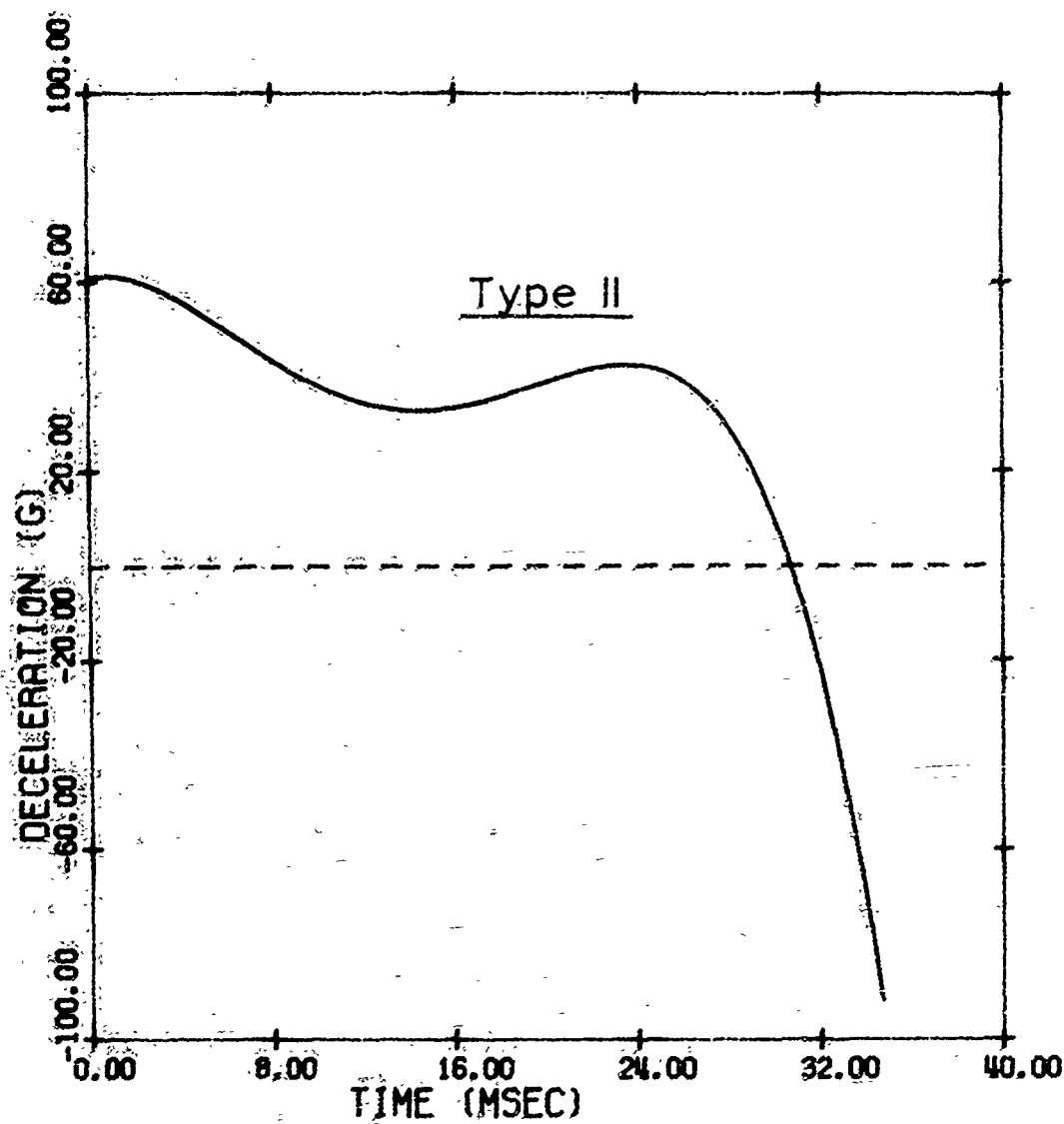


Figure 33.

pages 49 through 64 are examples of each type of curve for each gravity level. The curve parameters are tabulated in Tables VII and VIII in Appendix A.

The following trends were observed in the averages of the parameters at different gravity levels:

A. Type I Curves

1. \bar{t}_1 was always zero, \bar{t}_v was about 32% of \bar{t}_m , and \bar{t}_2 was about 67% of \bar{t}_m at all four of the gravity levels.
2. \bar{a}_v increased slightly with increasing gravity.
3. \bar{a}_2 was nearly constant over the range of gravities.

B. Type II Curves

1. \bar{t}_1 was nearly constant over the gravity range. \bar{t}_1/\bar{t}_m increased with increasing gravity.
2. \bar{t}_v was about 50% of \bar{t}_m and \bar{t}_2 about 80% of \bar{t}_m at all gravity levels.
3. \bar{a}_1 increased with increasing gravity.
4. \bar{a}_v increased with increasing gravity.
5. \bar{a}_2 increased with increasing gravity.

Generally, the deceleration-time curves are qualitatively like those that have been produced elsewhere with accelerometers. Quantitatively they are incorrect in some important ways. The curves do not start at impact with zero deceleration and the deceleration does not go to zero at \bar{t}_m . A negative deceleration at impact is possible, though assumed negligible in other areas of this work.

Zero deceleration at the end of the event is a definite requirement.

The explanation of errors in the curves must include at least two considerations. The first is the reading error involved in obtaining the distance-time data. The second is the least squares polynomial approximation of the true functional form. In an attempt to overcome the second source of error, numerical differentiation was tried. The size of the reading error, however, made the results unintelligible.

VI. Conclusions and Recommendations

Terrestrial Penetration Into Cohesionless Media

The following conclusions can be drawn from the results of this experiment:

1. The soil constant or function is the least well-defined variable in the problem.
2. Exact determination of the form of the soil resistance force would yield an exact solution to the problem.
3. The nose-shape of the projectile affects the maximum penetration that will result from impacting a cohesionless medium at low velocity. The importance of nose-shape is greater for projectiles of larger body diameter.
4. Figures 4, 5, 6, and 7 on pages 29 through 32, indicate that Young's empirical equation is the best fit to the observed penetrations of this experiment. The dependences on impact velocity and projectile mass are best described by Young's equation in the ranges covered by this experiment. Moore's equation is the best semi-analytical equation of the three described in this work.

Gravity Effects

The following conclusions can be drawn from this experiment:

1. An inverse relationship exists between maximum

penetration and gravity.

2. The soil constants of terrestrial soil-penetration equations are functions of gravity. They can be modified by a function, $\bar{G}(g)$, so that the equations agree with the results of this experiment in the range of gravity levels and impact velocities that was investigated.

3. At 1.00 g, the time-to-complete-penetration is a very weak function of impact velocity and may be assumed independent of impact velocity over the range of velocities of this work.

4. An inverse relationship exists between time-to-complete-penetration and gravity.

Deceleration-Time Curves

No definite conclusions can be drawn from the results of the deceleration-time curves that were developed in this paper. The trends that were noted in the results section of this paper are valid in that they described the variations of the averaged curve-parameters over the gravity range. The errors in the curves and the method in which they were produced make conclusions without further investigation hazardous.

General Conclusions

The similarity of the gravity dependences found in previous works might be significant. In the previously

described work of Smith and Franklin, the amount of energy that was input to the Ottawa Sand was approximately 10^{10} ergs per detonation. The average input of this experiment was 10^8 ergs per impact. The real differences in the experiments were differences in loading rate. The conclusion can perhaps be drawn that loading rate does not significantly affect the gravity-dependent, dynamic properties of cohesionless media.

The previously described experiment of Lynch and Higgins (Ref. 13) was perhaps a static problem (change of bearing capacity of cohesionless media with gravity) in which the bearing capacity was found directly proportional to gravity. The difference between this work and the others is, perhaps, that compressional and shear waves were not set up in the sand during the event. This, along with the evidence of Allen, Mayfield, and Morrison, Ref. 2) indicates that the gravity effects on shear and compressional wave velocities might be of major importance to the overall gravity effect observed in the dynamic experiments.

Recommendations

1. Further work in soil-penetration should be aimed at finding the exact form of the soil resistance force and the soil properties of which it is composed.
2. More investigation should be done on the variation of deceleration-time traces with gravity.
3. The effects of gravity on low velocity penetration

into other types of soil should be investigated.

4. Higher penetration velocities should be investigated with emphasis on the range of velocities that is near or above the compressional wave velocity of the target medium.

Bibliography

1. Adams, D. F., and D. R. Doner, "Determining the Material Properties of a Remote Target by Analyzing Deceleration-Time Impact Data", New York: Journal of Spacecraft and Rockets, AIAA, Vol.3, No. 6, pp. 885-889, June, 1966.
2. AFM 88-51, Materials Testing, Washington: Department of the Army and the Air Force, Feb., 1966.
3. Allen, W. A., E. B. Mayfield, and H. L. Morrison, "Dynamics of a Projectile Penetrating Sand", Journal of Applied Physics, Vol. 28, No. 3, March, 1957.
4. Beswick, A. G., Instrumentation for Investigating the Physical Properties of the Lunar Surface, Washington: National Aeronautics and Space Administration, TMX 54872, October, 1964.
5. Cherkasov, I. I., et al "Determination of the Density and Mechanical Strength of the Surface Layer of Lunar Soil at the Landing Site of the Luna 13 Probe", Translated from Kosmicheskoe Issledovaniya (Cosmic Research) Vol. 5, No. 5, pp. 746-757, Sept.-Oct., 1967.
6. Fung, Y. C., Foundations of Solid Mechanics, Englewood Cliffs, New Jersey: Prentice-Hall Inc., 1956.
7. Hanks, B. B., and J. L. McCarty, "Investigation of the Use of Penetrometers to Determine the Capability of Dust Materials to Support Bearing Loads", Washington: National Aeronautics and Space Administration, Tech. Note TN D-3200, 1964.
8. Hardin, B. O., discussion of "Foundation Vibrations", New York: Transactions of the American Society of Civil Engineers, Vol. 127, Part I, pp. 863-925, 1962.
9. Hoerner, S. F., Fluid-Dynamic Drag, Great Britain: Published by the author, 1958.
10. Johnson, S. W., J. A. Smith, E. G. Franklin, L. K. Moraski, and D. J. Teal, "Gravity and Atmospheric Scaling Equations For Small Explosion Craters in Sand", Wright-Patterson AFB, Ohio: Air Force Institute of Technology, AFIT TR 68-3, March, 1968.

11. Johnson, S. W., Associate Professor of Mechanics, Air Force Institute of Technology, Personal communication, July, 1968.
12. Karafiath, L. L., "Determination of the Coefficient of Friction Between Metals and Non-metals in Ultra-High Vacuum", Beth Page, New York: Grumman Aircraft Engineering Corp., Dept. Rpt. RE-311. December, 1967.
13. Lynch, E. J., and J. H. Higgins, "The Effects of Gravity On the Bearing Capacity of Cohesionless Soils", unpublished thesis, Air Force Institute of Technology, Wright-Patterson AFB, Ohio, 1964.
14. McCarty, J. L., A. G. Beswick, and G. W. Brooks, "Application of Penetrometers to the Study of Physical Properties of Lunar and Planetary Surfaces", Washington: National Aeronautics and Space Administration, Tech. Note TN D-2413, 1964.
15. McLachlan, N. W., Ordinary Non-Linear Differential Equations in Engineering and Physical Sciences, 2nd Edit., Oxford: Clarendon Press, 1956.
16. Mitchell, J. K., R. E. Goodman, W. N. Houston, and P. A. Witherspoon, Lunar Surface Engineering Properties Experiment Definition, 2nd Quart. Rpt. Contract No. NAS 8-21432, University of Cal. Berkeley: Space Sciences Lab., Ser. 10, Iss. 6, Feb., 1969.
17. Moore, H. J., United States Geological Survey, Menlo Park, Cal., personal communication, 8 May, 1968.
18. -----, personal communication, February, 1969.
19. Moraski, L. K., and D. J. Teal, "An investigation of the Effects of Gravity on Crater Formation in a Cohesionless Medium", unpublished thesis, Wright-Patterson AFB, Ohio, Air Force Institute of Technology, 1965.
20. Quigley, D. W., and J. K. Mitchell, "Remote Penetrometer Observations of the Lunar Surface", University of California, Berkeley, unpublished working paper, 1967.
21. Schmid, W. E., The Determination of Soil Properties In Situ by an Impact Penetrometer, Air Force Cambridge Research Laboratories, Bedford, Massachusetts, January, 1966, AD 634 043.

22. Smith, J. A., and E. G. Franklin, "Pressure and Gravity Effects on the Simulation of Meteorite Impact Craters", unpublished thesis, Air Force Institute of Technology, Wright-Patterson AFB, Ohio, 1967.
23. Swift, H., University of Dayton Research Laboratories, Wright-Patterson AFB, Ohio, Personal communication July, 1968.
24. Terzaghi, K., and R. B. Peck, Soil Mechanics in Engineering Practice, 2nd Edit., New York: John Wiley & Sons Inc., 1967.
25. Viktorov, V. V., and R. D. Stepenov, "Modeling the Action of an Explosion with Concentrated Charges in Uniform Ground", Engineering Collection of the Institute of Mechanics of the Academy of Sciences of the U.S.S.R., Vol. XXVIII, pp. 87-96, 1960. Trans. 1961, Sandia Corporation Library, Scientific Translation Service.
26. Womack, D. P., and W. R. Cox, Measurement of Dynamic Characteristics of Soils with Penetrometers, Washington: National Aeronautics and Space Administration, Contractor Rpt. CR-849, August, 1967.
27. Young, C. W., Low Velocity Penetration Study: Second Phase, Albuquerque: Sandia Laboratories, February, 1967.
28. -----, The Development of Empirical Equations For Predicting Depth of an Earth Penetrating Projectile, Albuquerque: Sandia Laboratories, May, 1967.
29. -----, and G. M. Ozanne, Compilation of Low Velocity Penetration Data, Albuquerque: Sandia Laboratories, June, 1966.
30. Young, C. W., Low Velocity Penetration Tests in Natural Earth Targets of Selenite and Gypsite, Albuquerque: Sandia Laboratories, April, 1965.

Appendix A

Tabulated Raw Data

The following pages contain tabulated raw data from both the laboratory and flight phases of the experiment. The sequence numbers apply to shots at a given gravity level. They are chronological within each level.

TABLE III

Penetration Data: 2.00 g(Ottawa Sand)

SEQUENCE NUMBER	PROJECTILE	V_o (cm/sec)	P_m (cm)	t_m (msec)
1	A1-2-F	1371	12.1	18.30
2	"	1371	11.6	14.88
3	"	1331	10.9	16.12
4	"	1277	11.0	14.88
5	"	1344	16.5	25.42
6	"	1424	16.5	25.42
7	"	1387	14.7	21.70
8	"	1408	15.3	23.56
9	"	1177	15.5	28.04
10	"	1280	13.7	21.70

TABLE IV

Penetration Data: 1.00 g(Ottawa Sand)

SEQUENCE NUMBER	PROJECTILE	V_o (cm/sec)	P_m (cm)	t_m (msec)
1*	A1-2-F	1312	13.4	21.08
2*	"	1248	12.4	19.84
3*	"	1390	16.4	27.90
4*	"	1315	16.0	29.76
5*	"	1395	16.0	26.04
6*	"	1376	14.7	23.56
7*	A1-1-F	1277	13.3	18.60
8	A1-2-F	937	11.7	25.90
9	"	895	10.7	24.60
10	"	937	9.9	22.10
11	:	1250	11.3	20.50
12	"	1125	11.8	20.50
13	"	1365	12.5	20.80
14	"	1375	12.9	22.10

* = fired in level flight

TABLE IV (cont.)

(t_m not available)

SEQUENCE NUMBER	PROJECTILE	V _o (cm/sec)	P _m (cm)
15	A1-2-R	1140	14.4
16	"	1290	15.1
17	"	1500	16.0
18	"	1690	17.3
19	A1-2-F	1120	14.4
20	"	1290	14.6
21	"	1500	15.7
22	"	1620	16.0
23	A1-2-R	945	15.9
24	"	1100	16.2
25	"	1270	16.8
26	"	1410	18.3
27	A1-1-F	930	14.5
28	"	1080	15.4
29	"	1240	16.4
30	"	1380	17.3
31	A1-2-F	847	14.6
32	"	837	11.7
33	"	1140	12.0
34	"	1140	12.2
35	"	1270	12.9
36	"	1270	13.4

TABLE IV (cont.)

SEQUENCE NUMBER	PROJECTILE	V _o (cm/sec)	P _m (cm)
37	A1-2-F	1470	14.4
38	"	1470	14.9
39	A1-1-F	943	14.3
40	"	943	13.6
41	"	930	13.2
42	"	1140	13.4
43	"	1120	13.8
44	"	1130	14.0
45	"	1240	14.8
46	"	1225	15.2
47	A1-2-F	1245	15.9
48	A1-1-F	930	14.4
49	"	930	13.7
50	"	930	13.1
51	A1-2-F	835	11.5
52	"	1120	11.6
53	"	1270	12.0
54	A1-2-R	1320	12.2
55	"	1330	12.3
56	"	1330	12.3
57	"	1320	12.3
58	"	1320	12.3
59	"	1320	12.3
60	"	1330	12.4

TABLE IV (cont.)

SEQUENCE NUMBER	PROJECTILE	V _o (cm/sec)	P _m (cm)
61	A1-2-R	1320	12.4
62	"	1320	12.4
63	"	1330	12.3
64	A1-2-F	1330	11.6
65	"	1330	11.4
66	"	1340	11.3
67	"	1320	11.4
68	"	1330	11.3
69	"	1330	11.4
70	"	1320	11.6
71	"	1330	11.6
72	"	1330	11.6
73	"	1320	11.6
74	A1-2-R	1240	13.2
75	"	1250	13.2
76	"	1240	13.1
77	"	1240	13.0
78	"	1240	12.8
79	"	1240	12.9
80	"	1240	13.0
81	"	1240	13.0
82	A1-2-F	1250	12.0
83	"	1250	11.7
84	"	1250	11.7

TABLE IV (cont.)

SEQUENCE NUMBER	PROJECTILE	V_o (cm/sec)	P_m (cm)
85	A1-2-F	1250	11.6
86	"	1250	11.6
87	"	1250	11.4
88	"	1250	11.5
89	"	1250	11.6
90	A1-1-R	1240	14.1
91	"	1240	14.7
92	"	1240	15.0
93	"	1230	15.0
94	"	1220	14.8
95	"	1220	14.6
96	"	1220	14.5
97	"	1230	14.5
98	A1-1-F	1240	13.0
99	"	1240	12.8
100	"	1250	12.7
101	"	1260	12.7
102	"	1270	12.7
103	"	1240	12.6
104	"	1240	12.6
105	"	1260	12.6

TABLE V

Penetration Data: 0.38 g(Ottawa Sand)

SEQUENCE NUMBER	PROJECTILE	V_o (cm/sec)	P_m (cm)	t_m (msec)
1	A1-2-F	1322	16.7	28.52
2	"	1277	15.7	24.18
3	"	1277	15.5	25.11
4	"	1267	15.6	25.62
5	"	1277	15.9	31.62
6	"	1234	16.0	28.21
7	"	1277	16.1	28.52
8	"	1306	15.9	24.18
9	"	1277	16.6	26.35
10	"	1277	16.3	31.93
11	"	1067	14.0	31.92
12	"	1114	15.1	-----*
13	"	1056	15.2	29.45
14	A1-2-R	1097	16.4	28.21

* t_m not available from films

TABLE VI

Penetration Data: 0.17 g

(Ottawa Sand)

SEQUENCE NUMBER	PROJECTILE	V_o (cm/sec)	P_m (cm)	τ_m (msec)
1	A1-2-F	1253	18.0	30.70
2	"	1395	17.7	34.74
3	"	1376	18.5	34.36
4	"	1387	18.4	31.50
5	"	1301	19.3	35.96
6	"	1408	19.1	34.72
7	"	1331	18.9	31.00
8	"	1277	18.5	29.76
9	"	1173	15.9	34.10
10	"	1163	16.7	33.74

TABLE VII

Deceleration-curve ParametersType I Curves

SEQUENCE NUMBER	a_1 (g)	t_v (msec)	a_v (g)	t_2 (msec)	a_2 (g)	t_m (msec.)
<u>0.17 g</u>						
1	110	10.5	25	21.5	53	30.70
3	140	11.0	30	20.0	38	34.36
4	165	9.5	27	18.0	37	31.00
5	70	14.0	33	23.0	36	35.96
6	52	15.5	30	27.0	36	34.72
<u>0.38 g</u>						
1	170	11.5	33	21.0	44	27.90
4	145	9.0	32	17.5	47	25.42
6	53	6.5	42	17.0	47	27.90
10	145	10.0	24	20.0	42	32.24
<u>1.00 g</u>						
3	190	9.5	42	16.0	46	27.90
4	198	9.5	28	16.0	38	29.76
<u>2.00 g</u>						
5	120	9.5	39	17.0	44	25.42
7	103	10.5	37	18.5	45	25.42

TABLE VIII

Deceleration-curve ParametersType II Curves

SEQUENCE NUMBER	a_1 (g)	t_1 (msec)	a_v (g)	t_v (msec)	a_2 (g)	t_2 (msec)	t_m (msec)
<u>0.17 g</u>							
2	62	1.0	33	14.5	43	23.5	34.74
8	47	4.0	26	15.5	47	27.5	29.76
<u>0.38 g</u>							
2	45	4.0	11	12.0	43	13.5	23.56
3	85	3.5	24	13.0	54	20.0	25.42
7	62	4.5	20	13.5	67	23.0	28.83
8	62	2.5	37	11.0	47	17.5	24.18
<u>1.00 g</u>							
1	92	4.5	30	12.0	56	16.0	21.08
2	77	5.0	27	11.5	53	17.0	19.84
5	73	1.0	37	10.5	59	19.0	26.04
6	70	3.0	54	10.0	73	17.5	23.56
<u>2.00 g</u>							
3	150	3.0	40	8.0	180	13.0	16.82
6	100	1.5	33	11.5	50	18.5	21.70

Appendix B

Properties of the Target Medium

The cohesionless medium used in the experiment was obtained from Soiltest Corporation, Evanston, Illinois. It was trademarked Density Sand, CN-501, but is better known as Flint Shot or Ottawa Sand. Some properties of this medium are given in the following pages.

Particle Size

Mechanical analysis is a method by which the particle size distribution of a granular soil can be determined. Analyses of several samples of the target medium showed that 99% by weight passed the U.S. Standard Sieve Number 20 and 97.4% by weight was retained on the U.S. Standard Sieve Number 40. This implied that 98.7% by weight of the same particles were between the limits of 0.4 and 2.0 mm in diameter. A typical grain size distribution curve is shown in Figure 34 on the following page. This distribution yielded the following grain size classification coefficients:

Coefficient of Uniformity. 1.38
Coefficient of Gradation 0.92
Effective Size 0.47 mm

The above coefficients indicated a poorly graded (uniform) sand. Under the Unified Soil Classification System it was classified SP, sand poorly graded (Ref. 24: 40).

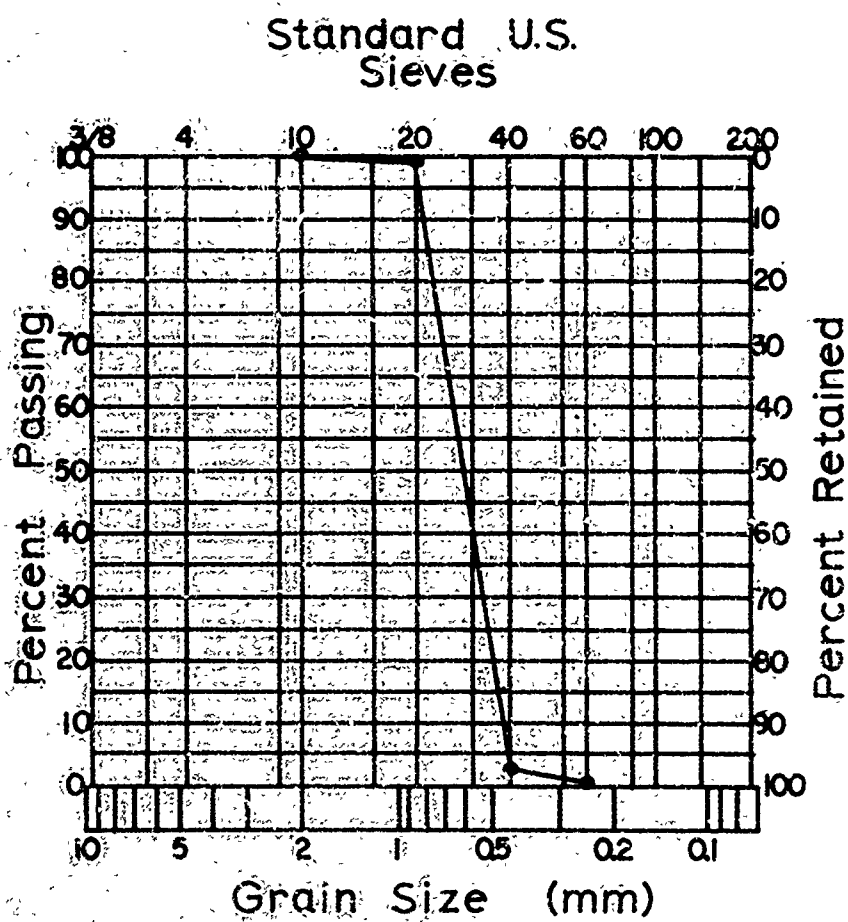


Figure 34. Mechanical analysis.

The uniformity of the sand was one of the basic reasons for its selection as the target soil. A well graded medium would have fine particles intermixed with the larger grains. These fine particles would tend to settle into the voids between the large particle and cause the sand to compact under vibration loads or repeated impacts.

Water Content

It was desirable to have a target medium that would maintain a nearly constant moisture content. It was impossible to test the target sand for water content at each firing, so the only way that a constant water content could be assured was to use a medium that had no water content at all.

The sand was tested for water content before and after the penetration tests were made. Four samples from the target were analyzed in accordance with the standard moisture content test as outlined in AFM 88-51 (Ref. 2). No traces of water were found in any of the samples and on this basis it was concluded that the water content of the target was negligible throughout the experiment.

Void Ratio

The packing condition of the sand grains in the target medium was measured by a standard soil property called the void ratio. The void ratio is defined by

$$e = \frac{V_v}{V_s} \quad (17)$$

where V_s is the volume of solid particles making up a sample, and V_v is the difference between V_s and the total volume of the sample. V_v is normally filled by air and water, but negligible water content had been established for the sand and V_v became the volume of the sample that was occupied by air.

It was important that a relatively constant void ratio be maintained during the experiments. Changes in the packing condition of the target would cloud the results of varying gravity.

The void ratio can most conveniently be determined from the formula

$$e = \frac{GV\gamma_w}{w_s - 1} \quad (18)$$

G = specific gravity of solids

γ_w = unit weight of water

V = total volume of soil sample

w_s = dry weight of solid particles in a sample

Five samples of the target medium were taken by pouring the sand slowly down the sides of a pre-weighed, graduated flask. The values of V and w_s could then be determined. Assuming a specific gravity of 2.67 and γ_w of unity (Ref. 24:27), a maximum void ratio (loosest packing condition) was determined to be 0.71. This gave a unit weight of 97.5 pounds per cubic foot.

Five other samples were taken and vibrated severely in the graduated flask until there was no noticeable reduction in their volumes. Values of V and w_s were taken for these samples and a minimum void ratio (densest packing condition) of 0.65 was determined. This gave a unit weight of 102.5 pounds per cubic foot.

From the maximum and minimum densities it was seen that the sand target would not be expected to vary in density more than 5.1% under the most extreme conditions of vibration.

Appendix C

Description of Equipment

The following is a detailed description of the equipment used in the experiment. It should clarify questions arising from the discussion of Section III.

The Aircraft

A KC-135A was used for simulation of the gravity levels required by the experiment. The basic configuration was a Boeing 707 as altered by the Air Force to fill the duties of an aerial refueling tanker. The aircraft was further modified by Aeronautical Systems Division, through civilian contract, to enable it to fly controlled parabolic maneuvers in which gravity simulation could be accomplished. The aircraft is capable of producing simulated gravity conditions from 0.00 to 2.00 g.

Alteration basically consisted of mounting accelerometers and gauges in the aircraft, placing electrical controls on the automatic pilot system, and padding the interior of the fuselage.

A photograph of the aircraft and a profile of a Zero-Gravity maneuver can be found on page 102 of Ref. 22.

Plywood Enclosure

A plywood box, 4 ft x 4 ft x 5 ft, previously used in AFIT thesis work aboard the aircraft (Ref. 22:103) was found and adapted to this experiment. The box had

previously been accepted for flight aboard the aircraft. This made acceptance of the project somewhat easier to obtain.

The only alteration of the box was repositioning of the lower window on the back side. All other adaptation consisted of attachments to the interior and exterior. The fully configured box is shown in Figures 35, 36, 37, and 38, on the following four pages.

Air Gun

The air gun was made up of five basic parts. They were the pressure chamber, the compressed air inlet line, the barrel and trigger assembly, the solenoid trigger, and the support angles.

Pressure Chamber. The pressure chamber was made from a cylindrical steel section, 1/2 inch thick, 8 inches in outer diameter, and 5 1/2 inches long. Circular steel plates, 1/2 inch thick and 7 1/2 inches in diameter, were welded to the open ends of the cylinder to form a closed chamber.

A hole was bored into the cylinder wall and was tapped to accept a pressure threaded compressed air inlet pipe. A circular area at the center of the bottom plate was polished to provide a mount for the barrel and trigger assembly. A smooth hole, 1/2 inch in diameter was bored through the plate at the center of the polished area. Six threaded holes were tapped into the polished area to a

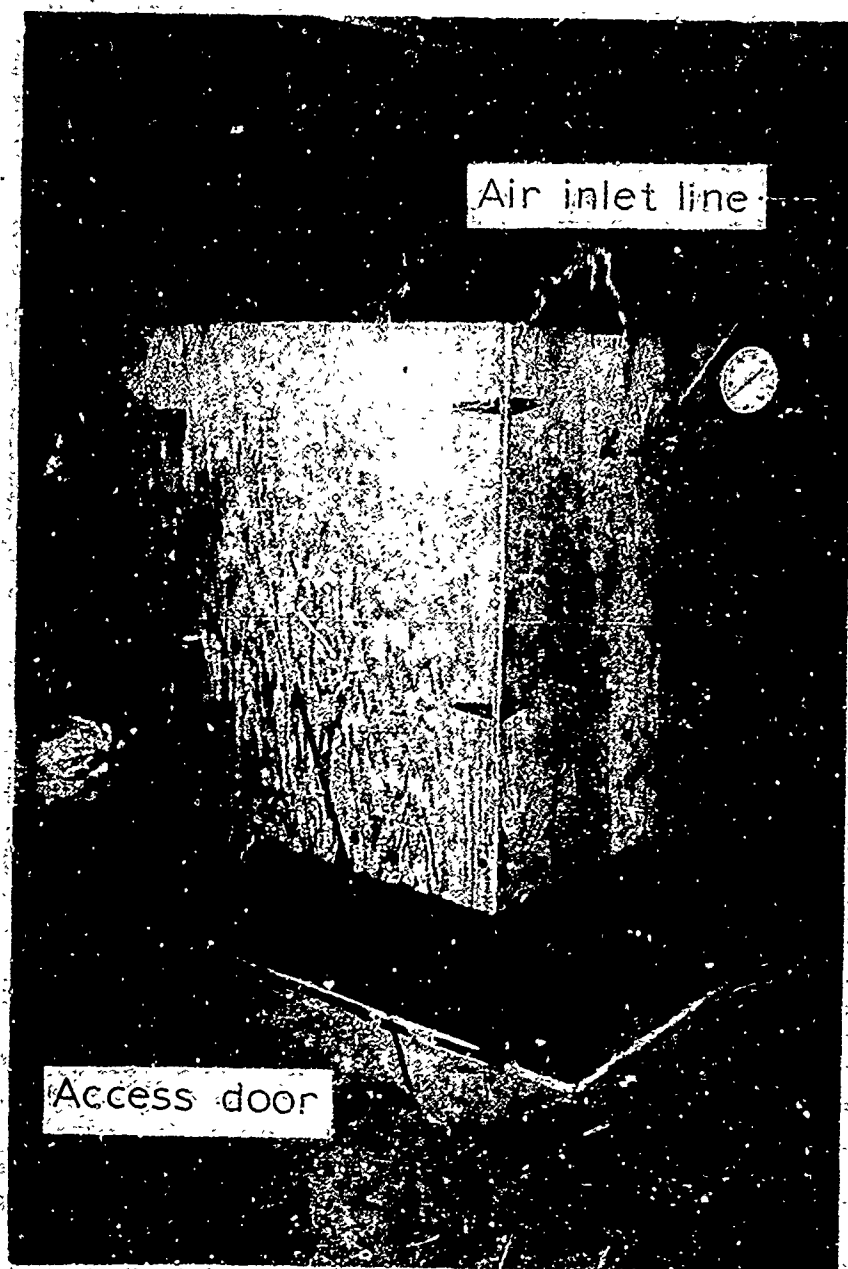


Figure 35.

GSF/MC/69-6



Figure 36.

GSF/MC/69-5

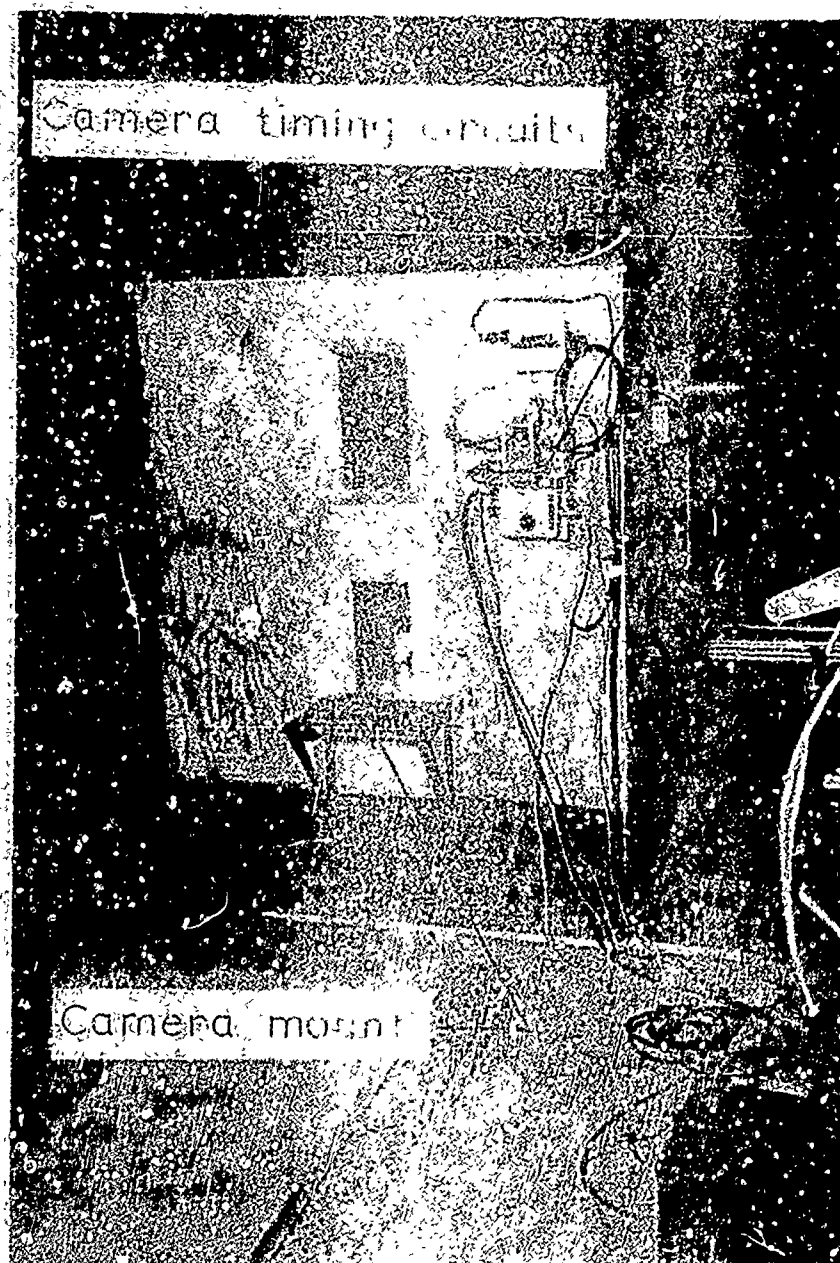


Figure 37.



Figure 38.

depth of $1/4$ inch. They were equally spaced about a circle with a 1 inch radius, concentric with the $1/2$ inch hole in the center of the polished area.

Four angular tie-down flanges were fillet-welded to the sides of the chamber at the bottom. These provided a means of attachment of the air gun to the support angles.

Compressed Air Inlet Line. The inlet line was a cast iron pipe, 30 inches long, threaded at both ends with a tapered die. One end was threaded into the hole in the side of the pressure chamber and the other was passed through a hole cut in the enclosing box. The outer end was fitted to a tee-connection to which was attached a U.S. Gauge, No. 19042. A shut-off valve was connected to the third branch of the tee by a nipple and a reduction coupling. A hose connection was fitted to the valve. This much of the inlet line was permanently attached to the experiment. (See Figure 35, page 92.)

Compressed air was brought to the line through a 150 pound, reinforced, rubber pressure hose from a regulator atop the 2000 pound storage bottle.

Barrel and Trigger Assembly. The barrel and trigger assembly was basically a barrel and a mounting plate to which were attached mounting posts for the trigger catch plate and the spring.

The barrel was a length of steel tubing, 12 inches long and $1/2$ inch in inner diameter. The mounting plate was brass. It was cut in a circle to fit the polished area

on the bottom of the pressure chamber. Six smooth holes were drilled through the mounting plate, one for each threaded hole in the bottom of the chamber. A smooth hole was drilled through the center of the mounting plate, concentric with the 1/2 inch hole in the chamber but larger in diameter by twice the wall thickness of the barrel. The barrel was fitted into this hole in the mounting plate and the barrel and mounting plate were welded together to form a solid unit.

A right-circular depression was cut into the mounting plate to a depth of 1/8 inch on the side opposite the barrel. This formed a seat for the rubber-washer pressure seal. This washer was 1 1/2 inch in outer diameter and 1/8 inch in inner diameter.

Two brass posts, 3 inches long, were threaded into holes tapped into the mounting plate so that they were parallel to the barrel and on either side of it. One post was sleeved to exactly 2 inches from the mounting plate. To this post was attached a trigger catch plate that had been cut from 1/8 inch steel sheet. The catch plate was 3 inches long and tapered from a 1 1/4 inch width where it was attached to the post to a 1 inch width on its free end. Both ends of the catch plate were rounded. The wider end was attached to the sleeved mounting post so that the plate could swing freely perpendicular to the barrel.

At the point where the catch plate met the barrel, a chord section of the barrel was cut out so that the edge of

the catch plate extended into the barrel to a maximum depth of 1/8 inch. The free end of the catch plate extended beyond the barrel and was connected to the other mounting post by a spring. This spring held the catch plate firmly in the notch in the barrel.

A wire lanyard was also attached to the free end of the catch plate but on the side opposite the spring. This was directly connected to the belt of the solenoid trigger on the side of the enclosing box.

Three holes were drilled into the barrel, 1 inch above the muzzle. The holes were equally spaced around a circumference and served as escape vents for the air blast which followed a projectile down the barrel. Their purpose was to dissipate this downward rush of air so that it would not follow the projectile into the sand bed.

The barrel and trigger assembly was fastened to the pressure chamber with six screws through the six holes in the mounting plate. (See Figure 39 on the following page.)

Solenoid Trigger. A 24 volt DC solenoid was used to provide a nearly constant trigger pull each time the air gun was fired. The solenoid was mounted on the outside of the enclosing box. The force with which it pulled a ferrous object into its core was transferred by the lanyard to the trigger catch plate to fire the gun.

The wire lanyard from the end of the catch plate was attached to a metal washer. The washer was placed over a cast iron nipple, and was held in place by a cap. The

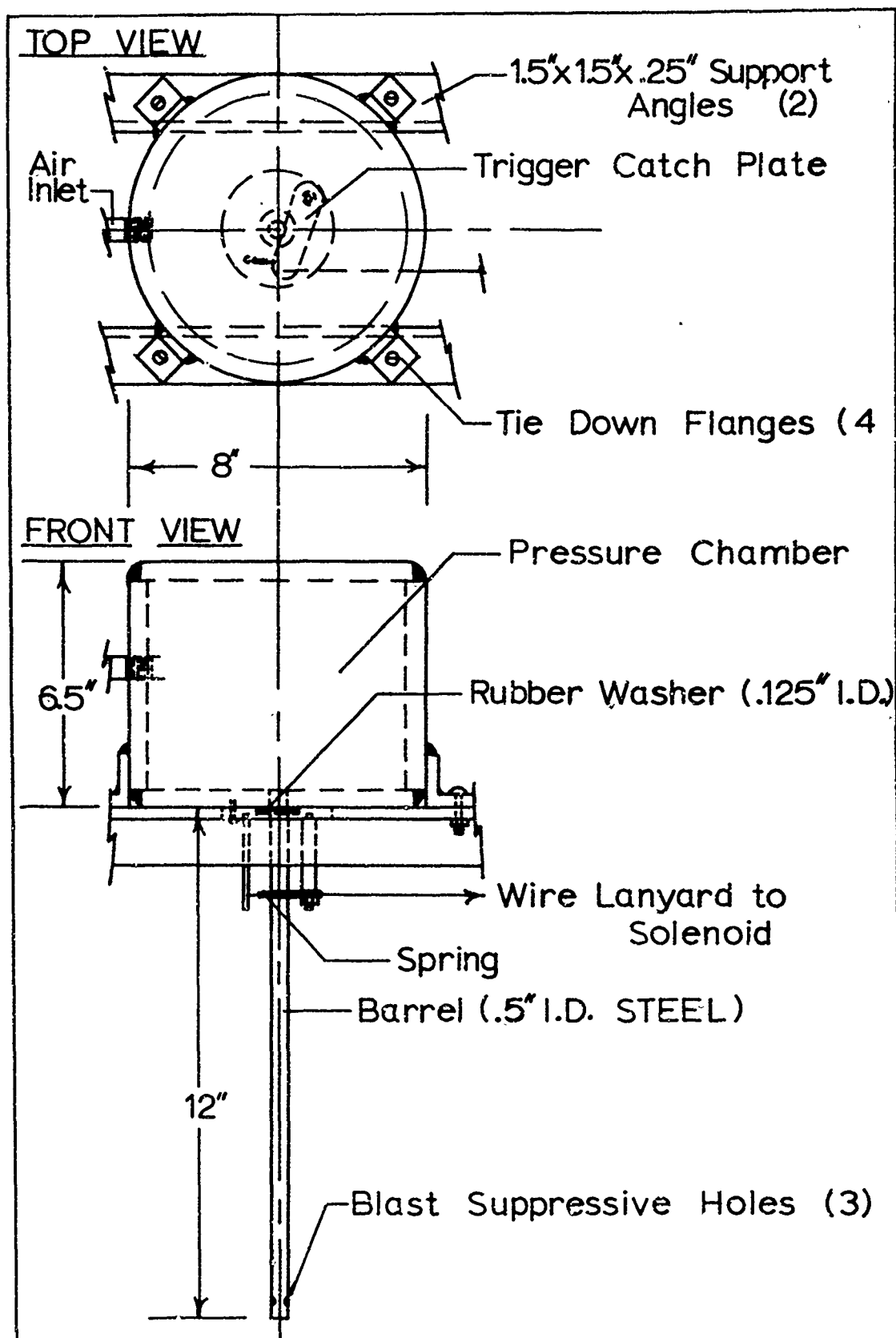


Figure 39. Compressed-air gun.

nipple was passed through a hole in the side of the enclosing box, on the side opposite the entrance of the compressed air inlet pipe. On the outside of the box, the protruding nipple was threaded into a union. The outer diameter of the union prevented the nipple from passing back through the hole in the box.

A hole was drilled through the short axis of a block of wood, 2 x 2 and 4 inches long. This hole was slipped over the union on the outside of the box. The block was then fastened to the box with wood screws so that the holes in the wood block and the box were concentric.

Another nipple was threaded into the open end of the union. The solenoid was then placed over the nipple and attached flush to the wood block with screws. The union was then trapped within the wood block and had about 1 inch of lateral freedom along the axis of the lanyard. (See Figure 40 on the following page.)

The electrical circuit of the solenoid consisted of a 24 volt DC power source and a normally open switch. During the ground tests in which high-speed photography was not used, a microswitch, spring-loaded to open circuit, was manually closed to fire the gun. When photography was used the electrical timing circuitry closed a relay after the proper delay, and this fired the gun.

The wire lanyard was adjusted so that it was tight enough to dislodge the trigger catch plate when the belt was pulled into the solenoid, but loose enough so that the

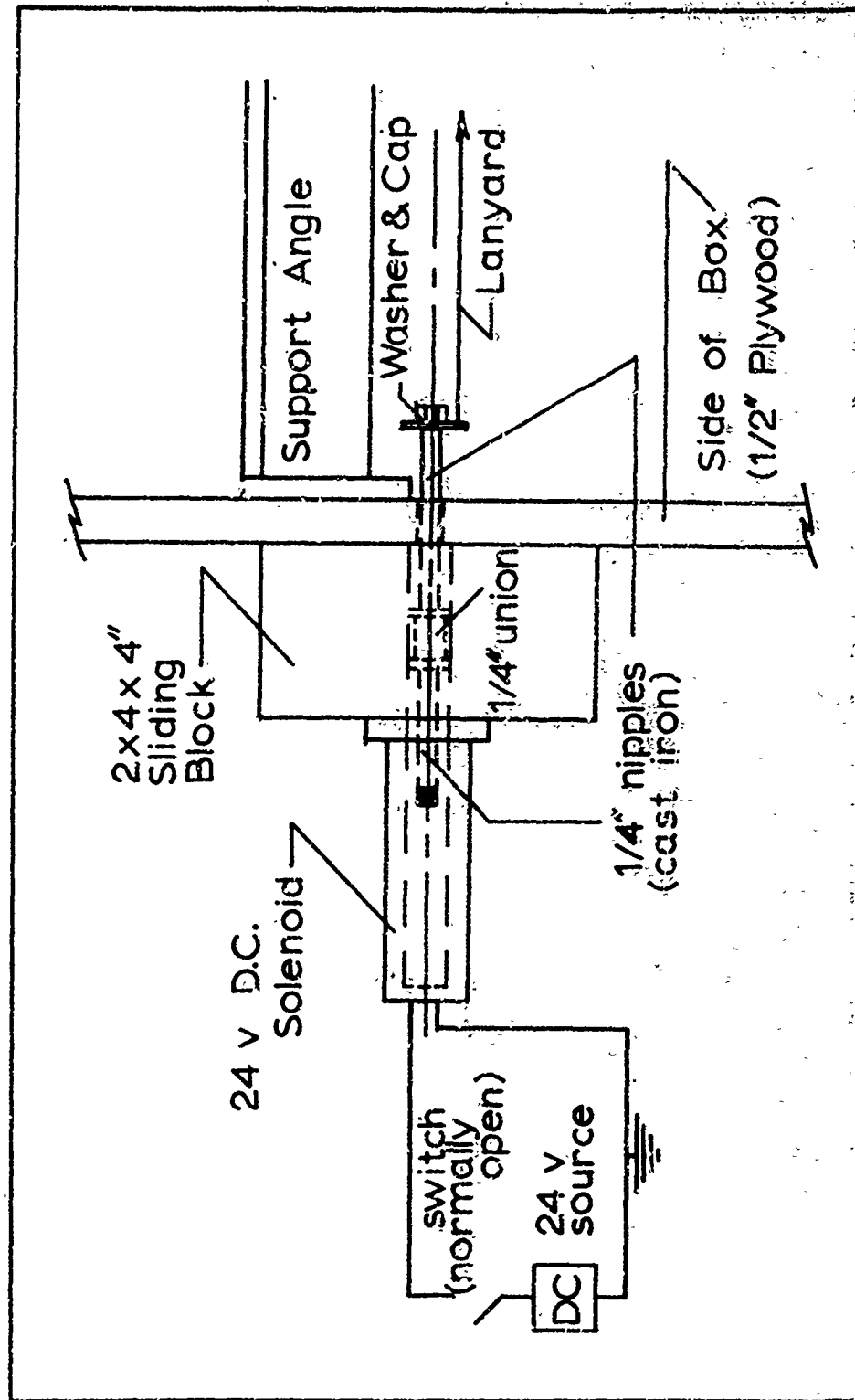


Figure 40. Solenoid trigger schematic.

spring could return the plate to the notch in the barrel.

The proper tension was found by trial and error.

Support Angles. Twin support angles were constructed from steel angle stock. They were 4 feet long overall, including steel plates welded to each end. Two holes were drilled in the horizontal legs of each angle. They were positioned to coincide with the holes in the tie-down flanges of the pressure chamber when the barrel was directly over the center of the sand target. When bolted to the sides of the enclosing box, these angles formed a solid platform for the air gun. The angles were placed in the enclosing box at a height which provided about 2 feet of free fall of the projectile from the muzzle of the gun to the surface of the sand bed. (See Figure 38, page 95.)

Operation. To operate the air gun, a projectile was chambered into the barrel. The back end of the projectile was held firmly against the rubber-washer pressure seal by the trigger catch plate. The catch plate passed through the chord section cut from the barrel and engaged a notch in the projectile. This completed the pressure seal of the chamber.

The shut-off valve was then opened and pressure was allowed to build up to the desired level in the chamber. The pressure level in the chamber was read on the gauge in the inlet line. At the desired level, the shut-off valve was closed. The gun was fired by either manually or electrically closing the switch in the solenoid trigger circuit.

The magnetic field created in the core of the solenoid pulled back the iron nipple. This motion was transferred along the lanyard to the catch plate which was pulled from the notch in the projectile. The pressure seal was broken and the compressed air in the chamber expanded down the barrel, pushing the projectile before it.

The pressure chamber was sealed with a special closed plate in place of the barrel and trigger assembly and hydrostatically tested to a pressure of 800 pounds per square inch prior to the first ground tests. Chamber pressure-velocity curves for the air gun were determined in the preliminary ground tests and are shown in Figure 41 on the following page. The maximum velocity which the air gun can produce with the available projectiles is not known.

Projectiles

The projectiles were made from either aluminum bar stock or aluminum tubing. The projectiles made from either material were identical except for their weights. Replaceable points were made, one flat and the other hemispherical. Both projectiles had a circumferential notch, 1/8 inch square, cut into their sides, exactly 2 inches from the back end. This notch was engaged by the trigger catch plate when the projectiles were loaded.

The main body of each projectile was a cylinder, 1/2 inch in diameter and 12 inches long. The loading end of each was tapped to accept the threaded replaceable points.

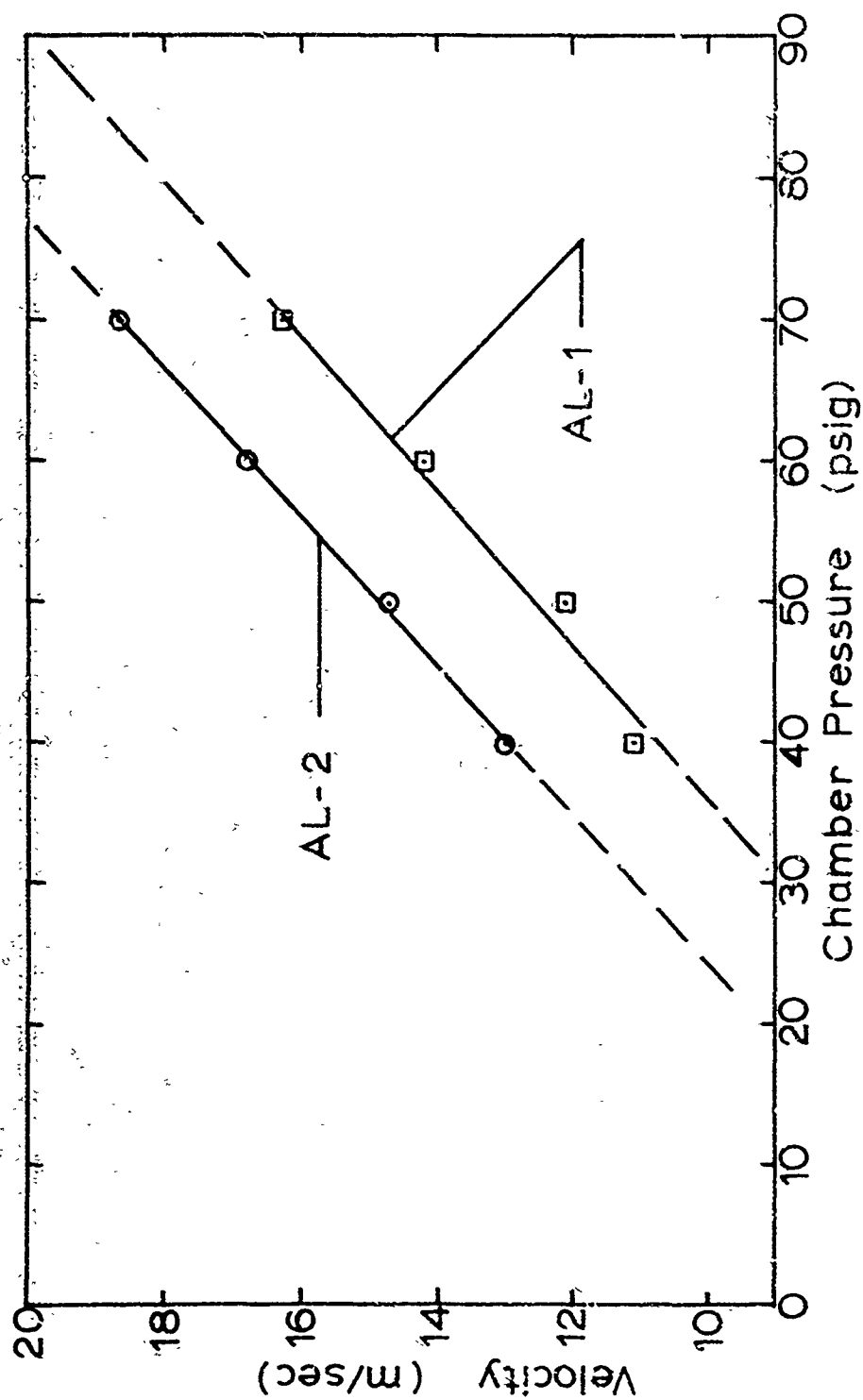


Figure 41. Air gun performance curves.

With either point on the projectile, the overall length became 13 inches. Figure 42 on the following page is a detailed photograph of the light weight projectile.

Velocity Measurement Systems

There were two methods of measuring impact velocity used in the experiment. One method made use of the sensitivity of a photo diode to changes in light intensity. The other used a double-exposure, high-speed photography technique.

Photo Diode Method. This method provided a means of measuring the time that a projectile of known length shaded a photo diode from a light source.

The photo diode was positioned near the path of the falling projectile and at a distance above the surface of the sand bed that equaled the length of the projectile. The time measured in this way was the time it took the projectile to cover the last 13 inches before impact. The velocities which resulted were averages over this distance. Negligible acceleration was assumed to convert them to impact velocities. Figure 43 on page 107 is a schematic of the system and Figure 44 on page 108 shows an example of the polaroid pictures taken by the oscilloscope camera of the response of the diode.

High-Speed Photography. This method made use of a pre-exposed grid in the plane of the path of the projectile. The grid was photographed on each frame of each 100

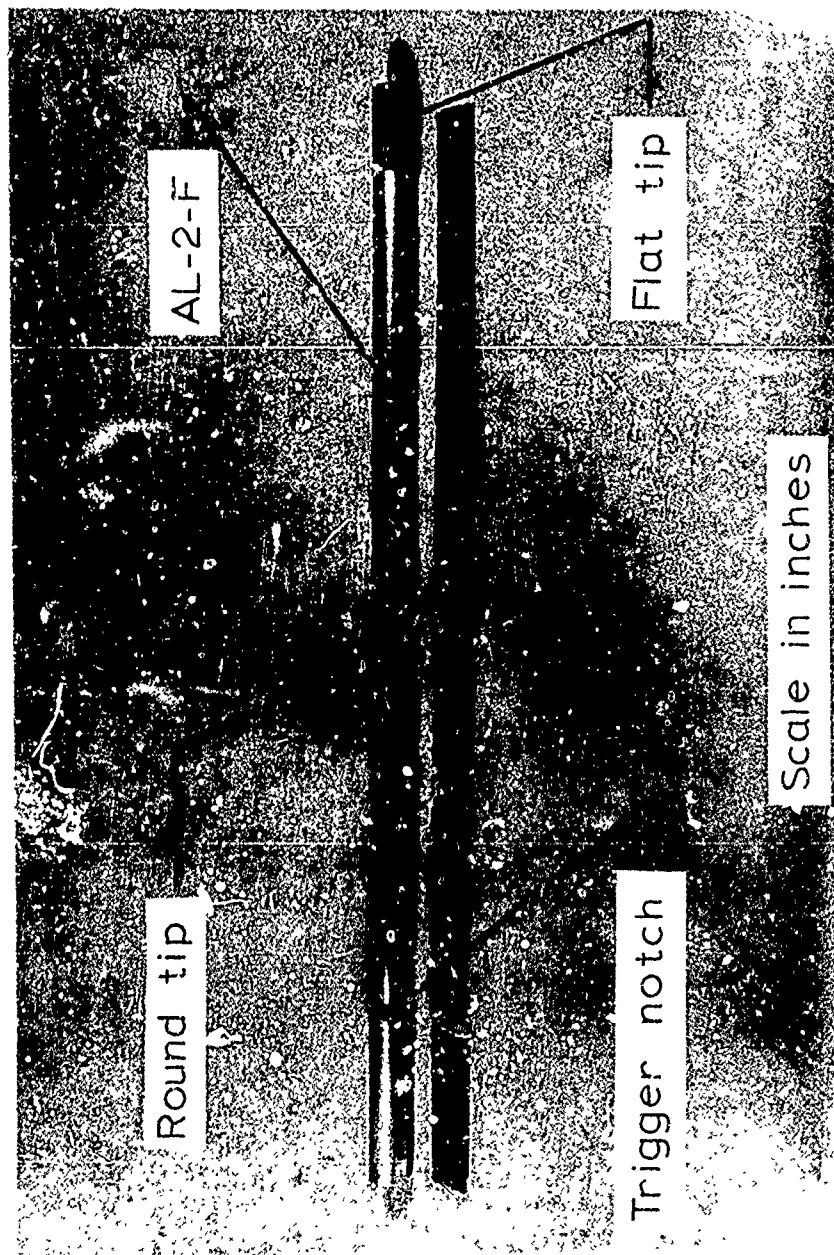


Figure 42.

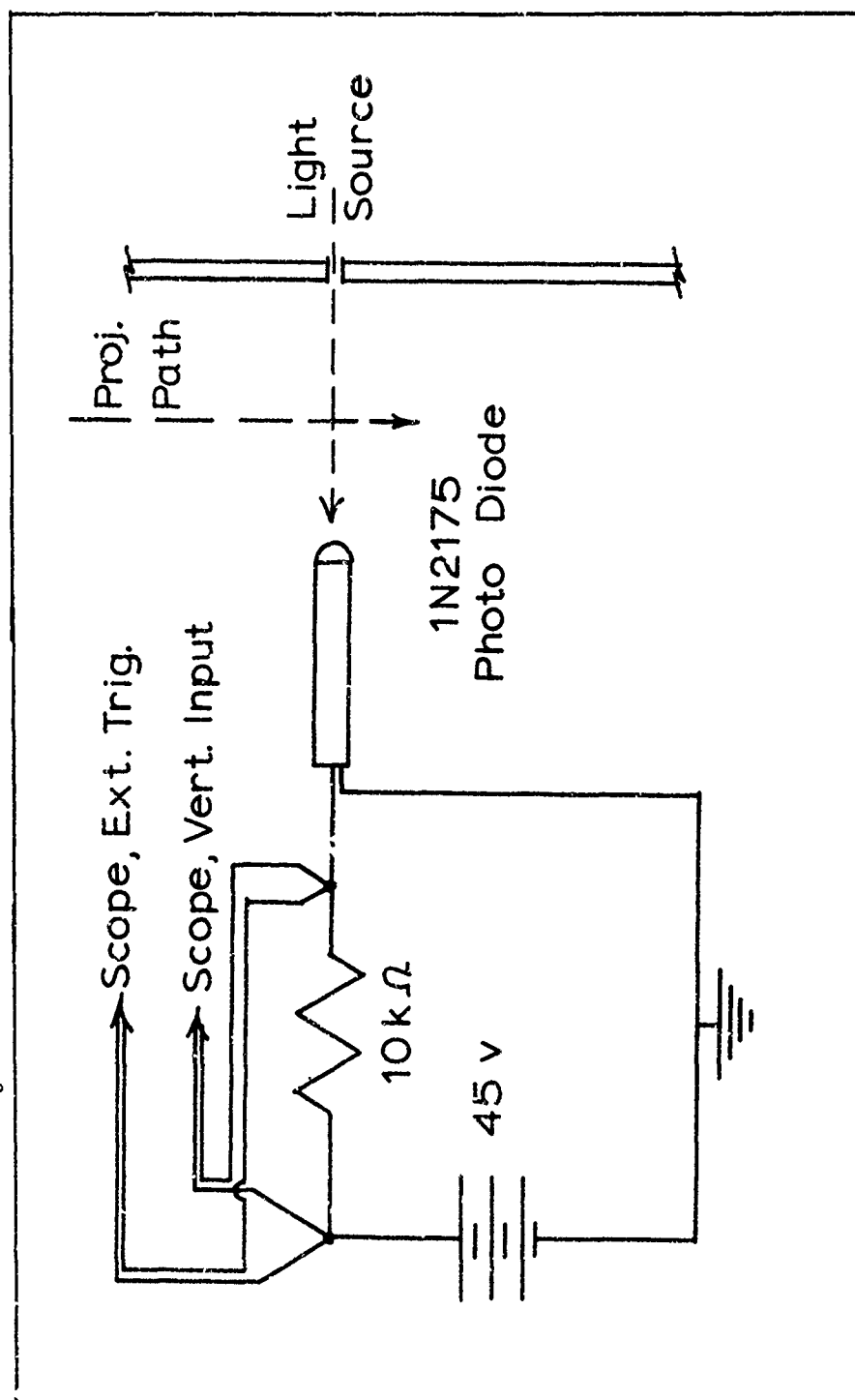


Figure 43 Photo diode schematic.

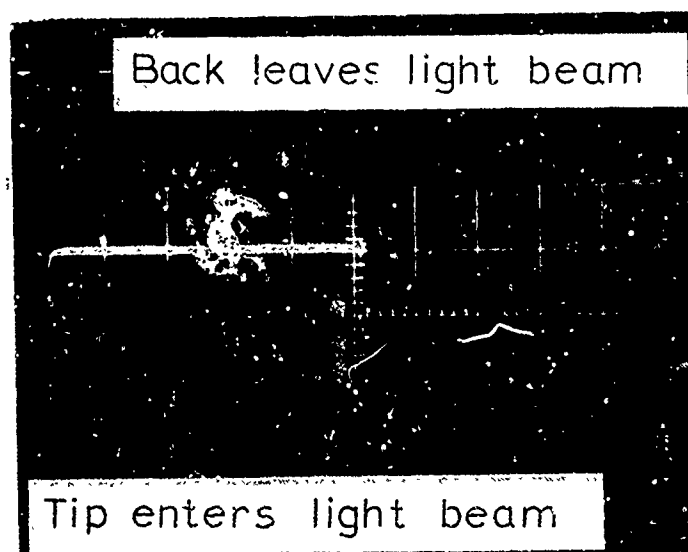


Figure 44 Sample oscilloscope trace.

foot roll of film at the same distance from the lens of the camera as the projectile was to be during the test. The grid gave a true distance scale in each frame. The film speed was marked with a millisecond timing pip to provide a time base.

The camera was a Fairchild Motion Analysis Camera, Model HS 101. It used 16 millimeter roll film and was run at 3200 frames per second. The lens was Elgert, 1.3 mm, f:1.5, wide angle.

The camera was mounted on a fixed platform attached to the outside of the enclosing box. It photographed the penetrations through a glass window. (See Figure 37, page 94.)

Four lights were mounted on the inside of the box to illuminate the penetration events.

The electrical circuitry required to correctly time the steps in the firing cycle was designed by Mr. Jack Warwick of the Technology Photography Division of ASD. Precise timing was necessary because the high-speed camera exposed a 100 foot roll of film in about 2.5 seconds. The cycle was started by closing one switch. The lights in the box came on immediately and were followed in 2.25 seconds by the camera. Exactly 1.3 seconds after the camera had started, voltage was applied to the solenoid and the gun was fired. The entire system shut down automatically when the roll of film had been used up.

Details of the camera, lighting, and exposure were handled by Mr. Merl Worland, also of the Technical Photo-

graphy Division. During the four flights, the camera was cared for by SSgt Dominic Miglionico and TSgt George Alvarado on different occasions. Both men were assigned to the Directorate of Flight Test, ASD, Wright-Patterson AFB, Ohio.

The wiring diagram of Mr. Warwick's circuitry is shown in Figure 45 on the following page.

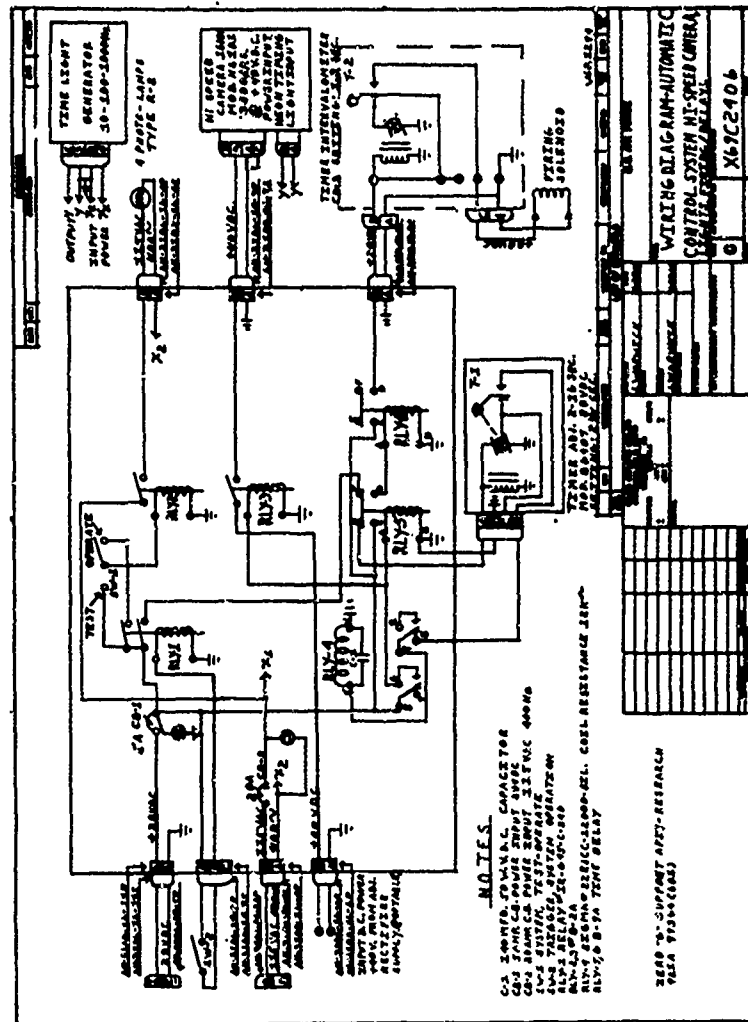


Figure 45. Wiring diagram.

Appendix D

Measurements and Sources of Error

Two types of measurements and calculations were required in this work. They were related to determination of impact velocity and maximum penetration.

Determination of Impact Velocity

Both methods of calculating impact velocity, photo diode and high-speed photography, were based on an assumption that the projectile was not accelerating during its flight from the gun to the sand. The assumption was better in the high-speed photography method because smaller increments of time were considered.

Photo Diode Method. An average velocity was determined for the projectile in its last 33 centimeters of flight before impact. The length of the projectile was known to be 33 centimeters, so the increment of distance used in the calculation is without error.

The sweep rate of the oscilloscope which recorded the response of the photo diode was 5 msec/cm and was given as accurate to plus or minus 3% by the manufacturer. The reading error involved estimation of the point on the photograph at which the trace began to return to base voltage. Estimation was required because the diode had a finite reaction time which was evident in the photographs. Based on the width of the trace, the accuracy of reading its length at raised voltage was plus or minus 0.1 centimeter.

The time increment was calculated by multiplying the length of the trace at raised voltage by the sweep-rate of the oscilloscope. For a length of 5.4 ± 0.1 cm and a sweep rate of 5.0 ± 0.15 msec/cm, the calculated increment of time would be 27.0 msec with a high of 28.4 msec and a low of 25.8 msec.

The resulting velocities would be the 33 cm distance increment divided by the different time increments, or 1220 cm/sec with a possible high of 1280 and low of 1160 cm/sec.

The assumptions of an ideal point source of light and a point face on the diode were not realized. These factors would increase the error involved, but to such a small degree that they are negligible next to the assumption of zero acceleration. Accepting this assumption, it would probably be conservative to state that this method of measuring impact velocities was accurate to ± 75 cm/sec.

High-Speed Photography Method. The pre-exposed grid used to determine projectile position was photographed so that parallax errors were avoided. The grid was constructed to an accuracy of ± 0.1 cm. This was checked by measuring the last 5.1 cm known length of the projectile at different depths in the grid. The reading accuracy of a given position of the projectile was determined to be ± 0.2 cm. This was done by having three different persons read the same film and record their results without prior knowledge of the results of the others.

The films were read by displaying them on the screen of

an Eastman Recordak viewer. At the highest magnification, about three frames at a time were displayed on the screen. A cardboard strip was marked and numbered so that it could be laid on the screen of the viewer and used as a ruler to aid in counting the number of lines from the top of the grid to the reference point on the projectile as it appeared in the frame. The position was estimated to the nearest tenth of a centimeter since the lines of the grid were 0.5 cm apart.

The velocity increment was determined by counting the number of frames between the millisecond timing-pips on the edge of the film. This could be done only to the nearest tenth of a frame. The result was a number of frames per millisecond which could be directly inverted to obtain milliseconds per frame. The average film speed of this experiment was 3200 frames per second accurate to ± 100 frames per second. The time increment per frame was therefore 0.31 msec/frame with an accuracy of ± 0.01 msec/frame.

Impact velocity was determined by reading the last five frames before impact. The time increment was about 1.65 msec and a typical distance increment over the five frames was 2.1 ± 0.2 cm. The resulting average velocities over this increment were 1270 cm/sec with a possible high of 1390 and low of 1150 cm/sec. At this range of velocities, the possible error was, therefore, 8.7%.

Determination of Maximum Penetration

Visual Method. A scale, graduated in millimeters, was used to measure the complement of penetration. Readings with it were accurate to ± 0.05 cm.

Determination of the height of the initial sand surface above the floor of the crater was done by laying the aluminum plate at the base of the projectile as it stuck up from the sand. The top of this plate then defined a horizontal reference plane, 0.6 cm above the initial sand surface. Irregularities beneath the plate were slight but could have caused its position to vary ± 0.1 cm.

Some projectiles were observed to be tilted from vertical after a complete penetration. The amount of tilt was never observed to be more than about two degrees. The scale measured only vertical distances above the plate but the error involved at this small amount of tilt was less than the accuracy of the scale.

High-Speed Photography Method. The errors in determining maximum penetration from the high-speed film were basically due to limits of the grid and reading capability. Another factor was the difficulty in determining the exact position of the projectile in the grid at impact. In some of the films, the bottom of each frame was poorly lighted. The only way to locate the frame of impact was to note in a good roll of film the position of the back of the projectile relative to a fixed point in the camera field when impact occurred. The grid in these cases was used only to

measure the vertical distance between the back of the projectile and the reference point.

When the frame of impact could be seen at the front of the projectile, the possible error was plus or minus one frame. This meant a position error of one-half the average distance traveled by the projectile at its impact velocity. At an impact velocity of 1300 cm/sec the error was ± 0.2 cm.

The overall error in penetration measurement was ± 0.4 cm.

Other Sources of Error

The following additional sources of error were noted:

1. Fluctuations in the atmospheric pressure aboard the aircraft were a possible source of error in light of the significant changes noticed from the laboratory to an elevation of 5000 feet in the aircraft. The magnitude of the error involved is not known.
2. Possible fluctuations in gravity level during the level flight tests would also affect maximum penetration. The magnitude of the fluctuations is unknown.
3. Variations in the void ratio of the target sand would have caused variations in the penetrations. The maximum expected change in void ratio was 5.1%, but the corresponding change this would cause in other soil properties cannot be determined and might be significant.

Appendix E

Derivation of a Semi-Analytical Equation

To show in depth the method used to develop semi-analytical equations, a derivation of Moore's equation (Eq. (7)) is presented in this section along with the derivation of an equation based on another form of the soil resistance force. The second equation includes Moore's suggested dependence on confining pressure, and adds the fluid dynamic drag consideration of a buoyant force dependent on the square of velocity. It also includes a possible dependence on ambient pressure.

Moore's Derivation

Assumptions. The basic assumptions of Moore's derivation are the following:

1. The target soil is a homogeneous mass and has no cohesion.
2. The energy available for penetration is the kinetic energy of the projectile at impact.
3. The soil resistance force is proportional to the confining pressure on the soil target, and acts opposite the motion of the projectile on the line of penetration.
4. The soil resistance force is independent of velocity.
5. The projectile is a cylinder with constant cross-section.

Method. Moore determines the work required to penetrate the soil to a depth, P_m , by integrating his assumed soil resistance force over the depth. He equates the result to the kinetic energy of the projectile at impact.

The soil resistance force assumed by Moore is

$$F = K\rho g z A_0 \quad (19)$$

where

g = gravitational acceleration

ρ = soil density

A_0 = cross sectional area

z = depth into the soil

K = a constant

The work required to overcome this resistance to a depth, P_m , is

$$K\rho g A_0 \int_0^{P_m} z \, dz = \frac{K\rho g A_0 P_m^2}{2} \quad (20)$$

The kinetic energy of the projectile at impact is

$$\frac{\rho_p A_0 L V_0^2}{2} \quad (21)$$

where

ρ_p = projectile mass density

L = projectile length

V_0 = impact velocity

Equating expressions (20) and (21), the following

solution for P_m is obtained

$$P_m = K' \left(\frac{\rho_p}{\rho} \right)^{\frac{1}{2}} \left(\frac{L}{g} \right)^{\frac{1}{2}} V_o$$

where $K' = (K)^{-\frac{1}{2}}$

An identical solution is obtained if one begins with Newton's equation of motion, Eq. (1), and neglects the weight of the projectile.

The differential equation then to be solved is

$$K\rho g z A_o = -M V \frac{dV}{dz} \quad (22)$$

where M is the mass of the projectile and the mass of soil moving with the projectile has been neglected.

Separation of variables gives an equation which can be integrated over the known limits of the event. The conditions which supply these limits are:

1. The event begins at $z = 0$, at which point $V = V_o$.
2. The event ends at $z = P_m$, at which point $V = 0$.

The resulting integral equation is

$$K\rho g A_o \int_0^{P_m} z \, dz = M \int_0^{V_o} \frac{V dV}{1} \quad (23)$$

from which the equation

$$K\rho g A_o P_m^2 = M V_o^2 \quad (24)$$

results.

The quadratic formula can then be used to solve for P_m , with the condition that P_m must be positive. The result is

$$P = K' \left(\frac{M}{\rho g A_0} \right)^{\frac{1}{2}} V_0 \quad (25)$$

which is identical to Eq. (7), if $\rho_p A_0 L$ is substituted for M .

Non-Constant Cross-Sectional Area. The head of a projectile is normally not flat. The results of this thesis, compared with the nose-performance coefficients empirically determined by Young, indicate that the coefficients are not constants for a given shape, but vary at least with projectile body diameter. The variation of cross-sectional area over the nose of a projectile can be included in the semi-analytical approach to a solution if the following assumptions are included:

1. The soil resistance force acts vertically against the frontal area presented by the projectile.
2. The variation of frontal area with depth is a function that can be determined and is integrable over the depth of penetration.

An example of this situation would be a cylindrical projectile with a hemispherical nose. The variation of frontal area with depth is then

$$A(z) = \begin{cases} \pi(2Rz - z^2) & 0 \leq z \leq R \\ A_0 & R < z \leq P_m \end{cases} \quad (26)$$

where R is the radius of the hemispherical nose and the body of the projectile.

Including this in a semi-analytical solution based on Moore's theory of the soil resistance force, the equations to be solved become

$$K\rho g\pi(2Rz - z^2)z = -MV\frac{dV}{dz} \quad (27)$$

$$K\rho gA_0z = -MV\frac{dV}{dz}$$

Integrating these equations over the proper limits and adding the results to get total penetration, the expression to be solved for P_m is

$$K\rho gA_0P_m^2 = MV_0^2 + K\rho g\left(A_0R^2 - \frac{4\pi R^3}{3} + \frac{\pi R^4}{2}\right) \quad (28)$$

The solution for P_m is then

$$P_m = \left[MV_0^2 + K\rho g\left(A_0R^2 - \frac{4\pi R^3}{3} + \frac{\pi R^4}{2}\right) \right]^{1/2} \left[K\rho gA_0 \right]^{-1/2} \quad (29)$$

Qualitatively, this equation shows that nose-shape can affect maximum penetration, and that the effect of nose-shape decreases with the radius of the projectile

A Proposed Form of the Soil Resistance Force

Based on the terrestrial accuracy of Moore's equation (Ref. 19) and on the dependence of certain soil properties on confining pressure, it is reasonable that the soil

resistance force be assumed a function of this variable. Considerations of fluid dynamic drag (Ref. 7), indicate that there will be a buoyant force proportional to velocity squared and a force proportional to velocity acting on a projectile traveling in a homogeneous medium. If all of these terms are gathered into a form of the soil resistance force, the resulting expression will be

$$F = K\rho gz + K_1V + K_2V^2 \quad (30)$$

where K , K_1 , and K_2 are constants.

Substituting this expression into Newton's equation of motion results in the formation of a non-linear differential equation which does not readily lend itself to a closed form solution. If, however, the term proportional to the first power of velocity is neglected, a solution can be determined.

Ambient pressure can also be considered by reasoning that it makes up part of the confining pressure. That is, the pressure on an element of soil at a depth, Z , below the surface of a sand bed is equal to the ambient pressure at the surface plus the confining pressure due to the overburden of sand.

With these assumptions made, the soil resistance force takes the form

$$F = K(P_A + \rho gz) + K_2V^2 \quad (31)$$

where P_A is ambient pressure.

Substituting this force into Newton's equation and neglecting the weight of the projectile, a non-linear differential equation is generated which can be rearranged into the form

$$\frac{dV}{dz} + \frac{K_2}{M} V = V^{-1} \left(\frac{K(P_A + \rho g z)}{M} \right) \quad (32)$$

This is a form of Bernoulli's equation (Ref. 12:11) which has the general form

$$\frac{dV}{dz} + f(z)V = V^\mu g(z) \quad (33)$$

This has a closed form solution if f and g are continuous functions of z only, and μ is not equal to 0 or 1.

Eq. (32) can be seen to fit these conditions with

$$f(z) = \frac{K_2}{M} \qquad g(z) = \frac{K(P_A + \rho g z)}{M}$$

$$\mu = -1$$

From the general solution to the Bernoulli equation, the solution to Eq. (32) is

$$V^2 = B \exp \left[\frac{-2K_2 z}{M} \right] + 2 \exp \left[\frac{-2K_2 z}{M} \right] \left(- \frac{K P_A}{M} \int^z \exp \left[\frac{2K_2 z}{M} \right] dz - \frac{K \rho g}{M} \int^z z \exp \left[\frac{2K_2 z}{M} \right] dz \right) \quad (34)$$

which reduces to

$$V^2 = B \exp \left[\frac{-2K_2 z}{M} \right] - \frac{K(P_A + \rho g z)}{K_2} + \frac{K \rho g M}{2K_2^2} \quad (35)$$

where B is an arbitrary constant. The constant can be evaluated by applying the condition that $V = V_0$ at $z = 0$.

P_m can be determined by applying the condition that z equals P_m at V equals 0. The resulting expression is

$$0 = \left[V_0^2 + \frac{K P_A}{K_2} - \frac{K \rho g M}{2K_2^2} \right] \exp \left[\frac{2K_2 P_m}{M} \right] - \frac{K(P_A + \rho g P_m)}{K_2} + \frac{K \rho g M}{2K_2^2} \quad (36)$$

The constants, K and K_2 must still be determined and the equation is difficult to handle. It may not be worth the effort involved in solving for values of P_m , since the solution requires a computer. On the other hand, it is not impossible that the constants might be definable in terms of the soil properties.

Inclusion of the term in the soil resistance force which is based on linear velocity dependence, should improve the accuracy of the solution, especially in the range of

velocities that occur after the projectile has nearly come to a stop.

It is possible to differentiate Eq. (35) with respect to time and determine a possible functional form of projectile acceleration. The resulting expression has the form

$$-a_p = \frac{Kpg}{2K_2} + \left[v_0^2 + \frac{KP}{K_2} - \frac{KpgM}{2K_2^2} \right] \exp \left[\frac{-2K_2 z}{M} \right] \quad (37)$$

It can be seen, qualitatively, that, at impact, the magnitude of deceleration is proportional to the gravity field. The expression then decays monotonically with depth into the sand, and does not agree with the observed deceleration traces that have been found in this and other experiments. The inclusion of the linear velocity term might change the form of this expression significantly. A great deal of experimental verification is necessary before this expression can be used with any degree of confidence, and a closed form of a solution should be sought with a soil resistance force as defined in Eq. (30).

Appendix F

Computer Program For Plot Production

The program presented on the following pages uses the capability of the IBM 7094 computer and its support equipment to produce continuous plots of least squares polynomials generated to fit the data read from high-speed films.

The program calls two subroutines, PLSQ for the least squares fit and GRAPHM to place instructions for the plotter onto a tape. PLSQ is in the library of the computer equipment. GRAPHM was written by Capt. Ron Prater, a student in the AFIT doctoral program.

The main program which follows is written in the Fortran IV language. It will accept data in three different formats, two of which require both X and Y coordinates of the data and one which requires only Y coordinates and internally computes equally spaced X coordinates. The program obtains the coefficients of the best least squares polynomial of a desired order and uses them to compute values of the polynomial over a range of the independent variable. If desired, the program will obtain the best least squares polynomial and double-differentiate it before getting the values for a plot.

The following pages contain the entire main program. GRAPHM can be obtained either from Capt. Prater or Major S. Johnson of the Mechanics Department, Air Force Institute

GSF/MC/69-6

of Technology, Wright-Patterson AFB, Ohio.

```

C
C      PLOT DISTANCE OR DECELERATION VS TIME

      DIMENSION X(800,1), FX(800,1), TITLE(18), XNAME(3), YNAME(3),
      WORK(403), S(20), NPS(100), T(100,1), D(100,1), PT(100), PD(100)
      CALL PLOTS(WORK,603)
      READ(5,*) LNDK
      FORMAT(13)
      READ(5,6) (XNAME(I), I=1,3), (YNAME(I), I=1,3)
      FORMAT(3A6)
      READ(5,8) TEND
      FORMAT(F7.2)
      READ(5,21) NP, INDK, NFRM
      FORMAT(3I3)
      READ(5,5) (TITLE(I), I=1,18)
      FORMAT(6A6)

C      READ DATA IN CORRECT FORMAT
C
C      IF(NFRM)100,101,102
      100 READ(5,76) (T(I,1), I=1,1), (I=1,NP)
      76  FORMAT(2F7.2)
      GO TC 103
      101 READ(5,77) (T(I,1), D(I,1), I=1,NP)
      GO TC 103
      102 READ(5,77) (C(I,1), I=1,NP)
      77  FORMAT(4F7.2)
      V=0.
      DO 31 I=1,NP
      T(I,1)=V
      31  V=V+0.62

```

```

C
C      OBTAIN CCEFFICIENTS OF LEAST SQUARES POLYNOMIAL
C
C      103 DO 52 I=1,NP
C          PT(I)=T(I,1,1)
C          PD(I)=D(I,1,1)
C          CALL PLSC(PT,FC,NP,6,E,C,EMAX,ERMS,EMEQ)
C
C          52 TEST FOR D/T CR A/T
C
C          IF(LNDK)29,29,34
C
C          OBTAIN DCUBLE DIFFERENTIATED COEFFICIENTS FOR A/T
C
C          JJ=7
C          DO 51 I=1,4
C              C=B(JJ)
C              B(JJ)=B(I)
C              B(I)=C
C              JJ=JJ-1
C          DO 43 I=1,7
C              J=I-1
C              X=J
C              B(I)=X*B(I)
C              K=J-1

```

```

43      Y=K
      B(I)=Y*B(I)
      NP=0
      DO 39 I=1,7
      B(I)=-B(I)
      S=STEND/0.05
      M=S
      R=0.
      DO 15 I=1,M
      X(I,1)=R
      FX(I,1)=B(7)
      DO 16 J=2,5
      K=8-J
      FX(I,J)=FX(I,1)*R+B(K)
      R=R+.05
      DO 53 I=1,M
      FX(I,1)=FX(I,1)*1019.716
      GO TO 24

```

NEGATE COEFFICIENTS AND DISTANCES FOR D/T PLOT

```

29      DO 30 I=1,NP
      NPS(I)=1
      DO 33 I=1,NP
      D(I,1)=-D(I,1)
      DO 32 I=1,7
      B(I)=-B(I)

```

```

C
C
C      OBTAIN VALUES FOR CONTINUOUS PLOT
      S=TEND/0.05
      M=S
      R=0.
      DO 10 I=1,M
        X(I,1)=R
        FX(I,1)=B(1)
      DO 23 J=2,7
        FX(I,1)=FX(I,1)+R+B(J)
      10 R=R+.05
      CALL GRAPHM FOR PLOT
      CALL GRAPHM(NP,T,D,NPS,M,X,FX,TITLE,XNAME,YNAME,5.,5.,1)
      C (INDK)11,11,12
      23
      11 CONTINUE
      CALL PLOTE
      STOP
      END

```

Appendix G

Attempted Use of a Simulated Lunar Soil

A sample of the simulated lunar soil (Ref. 16), processed by the University of California at Berkeley, was obtained in the later stages of the experiment. There was no chance to do penetration tests aboard the aircraft, but some shots were fired into it on the ground.

The crushed basalt had a large percentage of fine particles which created a large dust cloud each time the gun was fired. The material was found to compact under repeated impact. The penetrations showed a lack of consistency which was probably due to the compaction.

One obvious difference between the Ottawa Sand and this material was that no crater was formed when the projectile penetrated. The material surrounding the projectile was not in contact with it at the surface (see Figure 46 on the following page) and the walls of the hole in the target seemed to spread with depth.

The following recommendations are made concerning further use of this material in penetration tests:

1. The air gun must either be moved farther above the surface of the target or the means of propulsion for the projectile must be changed.
2. A great deal of work must be done to determine a way in which the void ratio of the target can be controlled during penetrations.

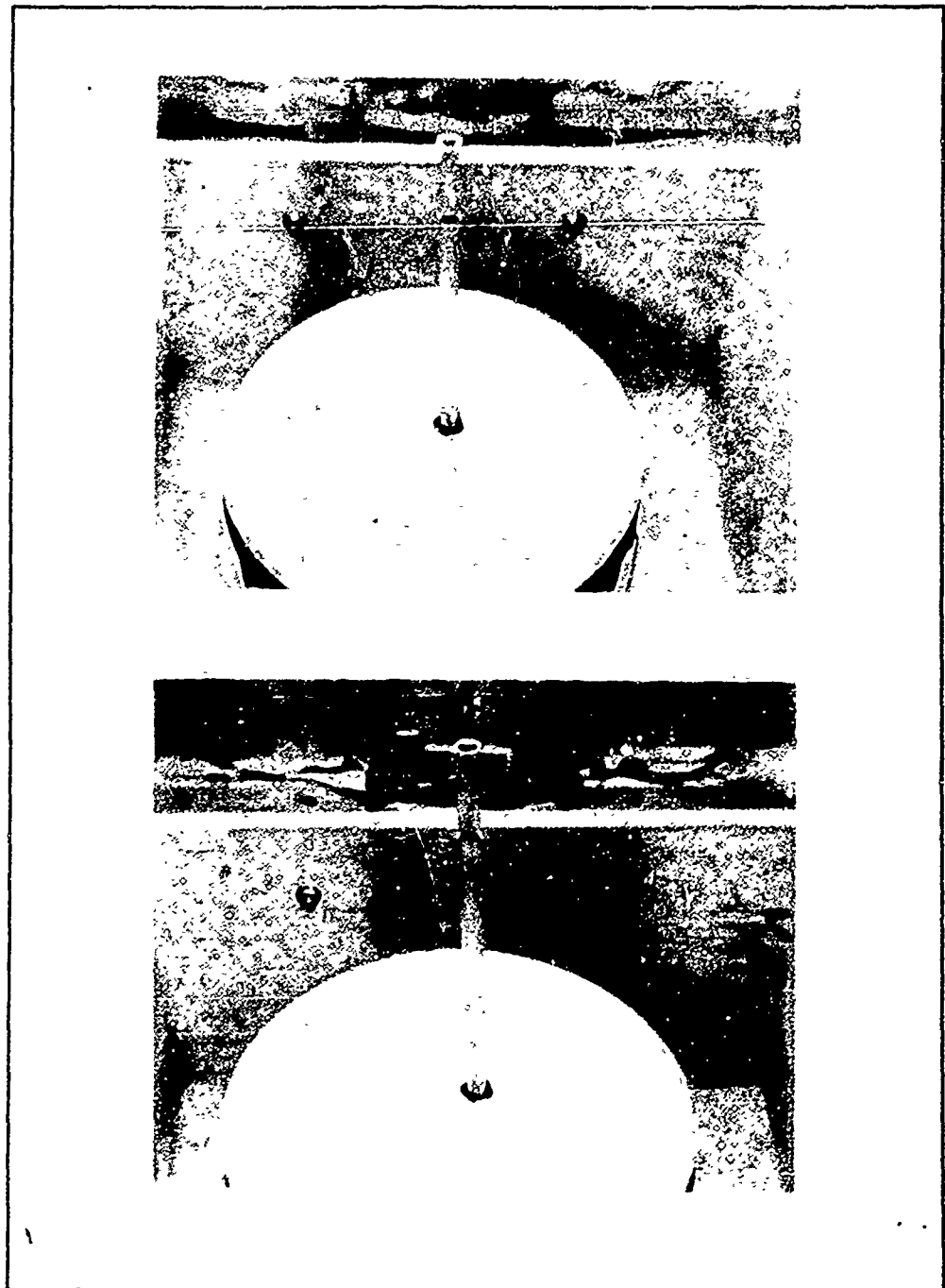


Figure 46. Penetration in crushed basalt.

GSF/MC/69-6

3. The water content of the medium must be checked as often as is found necessary to insure that it has not changed significantly over the time of the experiment.

GSE/MC/69-6

Vita

Anthony Paul Pyrzs was born on 15 may 1943 in Champaign, Illinois, the son of Anthony C. and Ursula A. Pyrzs. He graduated from Argo Community High School, Argo, Illinois in June 1961. In July of that year he entered the United States Military Academy at West Point, New York. He graduated in June of 1965 and was commissioned in the Air Force. Before coming to the Air Force Institute of Technology, he served with the 60th Civil Engineering Squadron at Travis AFB, California.

Permanent Address: 6057 S. 76th Avenue
Argo, Illinois

This thesis was typed by Mrs. Nancy Heatherly

Unclassified

DOCUMENT CONTROL DATA - R & D		
<small>Security classification of title, body of abstract and indexing annotation must be entered when the overall report is classified</small>		
1. ORIGINATING AGENCY (Corporate author) Air Force Institute of Technology School of Engineering (AFIT/SE) Wright Patterson AFB, Ohio 45433		2a. REPORT SECURITY CLASSIFICATION Unclassified 2b. GROUP
3. REPORT TITLE GRAVITY EFFECTS ON LOW VELOCITY PENETRATION OF A PROJECTILE INTO A COMESIONLESS MEDIUM		
4. DESCRIPTIVE NOTES (Type of report and inclusive dates)		
5. AUTHOR(S) (First name, middle initial, last name) Anthony P. Pyrz Captain USAF		
6. REPORT DATE June 1969	7a. TOTAL NO. OF PAGES 135	7b. NO. OF REFS 30
8a. CONTRACT OR GRANT NO. A. PROJECT NO. C. d.		8b. ORIGINATOR'S REPORT NUMBER(S) 7SF/MC/09-6 9b. OTHER REPORT NO(S) (Any other numbers that may be assigned this report)
10. DISTRIBUTION STATEMENT This document is subject to special export controls and each transmittal to foreign governments or foreign nationals may be made only with prior approval of the Dean of Engineering, Air Force Institute of Technology (AFIT-SE), Wright Patterson Air Force Base, Ohio 45433.		
11. SUPPLEMENTARY NOTES		12. SPONSORING MILITARY ACTIVITY
13. ABSTRACT The effects of gravity on the low velocity penetration of a projectile into Ottawa Sand are investigated in this study. A cylindrical aluminum projectile weighing 64.1 gm is fired at velocities in the range 800-1500 cm/sec into a bed of Ottawa Sand at gravity levels of 0.17, 0.38, 1.00, and 2.00 g. Maximum penetrations are compared at these levels. An inverse relationship is found between maximum penetration and gravity. Terrestrial soil penetration equations are discussed and compared with the data from the experiment. A method to transform a terrestrial equation into an equation valid at gravity levels in the range of the experiment is suggested. Deceleration traces are produced by computer from penetration-time data that is fit with a least-squares polynomial and mathematically differentiated. Double-peaked curves result at all gravity levels. Recommendations are made for further work in the area.		

DD FORM 1473
1 NOV 65

Unclassified
Security Classification

